Chemical patterning of surfaces for the development of biofunctional interfaces

María Jesús Pérez Roldán

FACULTAD DE
CIENCIAS
UNIVERSIDAD AUTÓNOMA DE MADRID

FACULTAD DE CIENCIAS
UNIVERSIDAD AUTÓNOMA DE MADRID

JRC
EUROPEAN COMMISSION

ihcp
Institute for Health and Consumer Protection

Chemical patterning of surfaces for the development of biofunctional interfaces

Thesis presented by/ Tesis presentada por:

María Jesús Pérez Roldán

To obtain the PhD in/ para optar al grado de Doctor en:

Advanced Materials and Nanotechnologies/
Materiales Avanzados y Nanotecnologías

Supervisors:

Dr. Pascal Colpo
Dr. Miguel Manso Silván
Dr. François Rossi

DEPARTAMENTO DE FÍSICA APLICADA

Octubre 2011

Dedicada a Salomé.

Table of contents:

Chapter 1

Introduction

1.1 Bio-interfaces

The development of new devices for molecular detection and advanced cell culture are constantly required to face with new challenges emerging from areas such as medicine, biology or environmental sciences (Catalona 1991, Marrazza 1999, Fischer 2003).

At this effect, the biological/non biological interface system is known to be an important cornerstone for the fabrication of such devices since it guaranties their reliability and performance and consequently has opened an important research area.

For instance, analytical devices for biomolecular recognition, e.g. biosensors, are based on the immobilization of a biological recognition element on a transducing surface, see figure 1.1 (Luong 2008). The biological recognition element interacts with the analyte to be detected, inducing a change of state on the transducer surface. The change of state in the physical transducer under a biorecognition event is transformed in a measurable signal, generally optical, electrochemical, or piezoelectric (Ravindra 2007, Luppa 2001) which can be subsequently recorded in a processing-monitoring unit.

Being highly related, it is evident that the efficiency of interaction between the biorecognition element and the analyte is crucial for high performance detection.

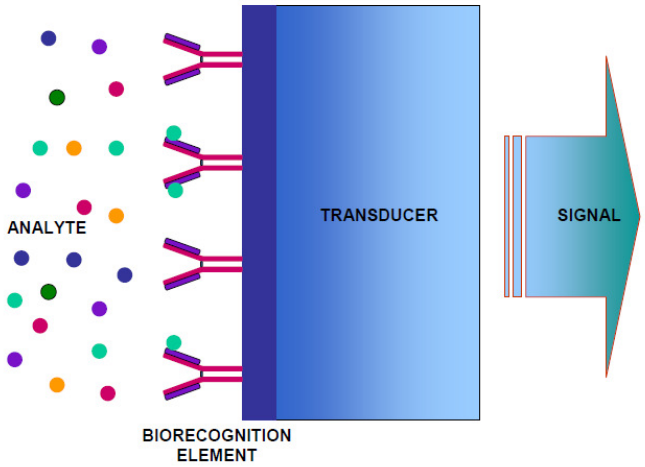

Figure 1.1 Scheme of a biosensor.

Consequently, the development of a proper biointerface that provides the immobilization of the biorecognition element (e.g. antibodies) in an active state and minimizes non-specific adsorption on the surface is mandatory for a highly sensitive and specific detection (Bonroy 2006). This problem is crucial when an antibody is used as recognition element since the biorecognition is possible only with a correct orientation of the antibodies, whose two antigen binding sites (on purple-coloured in figure 1.2) must be accessible to the analytes. Depending on the immobilization mode of the antibodies on the surface, the binding sites will be available or not for the antigen recognition.

Tissue engineering, cell based toxicological assay or biosensors and more generally *in vitro* assays are based on culturing cells on artificial surfaces (generally petri dishes, glass slides or electrodes). These non-biological surfaces have properties very different from the cell natural environment, which makes assay outcomes uncertain due to the high complexity of all phenomena involved. In particular, the interactions between cells and surfaces are mediated by integrins, which makes assay outcomes uncertain due to the high complexity of all phenomena involved. The interactions between cells and surfaces are mediated

by integrins, which are the major transmembrane proteins that link the cell cytoskeleton to specific ligands present on the surface (i.e., proteins of the extra cellular matrix (ECM)) (Werner 2006). Many researches are performed on the engineering surfaces in order to control nature density, spatial distribution and conformation of these ligands (ECM and signaling proteins) to control cell response such as proliferation and differentiation.

The development of surfaces or artificial microenvironments (2D and 3D) mimicking the "natural environment" of cells (cell lines or primary culture cells) in a specific mode, remains an important challenge that can be addressed by engineering bio-interface using materials that present a combination of bioadhesive or non-bioadhesive properties in order to favor or prevent the adhesion of biomolecules in a tailored manner (Lecuit 2007, Curtis 1997, Boyan 1996, Falconnet 2006, Mrksich 2002, Lord 2010).

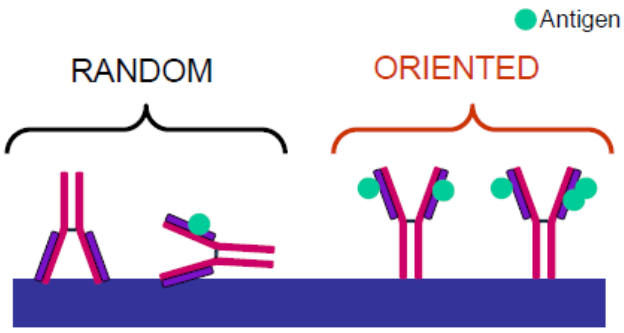

Figure 1.2 Protein immobilization.

Many surface functionalization techniques are available to provide biointerfaces with appropriate physico-chemical properties (Falconnet 2006). Surfaces can be functionalized with a range of different reactive functional groups (e.g. amine, carboxyl, polyethylene oxide (PEO)) by means of different techniques, for instance self-assembled monolayers (SAMs) (Love 2005, Mrksich 1996) or plasma polymerization (PP) processes (Sardella 2006, Brétagnol 2006 b, Siow 2006).

Combining these techniques with patterning processes, surfaces with bioadhesive/non-bioadhesive chemical contrasts can be developed to direct the protein-surface interaction only to the surface of a bioadhesive motif keeping the background free of proteins. Previous studies showed that these micro and nano chemical patternings provide not only a selective binding of proteins on the surface but also an improved orientation of the proteins immobilized, which is essential for carrying on assays based on biomolecular recognition (Brétagnol 2006 a, Ogaki 2010).

Nevertheless, the combination of surface functionalization and patterning is not straightforward since most of the techniques are based on the used of harsh reagents or external energy source (UV, plasma) that can alter the properties of the used polymers. On top of evident economic issues, the reproducibility and easiness of implementation in a biology laboratory are fundamental.

1.2 Aim of the thesis

The factors that influence biomolecule immobilization on solid surfaces are numerous and among them, the chemistry and the topographical properties of the surface are of paramount importance. The aim of this thesis was to explore the fabrication of surfaces with both a controlled topography and a specific chemistry by using a multidisciplinary approach.

The topographical properties of the surface were designed using techniques based on scanning lithography, such as electron beam lithography and focus ion beam lithography. Besides, a controlled chemistry was achieved combining these lithographic techniques with classical functionalization methods such as SAMs and PP.

SAMs can be constituted from organosilanes and organothiols. Organosilanes can assemble on SiO_2 and organothiols on gold and silver surfaces. However, PP can be applied to a broad range of materials. In PP, a monomer (low molecular weight molecules) is excited by interaction with plasma electrons. The resulting species (excited radicals and ions) react on the surface and are reorganized into high-molecular weight molecules (polymers) which form a film. Monomer and plasma

parameters determine the properties of the film deposited, so they were optimized to obtain the best functionalization of the surface.

With both methods, SAMs and PP, surfaces were designed to get bioadhesive/non-bioadhesive chemical contrasts. These chemical contrasts allowed the immobilization of biomolecules only on the bioadhesive areas of the surface.

The application of these surfaces showing chemical contrasts as biointerfaces on biosensors is of great interest for several reasons: First, these surfaces show a large reactivity, which allows controlled biomolecular interactions occurring on them. Secondly, the fabrication of chemical contrast at micro and nanometric scale can reduce significantly the amount of reagent required in the assays.

Chapter 2

State of the Art

This chapter describes the state of the art on biomolecular recognition, surface functionalization techniques, patterning techniques and biosensors. In particular, SPR biosensor technique is described.

2.1 Protein - Surface interactions

The interaction of biological systems with synthetic material surfaces is an important issue for many biological applications such as implanted devices, tissue engineering, cell-based sensors and biosensors (Kasemo 2002). Most of these applications require the immobilization of biomolecules or cells that have to be active for further interactions, such as cell proliferation for tissue generation and biomolecular recognition.

The immobilization mechanisms of proteins on surfaces are difficult to predict and control due to the complexity and diversity of the phenomena involved. Proteins have different levels of structure (primary, secondary, tertiary and quaternary), contain uneven hydrophobic and charged domains, have multiple interaction sites, tend to denaturate and often attach with random orientation on the surface. Indeed, a controlled orientation of the bound protein is crucial to guarantee the

correct interaction with other biomolecules or cells, since the functional domains of the bounded protein must be located in a way that allows the interaction.
The interactions of biomolecules with solid surfaces depend on the properties of the own biomolecules, of the bio-interface, including the solid surface properties, and the biological medium. Indeed, biomolecules can exhibit different properties (e.g. charge and hydrophobicity distribution) depending on the characteristics of the surrounding medium. The main mechanisms of immobilization of the biomolecules can be classified as physical adsorption, entrapment on polymeric matrices and covalent binding (Müller 2005, Shankaran 2007, Bilitewski 2006).

Physical adsorption is based on the direct interactions between biomolecules and surface. If the latter is not or poorly charged, low energy bonds (hydrogen bonds, van der Waals forces, or hydrophobic effects) are predominant. However, if the surface is charged, electrostatic interactions drive the interactions.
Van der Waals interactions are weak attractive forces that have a strong effect at close range and are based on dipole-dipole interactions. Biomolecules can create dipoles due to intramolecular interactions that disturb their electron clouds. These dipoles tend to align when biomolecules are immobilized in order to maximize the interaction with the electric dipoles of the molecules in the surface. Hydrogen bonding is a special case of dipole forces that occurs when a hydrogen atom is attracted by another electronegative element of a different molecule. As the hydrogen has a partial positive charge tries to find another atom (i.e. oxygen or nitrogen) with excess of electrons to share them and is attracted to the partial negative charge.
Hydrophobic interactions take place when molecules try to minimize their exposure to a polar surrounding, i.e. water. In such situation, molecules suffer conformational changes in their structure, since the hydrophobic interior of the biomolecule ‘unfolds’ to position itself against the hydrophobic interface. In figure 2.1 the distribution of the hydrophobic (red) and hydrophilic parts (blue), of the IgG molecule are shown.

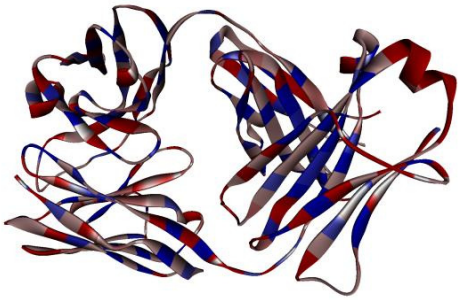

Figure 2.1 IgG hydrophobic distributions (in red high hydrophobic parts, in blue high hydrophilic parts).

Electrostatic interactions are weak forces that drive the interaction of charged surfaces with charged biomolecules. These interactions depend on the net charge of the surface and the biomolecules. Therefore, the control of the charge on the surface or on the biomolecules (e.g. by variation of pH) can turn these interactions into reversible mechanisms as the bounded species can be desorbed by variations of the pH, the ionic strength or the temperature.

The immobilization by covalent binding is achieved by setting up covalent chemical bonds between functional groups of the surface and functional groups of the biomolecules that are not involved in the molecular recognition process. The most widespread methods use –COOH, –NH2, –OH, and –SH as functional groups. This mechanism of immobilization involves the formation of irreversible chemical bonds between the biomolecule and the surface allowing a strong, and generally oriented, attachment. The process takes place by direct reaction with aldehyde and epoxide groups, or through an activation process with carboxylic or amine groups (Lofas 1995).

The entrapment of biological components within polymer membranes is another widely used immobilization technique (Ulbricht 2006, Livage 1999). This method offers a high loading of biomolecules with the retention of their activity. However, the formations of cracks or shrinkages and the changes in the material properties as a function of ageing are disadvantages to take into consideration.

2.2 Biomolecular assays

An accurate control of the immobilization of biomolecules at the biointerface can be carried out by different biomolecular assays. Some of the most common measurement formats are direct, sandwich and indirect competitive inhibition assays (Homola 2003, Shankaran 2007, Urban 2006, Fintschenko 1998)

In direct detection format, an analyte present in the biological fluid interacts with a biomolecular recognition element (antibody) immobilized on the sensor surface (see figure 2.2 a). This principle is generally used for the detection of large molecules (molecular weight ≥10 kDa).

The sandwich assay consists in two recognition steps, (figure 2.2 b). First, a target analyte is brought in contact with an antibody immobilized on the interface. Then a secondary antibody is flown over the sensor surface to bind with the previously captured analyte, increasing the number of bound biomolecules and thus also the sensor response. This method is generally employed for the detection of smaller molecules.

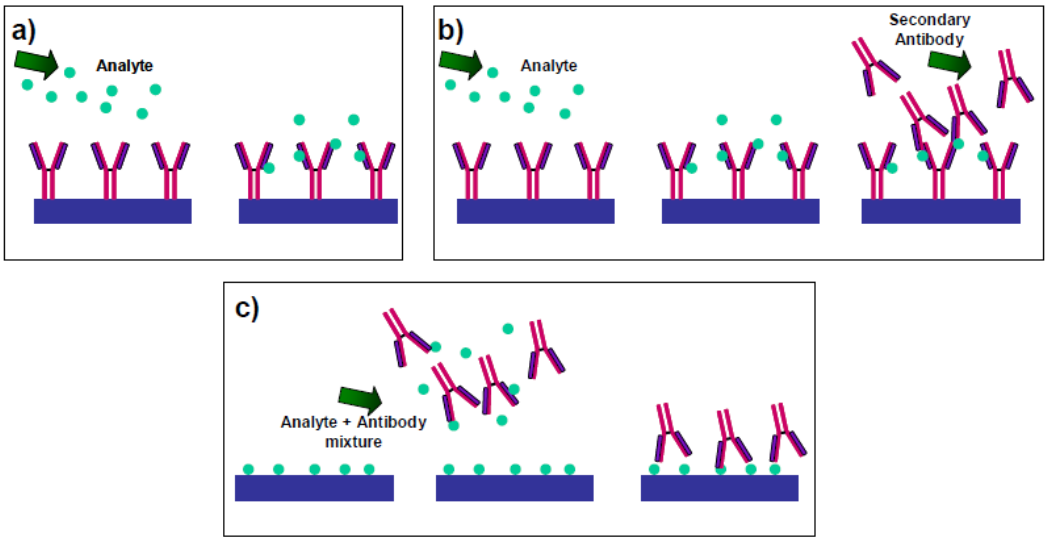

Figure 2.2 Immobilization assays: a) direct detection, b) sandwich assay, c) indirect competitive inhibition assays.

Indirect competitive inhibition assays generally consist of immobilizing a low molecular weight analyte on the sensor surface. The analyte is then mixed with the respective antibody and brought in contact with the sensor surface coated with analyte molecules, so that the unoccupied antibodies can bind to the analyte molecules, see figure 2.2 c. The concentration of the antibody is kept constant so that the response variations are proportional to the amount of the analyte mixed with the antibody.

2.3 Surface functionalization techniques

The physico-chemical properties shown by the surface of a biosensor transducer are a crucial factor to get a tailored binding of biomolecules on the surface. Widely used techniques of surface functionalization are self-assembled monolayers (SAMs) and plasma polymerization (PP).

2.3.1 SAMs

This technique is based on molecules that have the property to self-assemble spontaneously on solid surfaces forming a monolayer with a well-defined chemistry. SAMs are usually prepared by immersing a substrate in a solution containing a ligand that is reactive toward the surface.

There are two main classes of SAMs: alkanethiols ($HS(CH2)_n X$) that are normally deposited on gold or silver surfaces (Love 2005) and organosilanes deposited on silicon or silica (Mrksich 1996). They are made up of a head group that shows a special affinity for the substrate and a tail with a functional group at the terminal end, see figure 2.3. The functionalization of the surface will be determined by the functional group, e.g. oligo or poly(ethylene glycol) (OEG or PEG) chains are generally used in immunoassays, since they are highly hydrophilic and allow to reduce the non-specific adsorption (Lisboa 2007, Siegers 2004, Li 2005). Meanwhile, functional groups such as amine, carboxyl or epoxy groups (Belkin 2009) are used to enhance the protein adsorption, and consequently the cell adhesion.

Figure 2.3 SAMs immobilization.

SAMs provide ultrathin and ordered monolayers of organic molecules, good stability under extreme conditions of pH and temperature, as well as the possibility of regeneration. But some drawbacks such as the non-homogeneous coverage or their oxidation in atmospheric conditions are the limitations of this functionalization technique.

2.3.2 Plasma processes

Plasma processing is an interesting alternative for surface functionalization. It can be classified in 2 different techniques: plasma modification and plasma polymerization. Plasma modification utilizes gases such as Ar, N_2, O_2, NH_3, to modify or introduce surface chemical functionalities or to create radicals for further chemical grafting.

PP consists in the deposition of a conformal thin polymeric film with the possibility to provide a wide range of chemical moieties to the modified surface. The physico-chemical properties of the deposited film are influenced by the operating parameters (i.e. pressure, power, gas flow rate, etc.). The monomer selected determines the functionalization of the surface, e.g. acrylic acid produces carboxylic groups (Detomaso 2005), allylamine produces amine groups (Lejeune 2006), allyl glycidyl ether produces epoxy functionalized surfaces (Thierry 2008), whereas protein and cell resistant surfaces can be fabricated by plasma-deposited poly(ethylene oxide)-like (PEO-like) materials (Brétagnol 2006 b).

The major advantage of plasma polymers is related to the large range of properties that can be obtained, and their relative stability with time and against different solvents. Moreover, these techniques can be easily extended to a large

panel of surface chemistries without constraints in terms of substrates (plastics, glass, elastomers), on the contrary to SAMs for instance. However, the special and expensive equipment needed for their deposition and the change in chemistry produced by the plasma process (no chemical purity) are disadvantages for their application. Furthermore, the chemistry of plasma polymers is complex and depends strongly on the deposition conditions.

2.4 Patterning techniques

Numerous methods for producing micro and nano patterned areas are available. These techniques are usually classified as bottom-up and top-down techniques (Falconet 2006).

Top-down methods start from a bulk material, which after a proper operation is transformed in a material with micro and nanoscale features. These methods are based on lithographic techniques such as photolithography, Scanning Beam Lithography (SBL), Scanning Probe Lithography (SPL) or Soft Lithography (SL) (Gates 2004).

Photolithography (Adams 2010) is based on the exposition of a photosensitive resist to the light through a mask having opaque and transparent parts, for producing the pattern onto the resist.

SBL techniques (Vieu 2000, Wnuk 2011, Romano-Rodríguez 2007, Smith 1993), such as Electron Beam Lithography (EBL), Focused Ion Beam Lithography (FIBL) or X-ray Lithography (XRL), are based on chemical modification of resists or functional layers by scanning a high energy beam of electrons, ions or X-rays. EBL or X-rays depolymerizes or polymerizes the areas exposed from the resist; meanwhile FIBL can deposit or remove material.

SPL techniques (Wouters 2004, Ginger 2004, Xie 2006, Salaita 2007) (e.g., Dip Pen Nanolithography or Chemical Nanolithography) are based on the localized modification of a surface by oxidation or by material transfer using a sharp probe in contact with the surface.

SL technique (Xia 1998, Rogers 2005, Rolland 2004) uses soft organic materials to transfer a pattern on the substrate. A well-known method is microcontact

printing, that uses stamps, usually of polydimethilsiloxane (PDMS) structured at micro or nano-scale, and transfer the patterning by putting in contact the substrate with the stamp previously inked with the substance to transfer.

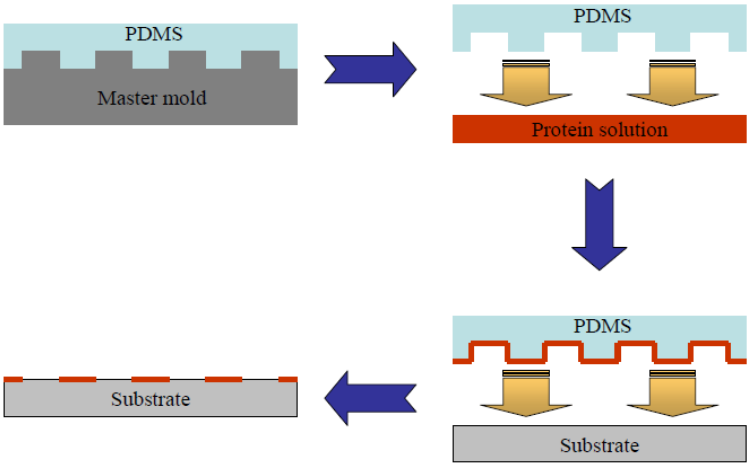

Figure 2.4 Patterning by microcontact printing: PDMS stamp is fabricated by pouring liquid PDMS against a master mold. PDMS is cured and released from the master, then is inked in protein solution to transfer the pattern on the substrate by printing

Bottom-up methods start out from building blocks, i.e. atoms, molecules and colloids that self assemble forming nanostructures on surfaces. Examples of these methods are Colloidal Lithography (CL) (Choi 2004, Yang 2006), Block Copolymers Lithography (BCPL) (Xu 2008, Roman 2003) or mixed Self-Assembled Monolayers (mixed-SAMs) (Th. Wink 1997).

BCPL uses different types of block-copolymers to form contrasted nano-regions. The more soluble block forms a shell around the less soluble block. Using a proper solvent the more soluble block is removed creating a nano-pattern of the second polymer on the surface.

CL is based on the capacity of colloid particles to form a two dimensional monolayer array on a surface. A monolayer of colloidal particles is deposited on the surface and used as mask for etching or sputtering processes.

In mixed SAM assembly, disordered patterns can be produced by mixing two thiols with different terminal groups, in such a way that a thiol with a functional head group is present at a low mole fraction, the surface concentration of one functional

group is reduced by the presence of the second thiol, allowing a minimization of the steric hindrance and non-specific interactions.

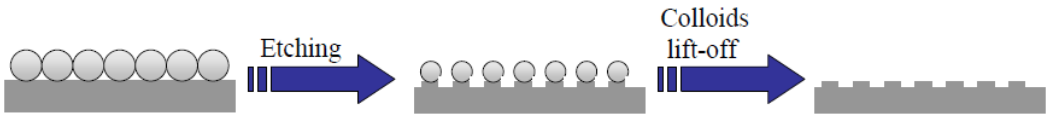

Figure 2.5 Patterning by colloidal lithography: A colloidal monolayer is used as mask for transferring the pattern into the substrate by etching processes

Furthermore, patterning processes can also be divided into parallel and serial techniques. In parallel techniques (e.g. SL or CL), large areas can be patterned by a complete fabrication process. Meanwhile in serial techniques (e.g. EBL or FIBL) the patterning is performed by step-by-step processes, which reduce their writing speed (i.e., the area that can be exposed per unit time).

Indeed, writing speed and resolution (i.e. the size of the smallest pattern feature that can be fabricated) are two important features characterizing the patterning techniques and very often are hard to reconcile, since the methods with very high resolution involve very slow writing speeds.

2.4.1 SEM based lithography: EBL and FIBL

Scanning Beam Lithography techniques as EBL or FIBL allow the fabrication of sub-micron and nanoscale features. These techniques are based on the modification of matter by its exposure to energetic particles, i.e. ions or electrons, generated on a SEM or a FIB system.

The processes generated by the interaction of these particles with the matter depend on factors such as charge, size and mass of the particles (Yao 2005 a, Yao 2005 b). Electrons having a small size pass between individual atoms, penetrating deeply inside the material, meanwhile ions that have higher cross section than electrons have a higher probability of interaction with atoms leading to a smaller range for a given energy.

When a solid material is submitted to ion bombardment several processes such as electronic and nuclear interactions with the treated substrate lead to rapid ion energy loss and ion implantation or sputtering depending on the energy with which

ions strike the surface (Giannuzzi 2005), see figure 2.6. Such processes may produce a direct writing of the material during lithography.

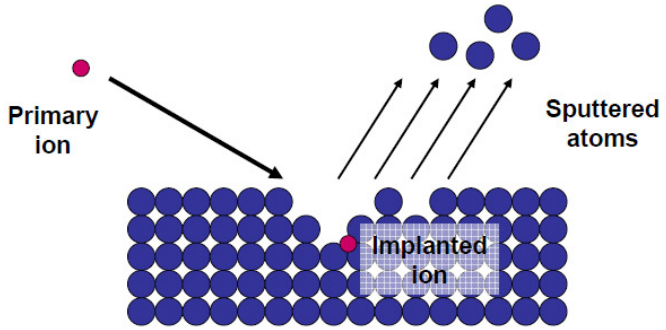

Figure 2.6 Scheme of ion interaction with matter.

Electron beam lithography (EBL) processes are based on the exposition of sensitive resists to the electrons for transferring the pattern. These resists are organic materials, such as polymers, that can be polymerized or, on the contrary, their chemical bonds can be broken after electron exposure. This modification of the resist creates a latent image that is materialized during chemical development. For positive resists, the development eliminates the exposed area, whereas for negative resists, the inverse occurs, see figure 2.7.

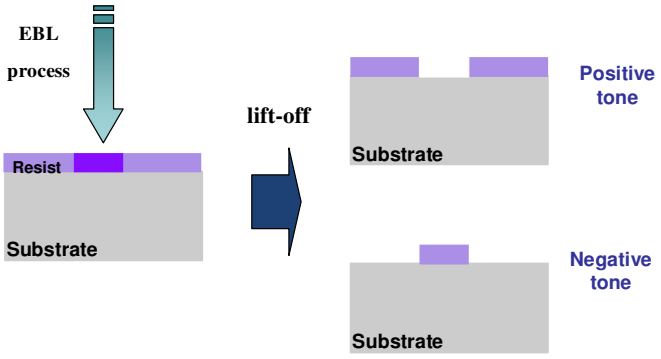

Figure 2.7 Positive and negative resist fabrication scheme.

Electron beam interaction with the resist and the substrate creates forward and backward scattered electrons. Forward scattering is responsible of the broadening

of the initial diameter (small angle scattering). Meanwhile backscattering, a large angle scattering, creates distortions on the designs, due to a low confinement of electrons on the shapes the system writes on. The distortions generated by the backscattered electrons are called proximity effect and depend on the atomic number (Z) of the material and the beam energy used in the process. Figure 2.8 shows the trajectory of electrons after their interaction with a PMMA film (200 nm) deposited on substrates with different atomic number: silicon (figure 2.8 a) and gold (figure 2.8 b). The simulation has been performed with the software CASINO v2.42.

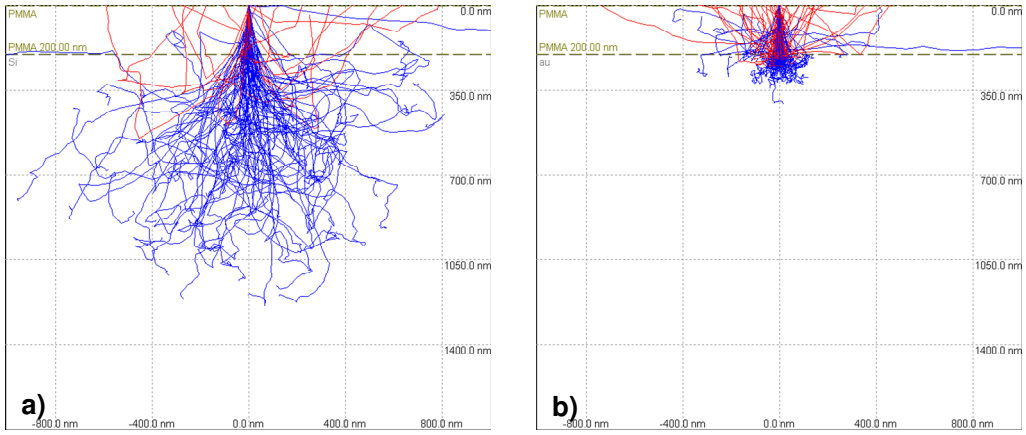

Figure 2.8 Trajectory of electrons in a PMMA film (200nm) deposited on a) silicon (Z=14) and b) gold (Z=79). The simulation is done with the software CASINO v2.42.

2.5 Biosensors: Surface Plasmon Resonance (SPR)

Biosensors are analytical devices based on biomolecular recognition that consist of a biological recognition element and a physical transducer. They can be classified by the transduction method or the biological molecular species they employ (Ferrari 2007). According to the transduction method, they can be classified as electrochemical, mass detection, optical methods, etc… (Gerard 2002). In electrochemical sensors (RüÌdel 1996, Drummond 2003, Katz 2004, Grieshaber 2008), the transduction event takes place by electron or ion transfer that results in the creation of an electrical signal. There are three different modes of operation: *potentiometric* (Bobacka 2003, Bühlmann 1998*)*, where the voltage

can be quantitatively related to the target analyte concentration, *amperometric* (Liu 2008, Trnkova 2008) where the current is related to concentration and *conductometric* (Shvarev 2001, Sergeyeva 1996, Ajay 2007), where the conductive properties of a medium between electrodes are measured. Mass detection methods are usually based on the use of piezoelectric crystals (Marx 2003, Cooper 2007). Applying an electrical signal at a specific frequency, these crystals resonate at a characteristic frequency, which depends on the type and mass of the crystal. Consequently, any material deposited on a quartz surface results in a change in the oscillation frequency related to the modification of the mass.

Optical sensors measure changes of light at material-liquid interfaces (e.g. absorption, reflectance, luminescence, SPR), which depend on optical properties of the interfaces and can be related to the amount of biomolecules immobilized at the interface (de Silva 1997, Homola 1999, Plowman 1999, Fan 2008). Among the optical sensors, SPR is widely used since it is a label-free detection system that provides a high specific detection.

In SPR, a beam of light strikes on a thin metallic film and a detector collects the reflected light. At a certain incident light wavelength and angle, a minimum in the reflectivity is observed. In these precise conditions, the changes in the SPR angle position can be monitored for sensing purposes, see figure 2.9, since these changes are related to changes on the refractive index at the interface. The principles of this phenomenon are presented in more detail in chapter 3.

The main features for SPR biosensing are the sensitivity (S) to refractive index changes, and the efficiency (E), with which the presence of analyte at a concentration C is converted into a change in the refractive index, being the lowest detection limit the lowest concentration of analyte that can be measured by the sensor.

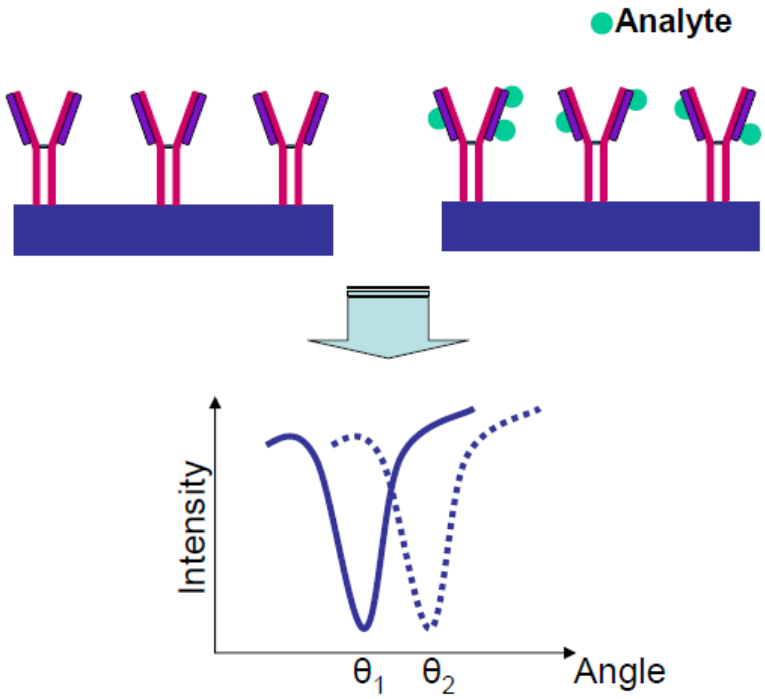

Figure 2.9 Schematic shifts in the resonance angle before (θ1) and after (θ2) a biorecognition assay.

There are a variety of application fields for this technique such as:

• Chemical SPR sensors: based on the measurement of SPR variations due to adsorption or chemical reactions, which causes changes in its optical properties. Examples of chemical applications of SPR include: monitoring detection of aromatic hydrocarbons adsorbing on Teflon film (Podgorsek 1997) or study of the chemisorption of NO_2 on gold has been used for NO_2 on gold (Ashwell 1996).

• Humidity detectors: using humidity-induced refractive index changes in porous thin layers and polymers (Weiss 1996).

• SPR-based temperature sensor: based on the thermooptic effect in hydrogenated amorphous silicon (Chadwick 1993).

• SPR as Affinity biosensors are the most widely employed, where SPR allows real-time analysis of biospecific interactions without the use of labeled biomolecules. The immobilization of the biological receptor takes place at the chemically modified gold surface, which is in contact with a buffer solution. This

immobilization produces a mass increase, and consequently a change in the refractive index in this region.

The shift in the resonance angle acts as a mass detector and allows a real-time monitoring of binding, providing kinetic data on the interaction. These affinity sensors have been used in studies of interactions between antigen-antibody, protein-protein or protein-DNA (Luppa 2001, Scarano 2010, Nelson 2000, Oh 2005).

2.6 Conclusions

A proper functionalization of the surfaces allows a controlled immobilization of biomolecules on them. To achieve such tailored functionalization, materials showing bioadhesive and non-bioadhesive properties are been deposited by SAMs and PP. These techniques allow the functionalization of the surfaces with customized functional groups, and in the case of PP, an added value is that the substrate is not a limiting factor.

Among all the available patterning techniques, EBL is considered one of the more flexible. This technique can produce accurate features with very high resolution at expense of a low speed of fabrication and high cost. The final result depends strongly on a great number of parameters, as the specifications of the SEM, the resist, the developer, the environmental conditions, the exposure parameters and in some cases, the post-exposure bake. In consequence, the final result of EBL will be conditioned by the characteristics of the electron beam, the resist and the chemical developer.

The aim of the present work is to produce patterned surfaces with appropriate physico-chemical properties to enhance or repel the adhesion of biomolecules, all the fabrication processes should preserve the bio-chemical properties of the materials. Even more, the presence of such materials, polymers in most of the cases, influence the lithographic parameters, so the fabrication process has to be adapted to fulfill creation of micro and nano structures showing a chemical contrast.

Chapter 3

Methods and Techniques

In this chapter the different methods, techniques and materials used in this thesis are described. The chapter consist of three parts: Fabrication, Characterization and Materials and a full description of the instruments employed in the work are included on them.

3.1 Fabrication techniques

This section consists of three main parts, plasma processes, lithography and pattern transfer. These techniques were employed for the patterns creation in this work.

3.1.1 Plasma Processes

Plasma processing is a surface engineering technique that can be divided into plasma modification, plasma etching and plasma polymerization. In the following, we will concentrate mainly on etching, sputtering and polymerization.

3.1.1.1 Plasma etching

Plasma etching produces active species that can chemically interact with a material to remove it, i.e. oxygen plasmas can interact with materials made up of hydrocarbons (as photoresists) and form volatile products, as CO_2 and H_2O, which are evacuated by the pumps, thereby removing it.

In this work, plasma etching was performed using an oxygen plasma carried out in a Magnetic Pole Enhanced-Inductive Coupled Plasma (MaPE-ICP). The reactor is based on a stainless plasma chamber with a cylindrical geometry. The water-cooled inductive coil is powered by a 13.56 MHz RF generator via a matching network composed of two driven vacuum capacitors (Advanced Energy RFX II generator 1.25 kW, matching network AZ90). The substrate holder can be biased by a secondary RF supply (Advanced Energy RFX 600) to control the energy of the impinging ions. The distance between the substrate holder and the dielectric window is 8 cm. The gas is injected using a ring tube placed at the top of the chamber. In this set-up, the ionic density, i.e. the ion flux is controlled by the current flowing in the inductive antenna, while the kinetic energy of the ions is controlled by the bias applied to the substrate holder.

3.1.1.2 Physical Sputter Deposition

Physical sputter deposition implies ion bombardment of a target, which results in the ejection of atoms from the target material. These atoms are directly transported to a substrate, where they are deposited.

In this work, gold and titanium were used as target material and the ion bombardment was provided by Ar+ ions. A flow of 100 sccm of Ar was injected into the vacuum chamber (UNIVEX350, oerlikon leybold: 370 mm wide, 500 mm high and 370 mm deep). A DC power supply (Pinnaple, Advanced Energy) was connected to the sputtering target at 45 W. The substrate holder was biased by a RF generator (Gambetti) at 120 V. The distance between the substrate holder and the sputtering target was 10 cm. The working pressure, monitored by a MKS baratron, was kept constant at 50 mTorr during the process.

3.1.1.3 Plasma Polymerization

Plasma Polymerization (PP) is a non-thermal discharge process, in which a monomer (low molecular weight molecules) is ionized and the resulting species are reorganized into high-molecular weight molecules (polymers). The chemical reactions taking place in PP are complex and involve multiple reaction pathways ending up in the formation of a broad range of species. So, the chemical and physical properties of a polymer product of a PP process are different from polymers produced by conventional polymerization processes, even if the monomer used in both processes is the same.

Generally, PP is carried out using a capacitively coupled plasma source. A glow discharge generated by a high frequency electric field is created from a monomer vapour between two parallel plate electrodes.

Operating parameters have an important influence on functionalization as they determine the species produced and the retention of the monomer in the deposited film. An increase in discharge power (W) increases the electron energy and the plasma density up to a certain saturation value. The plasma density increase produces a larger number of collisions between energetic electrons and molecules and subsequently a higher rate of fragmentation and re-arrangement of monomer molecules. This parameter, along with the flow rate (F) and the molecular weight of the monomer (M) were combined by Yasuda, to give the Yasuda factor W/FM (Yasuda 1978).

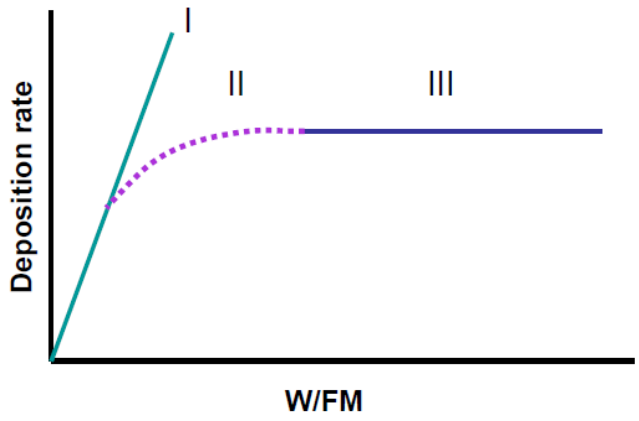

Figure 3.1 Dependence of plasma polymerization regions (I, II & III) on deposition rate and W/FM.

This factor is proportional to the concentration of activated species in the plasma and defines three different regions, see figure 3.1:
For low values of the Yasuda factor (region I) the deposition rate is linearly dependent of F, and for high values the deposition rate becomes independent of F (region III). Between both regions there is a transient region, region II. So, at low values of the Yasuda factor, region called power deficient regime, the power input rate is low and the result is a deposition film with properties very similar to the precursor but very poorly cross-linked. As the Yasuda factor increases, region III also called monomer-deficient region, there is sufficient discharge power but the deposition rate is determined by the monomer feed.

The polymerization process can be carried out by means of continuous (CW) but also with pulsed (PW) discharges. A pulsed discharge plasma is used when there is a need for mild treatment conditions. The pulsed plasma is characterized by the pulse period and the duty cycle. The duty cycle is given as the ratio of the pulse ON time to the total pulse time period, defined as:

$$D = \frac{t_{ON}}{t_{ON} + t_{OFF}} \qquad (3.1)$$

The average power with this method is therefore: $\langle P \rangle = P_{ON} D$ (3.2)
where P_{ON} is the power input during the plasma, also called peak power.

In the case of pulsed plasma, the use of a very low frequency generates a discharge very similar to the continuous discharge, except that the current will reverse every half cycle. In this case, the period is long compared to the time it takes for the plasma particles to come to equilibrium with the electric field. The plasma polymerization process take place during the “ON” period, although also during the “OFF” period a conventional polymerization (such as radical chain propagation) could take place increasing the retention of the functional group of the monomer in the deposited films.
In CW discharge plasmas, the degree of fragmentation of the monomer molecule is higher than with PW plasmas, which leads to a lower retention of functional groups.

In this work, both, continuous and pulsed plasma were used in plasma polymerization processes as described below.

The deposition of Poly Ethylene Oxide films was carried out in pulsed mode (peak power 7W, duty cycle 10% and pulse period 10 ms) in a homemade stainless steel reactor (300 x 300 x 150 mm^3) equipped with two symmetrical parallel plate electrodes (diameter 140 mm, electrode distance 5 cm). A RF generator is connected to the upper electrode, while the other electrode is grounded and used as sample holder. Pure diethylene glycol dimethyl ether (DEGDME) from Sigma Aldrich (CH_3-$OCH_2CH_2)_2O$) mixed with argon (15% DEGDME in Ar) are injected into the chamber by a feeding tube placed at a side of the chamber. Gas and precursor flow rates are controlled by MKS mass flow controllers. The working pressure, monitored by a MKS baratron, is kept constant at 20 mTorr.

Acrylic Acid was plasma deposited in a homemade reactor. The plasma chamber consists in a cylindrical stainless steel jacket (Diameter = 200 mm, Height = 350 mm) in which the sample is placed. The plasma is ignited between two internal stainless steel parallel plate electrodes and sustained by a RF unit operating at 13.56 MHz. The bottom electrode is grounded and acts as a sample holder, while the upper electrode is connected to the RF source. A vapour delivery system is connected to the chamber to vaporise the liquid precursor (Acrylic Acid of > 99% purity from Aldrich Chemical Co). Films were deposited in both methods, pulsed and continuous as described in detail in chapter 4.

3.1.2 Lithography (EBL, FIBL)

An external beam controller (Elphy Quantum, Raith GmbH) connected to a SEM (described in detail in 3.2.5) was used in electron and ion mode for the lithographic fabrication. The controller integrates the beam deflection system and the hardware for design, calibration and control of exposure conditions. The manipulation of the beam, with the coordination between translating substrates and blinking the beam on and off make possible the lithography process.

The procedure of the exposure comprises the following steps:

- design of the pattern with the software (Elphy Quantum) on a GDSII format.
- measurement of the beam current on the faraday cup to establish the exposure conditions.
- optimization of focus and stigmatism on a well known sample as a gold standard sample (formed by small grains of gold of variable size on a carbon structure).
- definition of reference systems for positioning.
- calibration of working field and magnification. With high magnifications the beam deflection with respect to the optical axis is small, which implies the reduction of the working field.
- determination of exposure parameters.
- irradiation.

Lithography processes based on ion beam exposure (FIBL) create the patterning by direct writing on the material, since ions can remove it. However, when the lithographic process is based on electron exposure (EBL), a chemical modification of the exposed material takes place. Generally on EBL, materials sensitive to the electrons, called resists, are used for the patterning creation.

The resists can be classified as positive and negative tone resists (Owen 1985). Positive tone resists are based on the degradation of exposed resist material. The break of backbone bonds causes polymer fragmentation. As a result, patterned features present an increased solubility when immersed in a solvent. Negative resists are based on the cross-linking of the polymer chains due to the beam charges. The consequence is a decrease in the solubility of the patterned areas.

Generally, before exposure, the substrate is raised to a moderate temperature (soft bake) to evaporate any excess of solvent molecules incorporated within the resist layer. This makes the thickness of the coating more uniform.

After exposure, a chemical development materializes the patterning on the resist. The excess of solvent molecules from the development phase is evaporated with a post-exposure bake. In this way, the polymer is also hardened for ulterior fabrication operations.

The resist most widely used in EBL processes is a positive tone resist: Poly(methyl methacrylate), PMMA. PMMA is suitable for defining very small features due to its high resolution (less than 20 nm) and shows minimal swelling during wet development.
The effect of an electron beam on PMMA is the break of carbon carbon-bonds in the polymer backbone.

In this work a positive resist layer of a 950 PMMA (4 % in anysole) was used. The resist was deposited by spin-coating (6000 rpm for 1 min) and baked at 50˚C in the oven (15 minutes). Such spin-coating conditions yield to a 200 nm thick film. Conventional polymeric resists are usually baked at temperatures above 150^{o}. In this work, for the creation of chemical contrast (see chapter 6 and 8) PMMA was deposited on a PEO-like film. To preserve the non-fouling properties of the PEO-like surface a soft baking (at 50^{o}) was carried out. This temperature is the maximum temperature guarantying the preservation of the chemical properties of the PEO films (Brétagnol 2007 a).
The regions of the resist exposed to the e-beam were removed by immersing the samples 30 seconds in a developer solution mixture of methyl isobutyl ketone (MIBK) and isopropyl alcohol (IPA) 1:3 and other 30 seconds on IPA, then they were rinsed with pure water, and dried with nitrogen. Lift-off of the resist was carried out by immersion in acetone, and then the sample was rinsed with pure water and dried with nitrogen.
The writing strategy of the system is based on the vectorial scanning technique, in which the beam is driven along straight lines, see figure 3.2. The determination of the exposure parameters is essential for the right reproduction of the designed features.
The amount of charge per unit area that receives the resist is called dose. The dose is established as the number of incoming electrons that are needed to fully develop the resist thickness. The dose value depends on the resist sensitivity and the development conditions. It is established experimentally. The adjustment of the dose is determined by the beam intensity, the time that the beam remains in each exposure point (dwell time) and the distance between exposure points (step size).

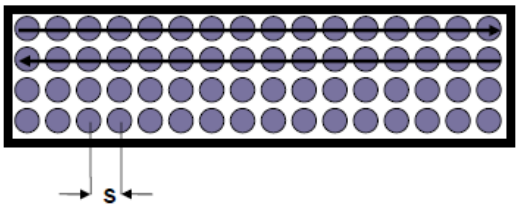

Figure 3.2 Rectangle exposed on vectorial technique with a step size s.

Elphy Quantum software provides alternatives for the exposure mode of lines and dots. With single line exposure mode lines can be defined with “zero” line width and be adjusted by the deflection speed, i.e. small line step size (large dwell time) implies higher delivered dose and in consequence larger line width. Similarly, in dots exposure mode the dwell time allows modulating the size of the resulting dots. Table 3.1 shows the relation between dose, beam intensity, dwell time and step size for the different exposure modes.

Area dose (μCcm^{-2})	Single line dose (pCcm^{-1})	Dot dose (pC)
$D_A = I_{beam} * T_{dwell} / s^2$	$D_A = I_{beam} * T_{dwell} / s$	$D_A = I_{beam} * T_{dwell}$

Table 3.1 Dose determination for area, line and dot exposure mode.

3.1.3 Pattern transfer

Once the pattern has been created on the resist, different methods can be used to transfer the pattern to the substrate (Dupas 2007).

Subtractive Pattern Transfer etching:

The pattern printed in the resist layer is used to etch the sample surface solely in those regions stripped of resist after development. This etching can be divided in wet and dry etching. In wet etching the sample surface is etched chemically by immersing it in a solution containing reactants specific to the substrate but inert

with regard to the material used as a mask. The main disadvantage of this method for producing nanometric patterns is that it acts isotropically. In dry etching the sample is etched by bombarding the surface with high-energy ions in a vacuum environment. Ions can remove the atoms on the surface and the process is highly anisotropic, but it is slow and non-selective.

Additive Pattern Transfer etching:

In this method, a new material is deposited on the openings made in the resist film during lithography. The deposition of the new material is generally done by plasma deposition or sputtering ensuring that the deposit formed above the resist and inside the patterns is discontinuous across the patterns. The resist layer is then simply dissolved in a suitable solvent, leaving only that part of the deposit located at the openings in the resist, i.e., in contact with the sample surface. The removal of the resist is called lift-off process. For a good result, several considerations have to be fulfilled:

- The deposition must be carried out at a temperature under the glass transition temperature of the resist, if not the patterns will be obliterated.

- The thickness of the deposited layer must be less than the thickness of the resist layer, otherwise the patterns may be completely blocked up with deposited material.

3.2 Characterization techniques

3.2.1 Atomic Force Microscopy (AFM)

AFM is a scanning probe microscopy (SPM) technique. In SPM techniques an extremely sharp tip (3-50 nm radius of curvature), located at the free end of a flexible cantilever, scans the surface guided by two piezoelectric crystals (for z and (x, y) displacements). When the tip is brought near the surface, the forces of interaction between the tip and the surface cause the deflection of the cantilever. These deflections are measured by an optical system that is based on a laser, some mirrors and a photodetector, see figure 3.3. The laser beam hits the surface of the cantilever with a certain angle and the beam is reflected into the

photodetector. Variations on the surface change the position of the laser beam on the photodetector.

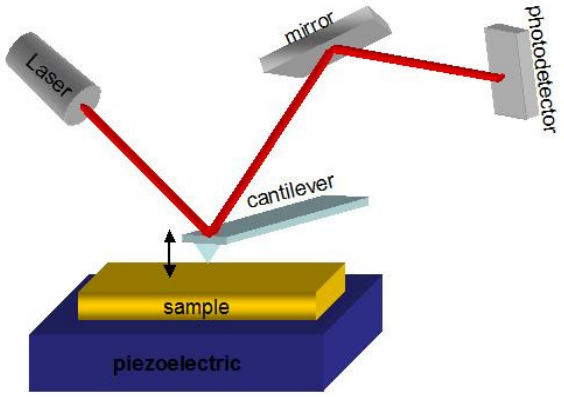

Figure 3.3 Scheme of AFM.

An electronic circuit with a feedback loop matches the signals coming from the photodetector and the piezoelectric crystal guiding the sample and allowing the system to work at a constant oscillation amplitude or frequency by adjusting the average tip-to-sample distance (intermittent contact mode).

Measuring the signal provided by the feedback loop to maintain constant the tip-to-sample distance at each (x,y) allows the scanning software to construct a topographic image of the sample surface, since the signal is proportional to the scanner vertical displacement.

AFM experiments were performed in intermittent contact mode with a “Solver” instrument equipped with a “Smena” head (NT-MDT solver, Moscow, Russia). The cantilever used to probe the surfaces was a standard silicon cantilever (NT-MDT v_{res}=150-300 KHz) equipped with a tip characterised by a 10 nm curvature radius and a cone angle of 22^{o}. The images analysis have been processed by the Nova RC1 software from NT-MDT solver.

3.2.2 Contact Angle

Contact Angle, θ, provides basic information about the wettability of the surfaces. The contact angle between a liquid (L), and a solid (S) in the gaseous medium (G) is defined as the tangent at the drop profile with respect to the surface plane, see figure 3.4. At equilibrium, the free energy in the three phases should be equal. We denote the solid-vapour interfacial energy as γ_{SG}, the solid-liquid interfacial energy as γ_{SL} and the liquid-vapour energy (i.e. the surface tension) as γ_{LG}. At the equilibrium the vectorial sum of the three components have to be zero (Young Equation):

$$\gamma_{LG}\cos\theta + \gamma_{SL} - \gamma_{SG} = 0 \qquad (3.3)$$

where θ is the equilibrium contact angle.

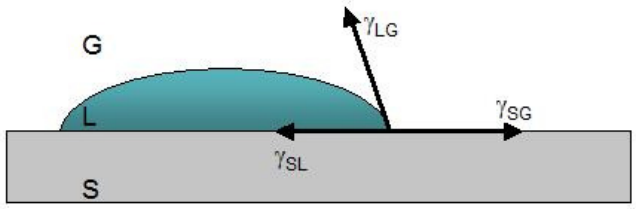

Figure 3.4 Scheme of the contact angle.

If the liquid drop spreads on the surface, low values of θ are obtained indicating a good wetting (hydrophilicity). On the opposite, no spreading of the drop reflects a poor wetting (hydrophobicity) and is indicated by high values of θ. When θ ranges from 0° to 30° the surface is called highly hydrophilic, up to 90° hydrophilic and if θ is larger than 90° hydrophobic.

The experiments were carried out spreading 3 µl of water on the surface. Images of the droplet profile at the surface were analyzed with the software provided by the contact angle meter, a Digidrop GBX goniometer (France). Five measurements were acquired and then averaged to obtain the advancing contact angle. Then after sucking of 1 µl from the droplet into the syringe the image of the droplet profile was analyzed. Five measurements were also acquired and then averaged to obtain the receding contact angle.

3.2.3 Ellipsometry

Ellipsometry measures the change in the polarization state of the light reflected from the surface of a sample.

Light with a known polarization arrives to the sample surface and becomes elliptically polarized when it is reflected. The amount of light that passes through a continuously rotating polarizer depends on the polarizer orientation relative to the electric field "ellipse" coming from the sample. The detector converts light to electronic signal to determine the reflected polarization. This information is compared to the known input polarization to determine the polarization change caused by the sample reflection. This is the ellipsometry measurement of the amplitude ratio, Ψ, and the phase difference, Δ.

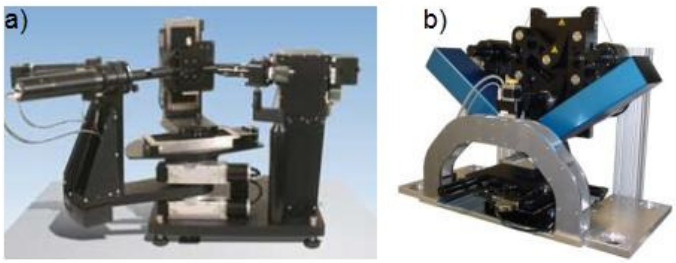

Figure 3.5 *Image of a) VASE ellipsometer, b) EP3 ellipsometer*

The measured response depends on the optical properties and thickness of the sample. Both properties can be obtained by fitting the experimental data with the software of the ellipsometer system. In our case the model has been fitted using the Cauchy relationship:

$$n(\lambda) = A + \frac{B}{\lambda^2} + \frac{C}{\lambda^4} \qquad (3.4)$$

Ellipsometry measurements were carried out with two different ellipsometers, see figure 3.5.

Variable Angle Spectroscopic Ellipsometer (VASE) from J. A. Woollam Co., Inc., model M2000V™ was used for non-structured surfaces. The measurements were performed in air at room temperature in the wavelength range 400 - 1100 nm, by steps of 10 nm, for three different angles of incidence: 55°, 65° and 75°. The resulting data were fitted using the VASE software.

Patterned surfaces were analyzed with a variable angle multi-wavelength imaging ellipsometer, model EP3 by Nanofilm Surface Analysis GmbH. The measurements were performed in air at room temperature and at a fixed wavelength of λ = 532nm. The angle of incidence was varied between 45° and 55°, with a step-width of 0.5° (20 measurements for each run). The resulting data were then fitted using the EP4 software.

3.2.4 Fourier Transform Infra-Red Spectroscopy (FTIR)

FTIR is an infra-red spectroscopy that guides the light modified by a target sample through an interferometer producing an interferogram, which contains all the sample characteristic infrared frequencies into it. By performing a Fourier transformation of the signal a conventional infrared spectrum is obtained. The resulting spectrum represents the IR absorption as a function of the wavelengths. As every absorption band corresponds to a characteristic frequency of vibration between the bonds of the atoms, the chemical groups present in the sample can be obtained. In addition, the intensity of the bands in the spectrum is a direct indication of the amount of material present.

Figure 3.6 Image Bruker Vector 22 FT-IR Spectrometer

The infra-red spectra were obtained using a Bruker Vector 22 FT-IR Spectrometer, see figure 3.6. The FTIR spectra were acquired in absorbance mode with 4 cm^{-1} of resolution in the region 600 - 3800 cm^{-1}. Before analysis, the baseline was subtracted from each spectrum. Experimental data were analyzed with OPUS software.

3.2.5 Scanning Electron Microscopy (SEM)

Scanning electron microscopy is characterized by rastering a sample with a focused beam of high-energy electrons to generate an image. The image is formed by collecting some signal from the beam-sample interaction. The signals include secondary (SE) and backscattered (BSE) electrons, which generate topographical and compositional images, respectively.

In this work, we used a FEI® Nova™ NanoLab™ 600i DualBeam™ equipped with two different sources, electronic and ionic, see figure 3.7. The sources are placed in two independent columns but the control system is common for both of them. Electrons are generated by a Schottky thermal field emitter (Sirion type). This is thermally assisted emission sources that consist in a filament heated by means of a current from which electrons are extracted by both thermal excitation and the application of an electric field, high enough to enable electrons to cross the surface potential barrier. Such combination provides a high stability, low noise, and low-cost operation.

Ions are generated by a liquid Gallium ion emitter operating with a Sidewinder™ field emission focused ion beam optics. On the ion emitter, the gallium is placed in contact with a tungsten needle and heated to the liquid state. The liquid gallium wets the needle and by application of a high electric field the gallium is ionized. These ions are accelerated with voltages varying between 5 kV and 30 kV.
Once the beam is formed, electric and magnetic focusing lenses and a deflecting system are responsible of guiding the beam on the substrate. Lenses force the beam to converge in some point of the optical axis and the deflection system deviates the beam through the sample surface. The complete process takes place

in high vacuum, hence two vacuum levels are differentiated, one for the source column and another one for the working chamber.

Figure 3.7 Image of FEI® Nova™ NanoLab™ 600i DualBeam™

The rest of the elements that constitutes the column are the apertures, astigmators and the beam blanker. The function of the apertures is limiting the beam by controlling the amount of current on the sample. The astigmator consists of a serial of poles (four or eight) that surround the optical axis system and is responsible of correcting the shape of the beam in order to make it circular. The beam blanker applies a potential to the beam that deflects it far from the column axis.

3.2.6 Surface Plasmon Resonance imaging (SPRi)

SPR is a phenomenon occurring at metal surfaces when an incident light beam strikes the surface at a particular angle for a given wavelength. The metal must have conduction band electrons capable of resonating with light at a suitable wavelength. Among the candidate metals (i.e. silver, gold, copper, titanium, chromium,…) gold is the most widely used since it produces a strong SPR signal in the near infrared region and is resistant to oxidation and atmospheric contamination. For SPR generation, a circa 45 nm thick layer of gold is usually deposited on a high refractive index support.

In the Au layer, the electrons are weakly bound and can move creating a collective oscillation with respect to the lattice. These oscillations produce longitudinal waves that describe a damped movement with a frequency ω_p, and their quantization, $\hbar\omega_p$, is called plasmon.

When these oscillations take place at the interface between a metal and a dielectric, they are called surface plasmons (Barnes 2003, Homola 1999).

Under certain conditions of total internal reflectance (TIR), the surface plasmons are excited in a resonance mode. That occurs when a thin conducting film of gold is placed at the interface between two optical media with different refractive index (n1>n2), see figure 3.8.

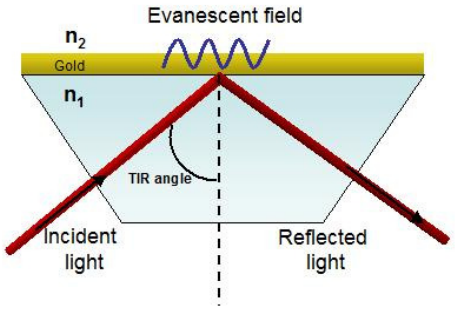

Figure 3.8 TIR conditions in SPR.

At a specific incident angle, greater than the TIR angle, the surface plasmons in the conducting film resonantly couple with the light due to the matching of respective frequencies. At this condition, the energy carried by photons is transferred to the plasmon. That occurs only if the energy and momentum of the photons and plasmons are exactly equal. Since energy is absorbed in this resonance, the reflected intensity drops at the angle where SPR is occurring.

The oscillation of the plasmons generates an electrical field that decays in the direction perpendicular to the metal–dielectric interface. The field typically extends about 100 nanometers perpendicularly above and below the metal surface.

For a given wavelength, the interaction between the electrical field of the plasmon and the material interface within the field determines the resonance conditions. So, any change at the interface results in a change of the resonance conditions i.e., a change of the angle at which the SPR occurs, see figure 3.9.

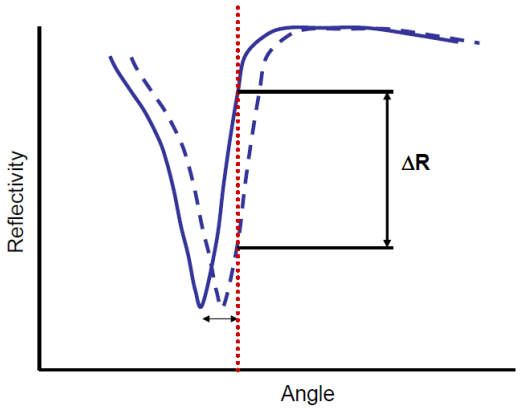

Figure 3.9 Change of the SPR angle monitored by the SPR system

As the momentum of the photons (k_{in}) is always smaller than the momentum of the surface plasmon (k_{SP}), three different configurations of SPR devices have been developed, prisms, gratings and optical waveguides. These allow increasing the momentum of the photons and fulfilling the resonance criterion:

$$k_{in} = k_{SP} \qquad (3.5)$$

This condition can be expressed as a function of the dielectric properties of both media, metal and dielectric as follows:

$$\frac{2\pi}{\lambda} n \sin\theta = \frac{\omega}{c}\left(\frac{\varepsilon_m \varepsilon_d}{\varepsilon_m + \varepsilon_d}\right)^{1/2} \qquad (3.6)$$

where λ is the wavelength of the incident light, θ is the angle of incidence, ω is the angular frequency, c is the propagation velocity in vacuum, and ε_m and ε_d the dielectric constant of metal and dielectric, respectively.

In the prism coupling technique, an incident beam passes through a high-density medium (such as a glass prism) and is totally reflected at the prism–metal layer interface. This method is called attenuated total reflection (ATR) coupler. The wave vector is modified by varying the phase velocity:

$$k_{in} = \frac{2\pi}{\lambda}\sqrt{\varepsilon_p}\sin\theta = k_{sp} + \Delta k \qquad (3.7)$$

where ε_p is the dielectric constant of the prism material .

Since the refractive index value of glass is greater than unity, the value of the wave vector k_{in} can be increased to match k_{sp}. In this way, there is a contribution (Δk) to the propagation constant due to the presence of the prism.

The resonance condition is described by the equations

$$\frac{2\pi}{\lambda}\sqrt{\varepsilon_p}\sin\theta_{SPR} = \frac{\omega}{c}\left(\frac{\varepsilon_1\varepsilon_2}{\varepsilon_1+\varepsilon_2}\right)^{1/2} \qquad (3.8)$$

where θ_{SPR} is the SPR resonance angle.

Thus, for each wavelength there is a single angle of incidence that matches the momentum of the surface plasmon.

To get the attenuated total reflection, two different configurations can be used: Kretschmann and Otto configurations, see figure 3.10.

In the Kretschmann configuration a very thin metal film is positioned against a prism, in this configuration the wave penetrates trough the metal and couples, at the outer boundary, with a surface plasmon. In the Otto configuration the metal surface is very close to the prism but not in contact. With an appropriated separation (typically few microns) the wave couples with a surface plasmon at the dielectric-metal interface.

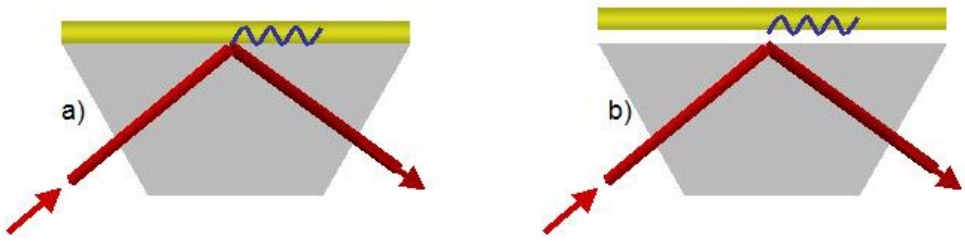

Figure 3.10 a) Excitation by Kretschmann configuration, b) Excitation by Otto configuration

The SPR measurements were performed with SPRi-PLEX+ instrument (GenOptics, Paris, France), which is equipped with a 12-bit charge-coupled-device (CCD) camera.

The samples for SPR analysis were purchased from Horiba (SPRi-Biochips™) or were fabricated on lab as follows: a coupling prism with a metallic film deposited on the top (5nm of Ti followed by 45nm of Au). Such coupling prisms allow

achieving the plasmon resonance with the Kretschmann configuration using an incident-light beam with a fixed wavelength of 810 nm.

In SPR measurements, the different areas of interest were selected using a CCD image, in this step, both position and size of the different areas of interest are determined. Then, the angle of the incident light beam with the sample surface was varied 10^0 (from 53^0 to 63^0 with a step of 0.3^0) and the plasmon curves from each area of interest were obtained. The working angle was then determined as the maximum of the first derivative of the reflectance as a function of the angle of incidence. The working temperature was fixed at 25^0 and the protein solutions were injected by an automated injector (Agilent ChemiLab). The protein immobilization was monitored from each area of interest by plotting the reflectivity changes versus time (sensorgram) at the working angle previously selected. By other side, the CCD camera takes images of the interface during the experiment, which allows monitoring variations in the reflected light at a fixed angle. The software of the system allows getting the difference image before and after the immobilization of the molecules on the interface. The difference image taken before protein injection is a complete black image, as can be seen in figure 3.11 a. In this way, every change in brightness obtained in the difference image taken after the protein injection is due to the immobilization of proteins on the surface, since the difference image after protein injection is the result of subtracting this complete black image from the new images obtained by the CCD camera an example is illustrated in figure 3.11 b. The brightness of the difference image was analyzed by the ImageJ software.

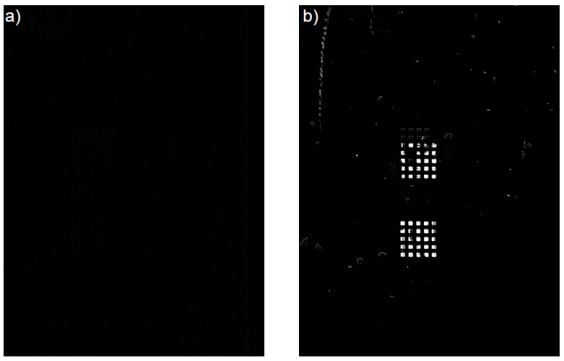

Figure 3.11 Difference image a) before and b) after injection of proteins.

3.2.7 Time-of-flight secondary ion mass spectroscopy (ToF-SIMS)

ToF-SIMS uses a pulsed ion beam to remove atoms and fragments from a sample surface. The atoms and fragments are ionized and accelerated into a mass spectrometer, where their mass is determined by measuring the exact time-of-flight from the sample surface to the detector. The particles travel through the ToF analyzer with different velocities, depending on their mass to charge ratio ($ke=½mv^2$).

Three operational modes are available using ToF-SIMS: surface spectroscopy for characterization of chemical composition, surface imaging for determining the distribution of chemical species and depth profiling for thin film characterization.

In the spectroscopy and imaging modes, only the outermost (1 - 2) atomic layers of the sample are analyzed. In the spectroscopy mode a full mass spectrum is obtained for each primary ion pulse. The chemical images are generated by collecting a mass spectrum at every pixel as the primary ion beam is rastered across the sample surface. For depth profiling an ion gun operating in DC mode removes material, and the same ion gun or a second ion gun is used in pulsed mode for the phase acquisition.

In this work, experiments have been performed with a ToF-SIMS IV (ION-ToF, primary 25 keV cluster Bi metal ion gun) operating either in high current surface spectroscopy mode (mass resolution ($m/\Delta m$) > 8000, lateral resolution < 7 µm) or imaging mode (lateral resolution of ~300 nm). In order to ensure static SIMS conditions total ion flux was maintained below 10^{13} cm^{-2}.

3.2.8 X-ray Photoelectron Spectroscopy (XPS)

XPS is a quantitative surface spectroscopic technique based on the photoelectric effect that allows the determination of the elemental composition of the materials present on a surface. When a material is irradiated with X-rays a photoelectron is emitted with a kinetic energy given by:

$$KE = h\nu - BE \qquad (3.9)$$

where BE is the binding energy of an electron emitted and KE is the kinetic energy of the emitted photoelectron and hν is the energy of the X-rays. By measuring KE it is possible to evaluate BE, thus obtaining information on the different elements present on the sample surface, whilst the atomic concentration of the elements can be obtained from the photoelectron peak intensities. Since the typical depth analyzed by XPS is around 10 nm, it gives information about the chemical composition on the outer layers of the surface.

XPS measurements have been performed with an AXIS ULTRA spectrometer (KRATOS Analytical, UK) equipped with a monochromatic Al Kα source (hν = 1486.6 eV). The analyses were performed at 90º take off angle (respect to the sample surface) and with a spot size of 400 μm x 700 μm on homogeneous surfaces and 27 μm in diameter on patterned samples.

Surface charging was compensated by means of a filament (1.9 A, 3.6 V) inserted in a magnetic lens system and all spectra were corrected by setting the C1s hydrocarbon component to 285.00 eV. For each sample, a survey spectrum (0 – 1150 eV), from which the surface chemical compositions (at.%) were determined, was recorded at pass energy of 160 eV. Sample compositions were obtained from the survey spectra after linear background subtraction and using the RSF (Relative Sensitivity Factors) included in the software derived from Scofield cross-sections. In addition one set of high-resolution spectra (PE = 20 eV) was also recorded on each sample. The data were processed using the Vision2 software (Kratos, UK) and Casa-XPSv2.3.15, (Casa software, UK). The core level envelopes were fitted with Gaussian–Lorentian function (G/L = 30) and variable full width half maximum.

3.2.9 X-ray photoemission electron microscopy (X-PEEM) at the Advanced Light Source in Berkeley, California

X-PEEM is a full field imaging technique based on the illumination of the sample with tunable synchrotron X-rays. Photoelectron and secondary electrons emitted by the X-ray irradiation are accelerated into an electrostatic imaging column, where the spatial distribution is magnified and detected by a CCD camera.

The X-PEEM measurements were carried out at the Advanced Light Source (ALS) on beamline 7.3.1 using right circularly polarized light (70 – 80 %). Photoelectron and secondary electrons ejected by absorption of monochromatic X-rays are accelerated into an electrostatic imaging column, where the spatial distribution is magnified and detected by a CCD camera.
A 100 nm-thick Ti foil was used to eliminate second-order light while radiation damage was minimized by using a fast shutter (0.1 s). The field of view was about 30 µm. C 1s stacks were obtained with photon energy ranging from 282 to 292 eV, with an energy resolution of 0.45 eV. Quantitative chemical mapping analyses were completed with the aXis 2000 software package, using the singular value decomposition (SVD) method. SVD is a matrix method optimized for highly over-determined data sets and produces results equivalent to least square analysis.
The beamline 7.3.1 used in these experiments can achieve a spatial resolution down to 30 nm, which allows to carry out measurements on micro and nano patterned areas.

3.2.10 ζ-potential

When a solid surface is placed into a liquid can acquire an electric surface charge that depends on its chemical properties and on the chemistry of the liquid in which it is immersed. In such situation, a double layer structure is generated. This double layer comprises a first layer (Stern layer), formed by ions adsorbed directly on the surface and a second layer (diffuse layer) composed of ions attracted to the surface charge via the coulomb force and electrically compensating the first layer. The potential at the plane of shear between surface and solution (where there is relative motion between them) is the zeta potential (Elimelech 1994).
The ζ-potential measurements in this work were performed using the streaming potential technique. This technique is based on the generation of a potential difference by the flow of a liquid over the sample surface under a pressure gradient, resulting in an electrolyte current.
In this work ζ-potential measurements were performed by using an electrokinetic analyzer (EKA), model EKS100 (Anton Paar KG, Graz, Austria) see figure 3.11. The streaming potential and the pressure drop between the electrolyte in- and

outlet were measured in order to obtain the ζ-potentials. The EKA determines dU_{Sr}/dp from the gradient of a plot of potential against increasing pressure difference.

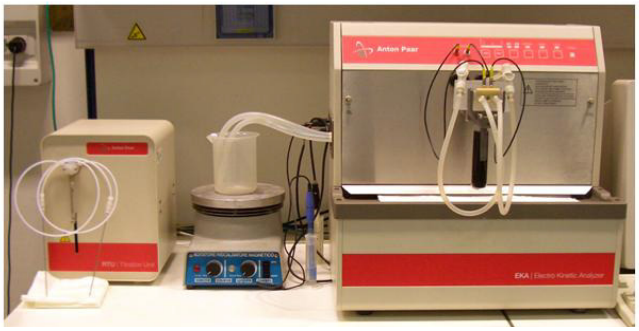

Figure 3.11 Electrokinetic analyzer (EKA), model EKS100.

For the measurements, the treated side of the sample is pressed against a PMMA spacer, which contains a row of seven parallel rectangular channels. The depth of the channels is much smaller than their width and a pressure drop is generated in the measuring cell that is dependent on the flow resistance and is detected by a differential pressure sensor. The values required for the calculation of the ζ-potential, such as pH, conductivity and temperature are measured by external electrodes and a temperature sensor. Moreover, the control and evaluation software "VisioLab for EKA" contains a temperature correction table for water, which is necessary to obtain the corresponding viscosity and dielectric constant for the actual temperature during measurements. The values for water can be used since the electrolyte solutions are diluted.

Furthermore, the software makes use of the Fairbrother-Mastin approach, which is based on the Smoluchowski equation

$$\zeta = \frac{dU_{Sr}}{dp} \cdot \frac{\eta}{\varepsilon \cdot \varepsilon_0} \cdot \frac{L}{Q \cdot R} \qquad (3.10)$$

where η is the liquid viscosity, ε is the liquid permittivity, ε_o is the permittivity in vacuum, R is the electrical resistance across the medium, and L and Q are the length and cross-sectional area of the channel, respectively.

As very diluted electrolyte solutions are used, the term *L/QR* is substituted by κ, the conductivity of the electrolyte solution:

$$\frac{L}{Q \cdot R} = \kappa \qquad (3.11)$$

As the sample is in contact with an insert made of PMMA, the measured ζ-potential is derived half from the sample and half from the PMMA. The ζ-potential of the sample can thus be calculated according to:

$$\zeta_s = 2 \cdot \zeta_m - \zeta_{PMMA} \qquad (3.12)$$

where ζ_s is the ζ-potential of the sample, ζ_m is the measured ζ-potential and ζ_{PMMA} is the ζ-potential derived from the PMMA insert.

3.3 Materials

3.3.1 Substrates

Silicon wafers (Resistivity: < 20 Ωcm, Thickness = 150 µm, Orientation (100)) were used for the XPS analysis, meanwhile both sides polished silicon wafers (Resistivity: < 100 Ωcm, Thickness = 3000 µm, Orientation (100)) were used for FTIR measurements.

SPRi-Biochips™ and SPRi-Slides™ were purchased from Horiba for SPRi experiments. Both, chips and slides are coated with a gold thin film. Prisms are made of a high refractive index glass prism.

Indium-tin oxide (ITO) coated glass substrates were used for cells seeding.

3.3.2 Biomolecules

The proteins used in this work are the followings:

Human Serum Albumin (HSA), Bovine Serum Albumin (BSA), Immunoglobulin G (IgG), Fibronectin (Fb), Transthyretin (TTR), Ubiquitin (Ubq), and Maltose Binding Protein (MBP).

- Albumin is a plasma protein essential for maintaining the osmotic pressure needed for proper distribution of body fluids. It acts as a plasma carrier and as transport protein for fatty acids, metabolites and drugs.
- Fb is involved in cell adhesion, growth, migration and differentiation, plays a crucial role in wound healing and is necessary for embryogenesis.

- IgG is involved in the immunologic response.
- TTR is a carrier of the thyroid hormone and retinol
- Ubq recycles unneeded proteins and it is involved in activation of protein kinases, and in signaling.
- Finally, MBP, a soluble periplasmic protein, is involved in the high-affinity maltose membrane transport system malEFGK (initial receptor for the active transport of and chemotaxis toward maltooligosaccharides).

The main properties of these proteins are summarized in table 3.2.

	Molecular weight (KDa)	Isoelectric point (pH)	Charge at pH 7.5 (mV)
HSA	69	5.8	-13.1
IgG	56	5.7	-7.9
BSA	69	5.9	-15.1
Fb	262	5.7	-57.7
Ubq	11	5.5	-5
MBP	40	5.3	-8.1
TTR	60	5.7	-5

Table 3.2 Main properties of proteins used in this work

Antibodies used for antibody-antigen recognition experiments are summarized in table 3.3.

	Molecular weight (kDa)	Isoelectric point (pH)	Charge at pH 7.5 (mV)
Ab-HSA	150	5.7	-7.9
Ab-IgG	150	5.7	-7.9
Anti-MBP	150	5.7	-7.9

Table 3.3 Main properties of antibodies used in this work

The properties of the thiols used for functionalization of the surfaces are summarized in table 3.4.

	Molecular weight (kDa)
1-Thio-β-D-glucose sodium salt	0.22
PEO-thiol	4

Table 3.4 Thiols used in this work.

Chemisorption of thiols on gold surface was performed as follows:
samples were covered with a solution of thio-glucose (1-Thio-β-D-glucose sodium salt) diluted in H_2O at a concentration of 1mM (overnight at 4 degrees on dark). Then, the surface was rinsed with H_2O and dried with nitrogen.
The chemisorption of the PEO-thiols was carried out by immersion of the samples in the thiol solution (5 mM in ethanol) in the dark during 12 hours. After the chemisorption process, the samples were cleaned with ethanol in ultrasounds during 10 minutes and rinsed with ultra pure water.

Proteins were diluted in buffer at different concentration. The buffers used in this work were: Phosphate buffered saline (PBS) (pH 7.4) and acetate (pH 4).
Images of the proteins present in this work have been obtained from the protein data bank (PDB) and processed with the Discover Studio Visualizer software.

3.3.2 Cells

The cells used in this work were Human Umbilical Cord Blood Neural Stem Cells (HUCB-NSC). Cells from this cell line have the ability to grow without transformation process, moreover, during standard culturing conditions HUCB-NSC abide expression of pluripotency markers (*Oct4, Sox2,* and *Nanog*) and

demonstrate potential to differentiate into the various neuronal cell types (Buzanska 2010, Jurga 2009).

The experiments were performed seeding the HUCB-NSC cells in a serum containing medium at $5*10^4$ cell/cm^2 cell density in a 3 cm diameter Petri dish containing the patterned sample. After 1 day of incubation at 37°C, at 5% CO_2, floating cells were removed by washing with PBS.

Chapter 4

Deposition and Characterization of ppAA

Plasma polymerization is a reliable technique used for deposition of polymer thin films with tailored properties. The monomer and the operating parameters are factors that control the physico-chemical properties of the film.

In this work, plasma polymers from acrylic acid (ppAA) have been deposited in order to produce bioadhesive films with carboxylic functionalities. Since the bioadhesive character of the ppAA films depends on the retention of carboxylic groups, a complete characterization has been carried out in order to optimize the deposition conditions. For that purpose, two different deposition methods, continuous and pulsed mode, were carried out and the samples were characterized by means of XPS and FTIR. Additional analyses were performed by ellipsometry, contact angle and ζ-potential.

4.1 Effect of the power applied on the carboxylic retention

The effect of the power applied on the deposition process was analyzed by means of XPS and FTIR. During the deposition process, the precursor was heated at $40^{O}C$ and the pressure before ignition of the plasma was set at 4.1×10^{-2} Torr at a precursor flow rate of 2 sccm. Two different deposition methods, continuous and pulsed mode, were used, whilst the deposition time was five minutes for samples analyzed with XPS and ten minutes for samples analyzed with FTIR.

For guidance in the XPS analysis, the C1s XPS peak was fitted with four distinct components. These components were, respectively, attributed to C0 at 285.0 eV (corresponding to C- C and/or C- H moieties), C1 at 286.5 eV (corresponding to C-OH and/or C-O-C moieties), C2 at 287.5 eV (corresponding to –C=O/O-C-O moieties) and a fourth component, C3, at 289.2 eV (corresponding to O-C=O moieties). In particular, the component at about 289.2 eV, was studied to determine the evolution of the COOH moieties (Kelly 2003). Finally, a component C beta at 285.6 eV (corresponding to the C-COOH/R) having the same intensity as C3 component was also added to account for the carbon bonded to the COOH/R moieties.

The FTIR spectra from the ppAA films deposited in this work are in agreement with typical FTIR spectrum of poly acrylic acid films (Sato 2006, Moharram 2002) and related works of plasma deposited acrylic acid films (Rossini 2003, Lejeune 2005, Cho 1990, Jafari 2006). The spectra obtained present the bands relative to the stretching vibration bands of C=O around 1700 cm^{-1}, C-H around 2930 cm^{-1} and C-O around 1170 cm^{-1}. The intensity of C=O is correlated with the carboxylic retention in the film.

As the intensity of the bands depends on the thickness of the deposited film, the acrylic acid retention at each temperature was measured by the ratio of C=O/C-H, in order to evaluate the carboxylic retention without any influence of small variations on the thickness of the deposited films.

4.1.1 Continuous mode

A series of samples were deposited varying the power from 5 to 25 W, in steps of 5 W. FTIR and XPS analyses were carried out on samples as deposited and after 5 minutes of sonication in ultra pure water in order to evaluate the effects of possible partial solubility of the films.

The evolution of the C=O/C-H ratio from FTIR and the COOH % (component C3 of C1s peak) determined by XPS showed the same trend, see figure 4.1: a higher carboxylic retention when a low plasma power was applied. Furthermore, on samples sonicated in ultra pure water (5 minutes) a high stability at the different powers applied was observed. The highest retention of COOH moieties was

reached at 5 W, but in such conditions some samples showed poor polymer adhesion to the substrate, and part of the deposited film was removed.

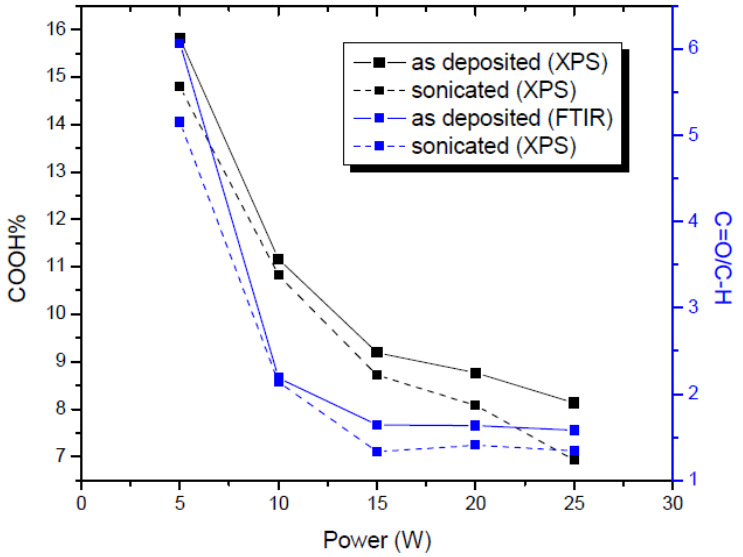

Figure 4.1 C=O/C-H ratio of FTIR (blue) and COOH% of XPS spectrum (black) as a function of the power applied as deposited (solid line) and after 5 minutes of sonication in ultra pure water (dash line).

To guarantee the adhesion, preserve the stability in water and achieve a good retention of carboxylic groups (around 11 % after 5 minutes of sonication in ultra pure water), the power applied on the deposition of ppAA was set at 10 W. At these conditions COOH % peak from XPS (see figure 4.2) and C=O/C-H ratio from FTIR (see figure 4.3) show that the film does not dissolve in water and loose very few functional groups (around 2.5 %). In table 4.1 the values of the C1s peak components are shown for ppAA films as deposited and after 5 minutes of sonication in ultra pure water.

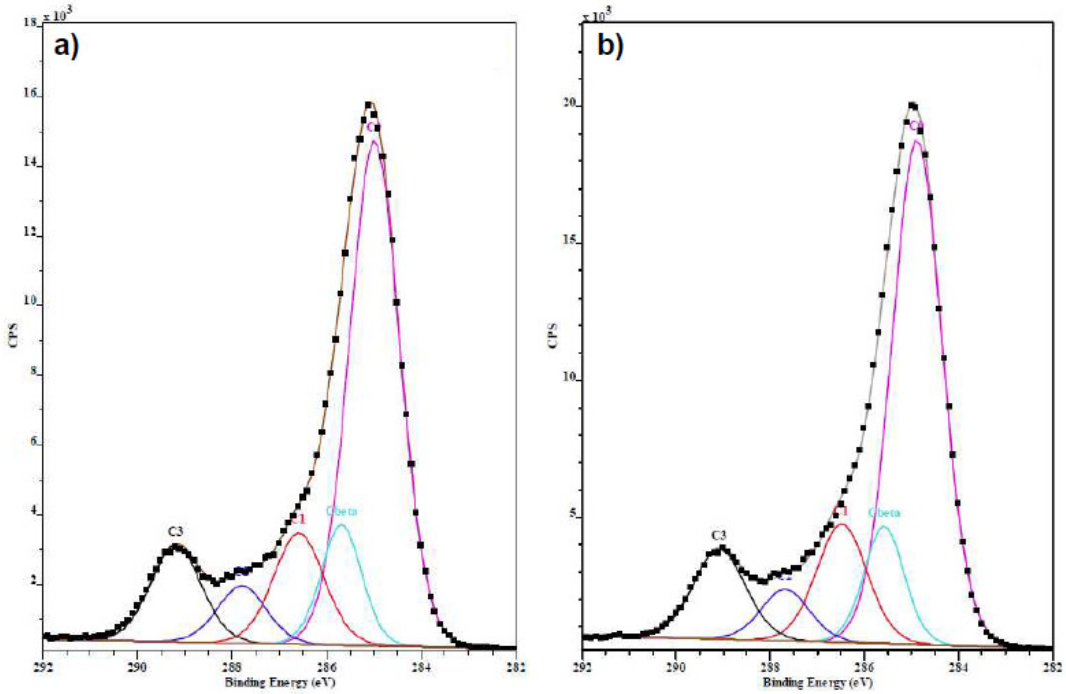

Figure 4.2 C1s core level spectra of ppAA films deposited at 10 W in continuous mode a) before, b) after 5 minutes of sonication in ultra pure water.

	As deposited				After 5 minutes sonication in water		
Name	**Pos.**	**FWHM**	**% Area**		**Pos.**	**FWHM**	**% Area**
C0	284.99	1.250	58.40		284.88	1.250	58.64
C1	285.69	1.000	11.17		285.58	1.000	10.89
C2	286.59	1.250	12.87		286.48	1.250	13.79
C3	287.79	1.200	6.40		287.68	1.200	5.81
C4	289.19	1.250	11.16		289.08	1.3	10.88

Table 4.1 C1s XPS peak components of ppAA films deposited at 10 W in continuous mode before and after 5 minutes of sonication in ultra pure water.

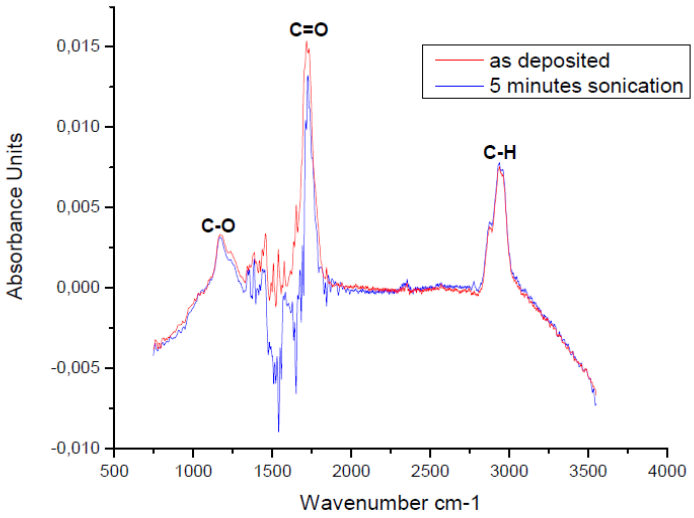

Figure 4.3 FTIR spectra with precursor of ppAA films deposited at 10 W in continuous mode: red as deposited, blue after sonication in ultra pure water.

4.1.2 Pulsed mode

In pulsed mode, two parameters were fixed in the deposition process: the duty cycle (DC = 5 %) and the pulse period (t_{ON} + t_{OFF} = 100 ms). A low duty cycle has been selected to increase the retention of carboxylic groups (Swaraj 2005, Detomaso 2005). A series of samples were deposited varying the power from 10 to 50 W, in steps of 10 W. FTIR and XPS analyses were carried on samples as deposited and after 5 minutes of sonication in ultra pure water.

From the COOH % peak of XPS and the FTIR ratio of the C=O/C-H bands two deposition regimes as a function of the power applied could be distinguished (Figure 4.4). A first regime characterized by films soluble in water is observed at power lower than 30 W. In this regime, as deposited films show a very high retention of carboxylic groups (up to 25 %) with a decrease as the power is increased, decrease that is sharper in the FTIR ratio of the C=O/C-H bands. After sonication in ultra pure water, films are completely removed, indicating a low stability of the film.

For power higher of 30 W, a second regime is observed. In this regime, as deposited films show a retention of COOH around 21 % that drops down to about

13 %, after sonication in ultra pure water. However, films are stable in water in this regime.

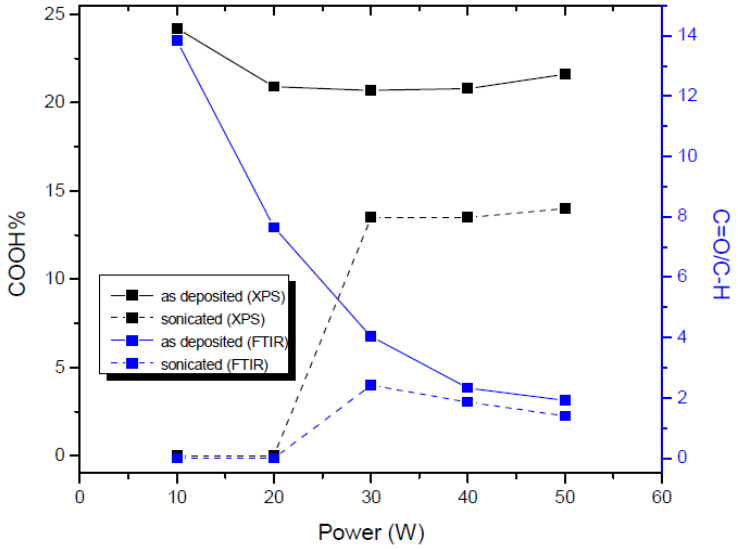

Figure 4.4 C=O/C-H ratio of FTIR (blue) and COOH% of XPS spectrum (black) as a function of the power applied as deposited (solid line) and after 5 minutes of sonication in ultra pure water (dash line).

As occurs in continuous mode, the adhesion to the substrate increases as the power applied is increased; thus, in order to have an adherent film with a high carboxylic retention (around 13 %), a deposition power of 40 W has been chosen. The optimal properties of this film can be derived from the comparison of the XPS (Figure 4.5) and FTIR spectra (Figure 4.6) before and after water sonication, which demonstrate a low loss of functional groups (around 24 %). The values of the C1s peak components are shown in table 4.2 for ppAA films as deposited and after 5 minutes of sonication in ultra pure water.

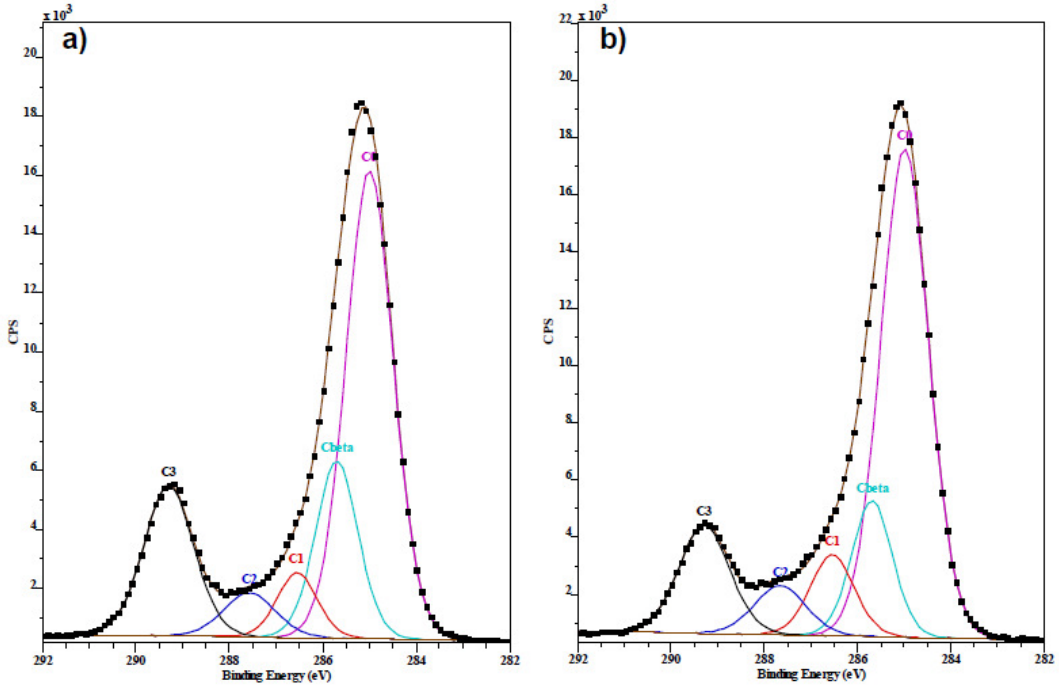

Figure 4.5 C1s core level spectra of ppAA films deposited at 40 W in pulsed mode a) before, b) after sonication.

	As deposited				After 5 minutes sonication in water		
Name	**Pos.**	**FWHM**	**% Area**		**Pos.**	**FWHM**	**% Area**
C0	285.00	1.189	52.71		284.99	1.216	58.01
C1	285.70	1.064	17.85		285.69	1.020	13.53
C2	286.55	1.000	6.14		286.54	1.100	8.71
C3	287.57	1.300	5.47		287.66	1.300	6.24
C4	289.30	1.252	17.83		289.29	1.278	13.52

Table 4.2 C1s XPS peak components of ppAA films deposited at 40 W in pulsed mode: before and after 5 minutes of sonication.

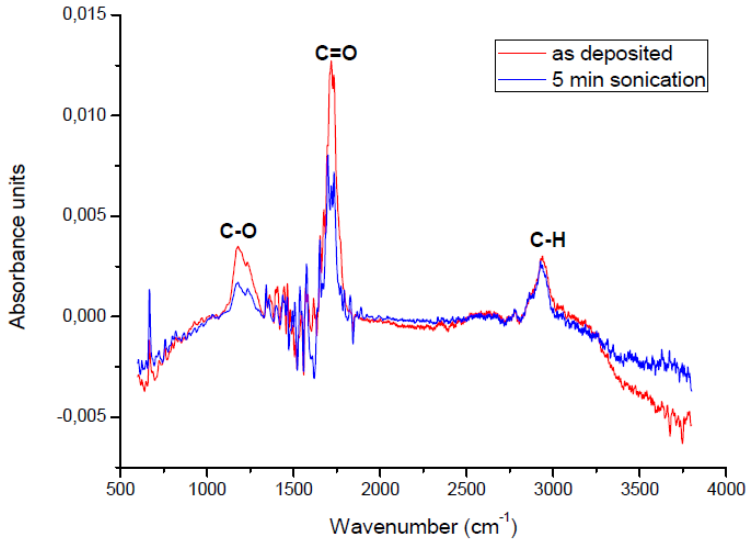

Figure 4.6 FTIR spectra with precursor of ppAA films deposited at 40 W: red as deposited, blue after washing.

For both deposition methods, pulsed and continuous, a reduction on the carboxylic retention is observed, as the power applied in the plasma process is increased. Such variation is due to a higher fragmentation of the precursor as the power is increased, yielding to a lower retention of the precursor and a higher cross-linking of the deposited film.

4.2 Characterization with ζ-potential, contact angle and ellipsometry

ζ-potential measurements were performed using an automatic titration program that measured the ζ-potential as a function of pH. In figure 4.7 the ζ-potential curves of ppAA films deposited in continuous and pulsed modes are reported. The data indicate that the ppAA film have a positive global charge when they are immersed in a pH lower than 3.1 (the isoelectric point), while a negative global charge is observed for pH values higher than 3.1.

The ζ-potential curve (Fig. 4.7) shows the acidic behaviour of ppAA films deposited in continuous and pulsed modes. The positive sign of the ζ-potential in

the acidic range is caused by the absence of dissociation of the carboxylic groups. Meanwhile, the small variation of the curve in the alkaline range is shows almost no dissociation of the carboxylic groups. Indeed, films deposited in pulsed mode present a plateau for pH higher than 6 that indicates the complete dissociation of the carboxylic surface groups at these pH values.

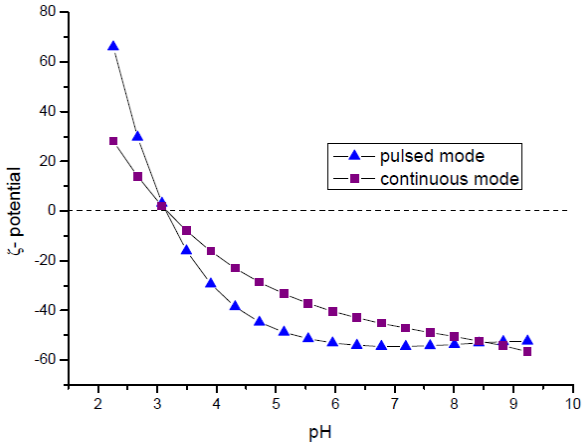

Figure 4.7 ζ-potential versus pH curves for ppAA films deposited in pulsed (at 40 W) and continuous mode (10 W).

Since the aim of this work is the use of ppAA layers as bioadhesive films, the global charge that the ppAA surface shows at different pH is an important feature when electrostatic interactions are taking place between surface and biomolecules.

The films analyzed by contact angle showed a hydrophilic character (angles below 90^{O}) for both deposition modes

	Advancing angle (^{o})	Receding angle (^{o})
Continuous mode	47 ± 2	24 ± 2
Pulsed mode	55 ± 2	29 ± 4

Table 4.3 Advancing and receding angles for films deposited at continuous and pulsed modes.

The ellipsometry data treated by a Cauchy model allowed determining a deposition rate of 17 nm/min for continuous mode and 5.5 nm/min for pulsed mode.

Measurements at a fixed angle (60^{O}) in a wavelength range between 400 to 1100 nm were carried out using a liquid cell in order to evaluate the behavior of the film immersed in water. The experiment was performed during 120 minutes and data were saved in a dynamic mode every 5 minutes.

The stability of the thickness during the experiment indicates no swelling of the polymer film by the liquid, see figure 4.8.

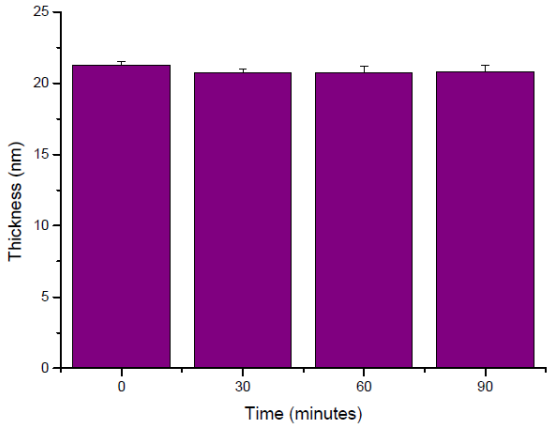

Figure 4.8 Thickness versus time of a ppAA film deposited on silicon on continuous mode (10 W).

4.3 Discussion and conclusions

Two different deposition methods, continuous and pulsed mode, have been used for the preparation of the ppAA films. Pulsed mode was characterized by two deposition regimes, a regime applying a power lower than 30 W in the deposition, where soluble films in water were obtained. The second regime was observed for power higher than 30 W, where an increase in the stability in water was reached. On the other hand, in continuous mode a unique regime was found, with films stable in water in all conditions. For both deposition modes a reduction of the carboxylic functions was observed as the power applied was increased, as confirmed by XPS and FTIR techniques. The carboxylic retention obtained on both

deposition modes is in agreement with the values reported in several works (Detomaso 2005, Rossini 2003, Swaraj 2005).

Keeping constant the other parameters (pressure, precursor flux and temperature), to obtain ppAA films stable in water, showing a good adhesion to the substrate and a good retention of carboxylic groups, a power of 40 W in pulse mode and 10 W in continuous mode were selected. Under these conditions, both films show the same isoelectric point (3.1), and a similar retention of carboxylic groups (13% in pulsed mode and 11% in continuous mode). However, the deposition rate is slower in pulsed mode, 5.5 nm/min against the 17 nm/min in continuous mode, which means a higher investment of time in the deposition process. Ellipsometry measurements of a film deposited on continuous mode showed almost no change of the thickness of the film, indicating no swelling of the ppAA film by the liquid.

Chapter 5

Direct polymerization of AA structures on a PEO-like matrix

As described in chapter 4, the physico-chemical properties of films deposited by plasma polymerization (PP) can be tailored by tuning deposition process parameters. Such parameters determine the thickness, the stability in water, the cross-linking degree or the chemistry of the deposited films. Among those parameters, the RF power forwarded to the electrodes is essential, since it determines the electron energy in the plasma discharge. The lower power deposition results in a low cross-linking of the film. This possibility of low power regime opens the path to the selective completion of the polymerization by a subsequent technique that supplies energy to the film.

Bretagnol et *al.* (Bretagnol 2007 b) reported a resist free lithographic technique, based on the deposition of a low cross-linked plasma deposited acrylic acid (pdAA) film, which was subsequently cross-linked by locally supplying energy from an electron beam. In this process, the pdAA film acts as a negatively tone resist on the lithographic process, enabling the creation of micro and nano features on the surface, since the cross-linking takes place only in the areas exposed to the electrons, while the rest of the film remains soluble in water and can be removed easily by sonication.

In the previous chapter, the plasma parameters for the deposition of poorly cross-linked films were determined.

In this chapter, the EBL conditions for the cross-linking of the pdAA onto silicon substrates will be determined as a first step. Moreover, patterns obtained by this process will be characterized in order to evaluate their application for the immobilization of biomolecules on the bioadhesive areas, i.e. on the EBL cross-linked pdAA films.

Then, in order to create functional patterns with a chemical contrast, the patterning process will be performed on a non-fouling PEO-like film previously deposited, in such way bioadhesive patterns are created on a non-bioadhesive matrix (Bretagnol 2007 b) constituting a complete device as schematized in figure 5.1.

Then, the patterns were characterized by AFM, XPS and X-PEEM. XPEEM experiments were carried out in collaboration with the group of Adam Hitchcock (BIMR, McMaster University, Hamilton, ON, Canada).

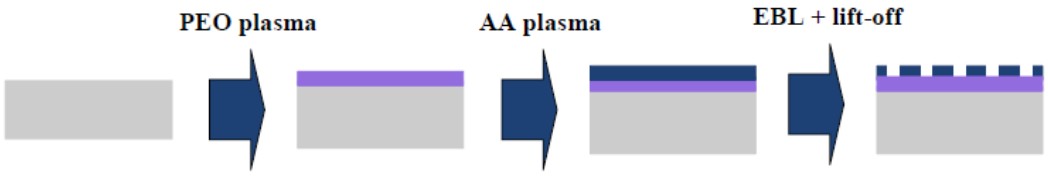

Figure 5.1 Fabrication process: direct polymerization of pdAA by EBL.

5.1 pdAA cross-linking with e-beam

The plasma deposition conditions were selected to obtain pdAA layers soluble in water (to be used as developer) as illustrated in figure 5.2. The plasma discharge was carried out in pulsed mode with a frequency of 10 Hz and a 5 % of duty cycle. A peak power of 10 W (average power of 0.5 W) was applied for 10 minutes with a flow rate of 2 sccm of acrylic acid and a pressure of 4.1 x 10^{-2} Torr. In such conditions, a layer of about 60 nm, with a low degree of cross-linking, a weak adhesion to the bare Si substrate, and a high carboxylic retention (23.7 %) was obtained, as illustrated in the C1s core level spectrum in figure 5.3.

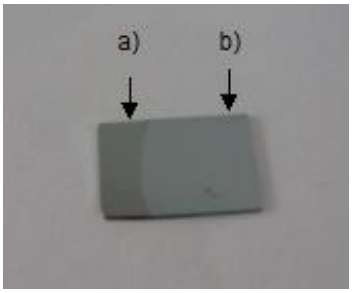

Figure 5.2 Image of a pdAA (10 W in pulsed mode) coated silicon substrate a) as deposited, b) after immersion in ultra pure water.

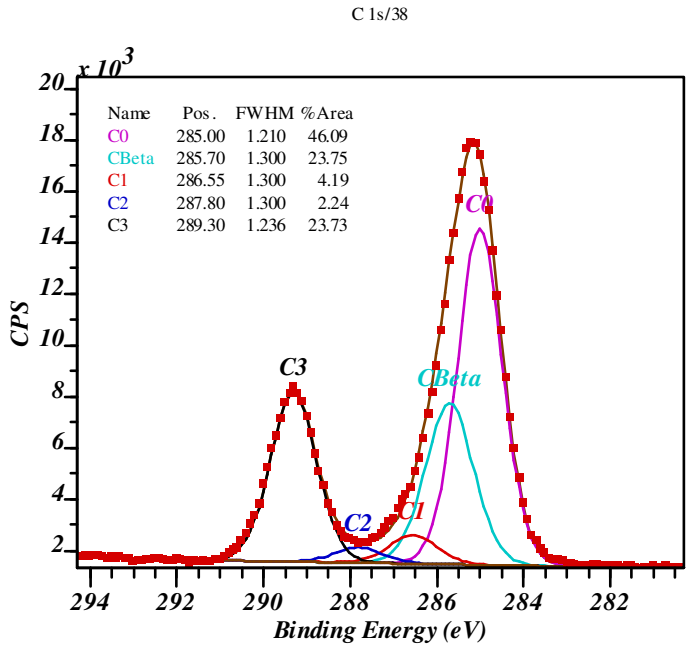

Figure 5.3 C1s core level spectrum of pdAA film as deposited (10 W)

During the EBL process, the SEM was operating at 20 KeV and the doses applied in the EBL process varied from 500 to 8000 μCcm^{-2}, to optimize the conditions for the pdAA cross-linking. Moreover, in order to determine the minimum dose needed for the cross-linking a 4 x 4 matrix with circles of 10 μm of diameter was fabricated by increasing the dose by 500 μCcm^{-2} steps at each circle. Then the sample was sonicated in ultra pure water for 5 min and dried under nitrogen.

Images of the samples taken with a SEM and an optical microscope after sonication in water revealed that areas patterned with doses lower than 1000

μCcm^{-2} were still soluble in water, thus indicating that the energy delivered to the pdAA was not enough to cross-link the film. The optical image in figure 5.4 shows the patterned circles after 5 minutes in ultra pure water. From the image, it can be seen that circles patterned at low doses (500 - 1000 μCcm^{-2}) disappeared after washing, indicating the solubility of the area in water.

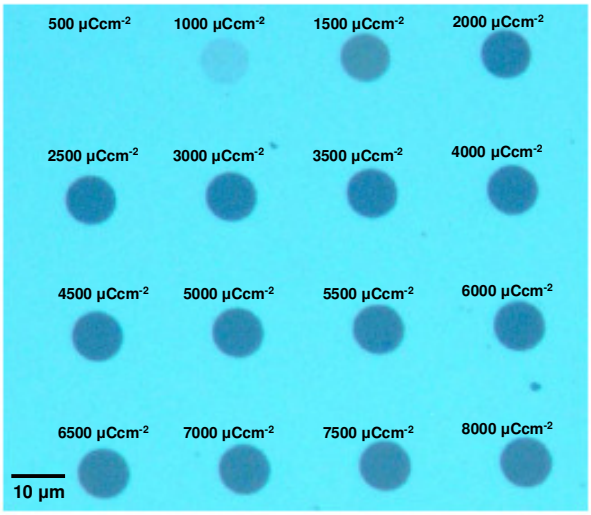

Figure 5.4 Optical image of patterned circles at doses from 500 (up-right corner) to 8000μCcm^2 (down-left corner) after 5 minutes in ultra pure water.

Several samples were analyzed by SEM before and after immersion for longer periods in water (up to 1 hour soaking). The related images (not shown) indicated the solubility of areas patterned with doses ranging from 1000 - 1400 μCcm^{-2}.

The chemical composition of the exposed areas was analyzed by XPS after sonication. Squares of 100 x 100 μm^2 were irradiated with different doses (1200, 1500, 1700 and 2000 μCcm^{-2}). High-resolution C1s core level spectra of the exposed areas after sonication were obtained and the C1s envelope was deconvoluted as described in chapter 4, section 2 to determine chemical changes induced by the EBL process.

A diminution in the carboxylic retention was observed when the dose applied in the lithographic process was increased, as illustrated in figure 5.5. As concluding

result, doses below 1700 μCcm^{-2} produce high retention of carboxylic functional groups (> 8%) in the film.

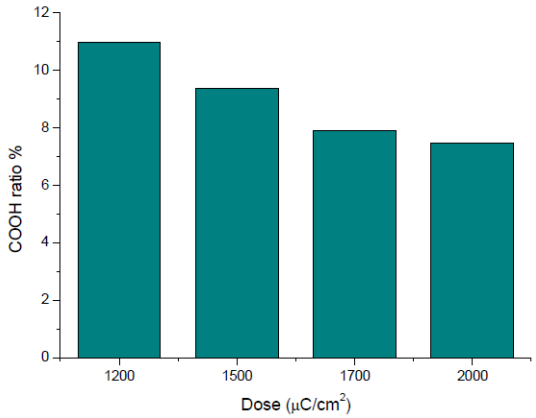

Figure 5.5 COOH % content (obtained from C1s XPS spectra) at different doses after 5 minutes of sonication in ultra pure water.

Since the goal of this process is to achieve a tailored immobilization of biomolecules in the patterned areas, the structures must have a good stability in water and biological media while maintaining a sufficient COOH retention to allow the biomolecule attachment. In this respect, a good compromise between adhesion to the substrate (poor adhesion was observed even at 1400 μCcm^{-2}), water stability and carboxylic retention (high retention with doses below 1700 μCcm^{-2}) is thus achieved with a dose of 1600 μCcm^{-2}.

A medium magnification photoemission image of a patterned area (squares of approximately 80 μm x 80 μm) prepared under optimal conditions is shown in Figure 5.6 a). The pixels in red represent fragments from the irradiated pdAA (at 285 eV BE) and the pixels in green are representative of the silicon substrate (at 99 eV BE). Microspectroscopy performed with 27 μm spotsize reveals that a C1s core level spectrum typical of the pdAA in the irradiated regions, whilst in the silicon substrate a low carbon signal at 285 eV, related to hydrocarbon contamination is detected. This result indicates that the EBL process was successful.

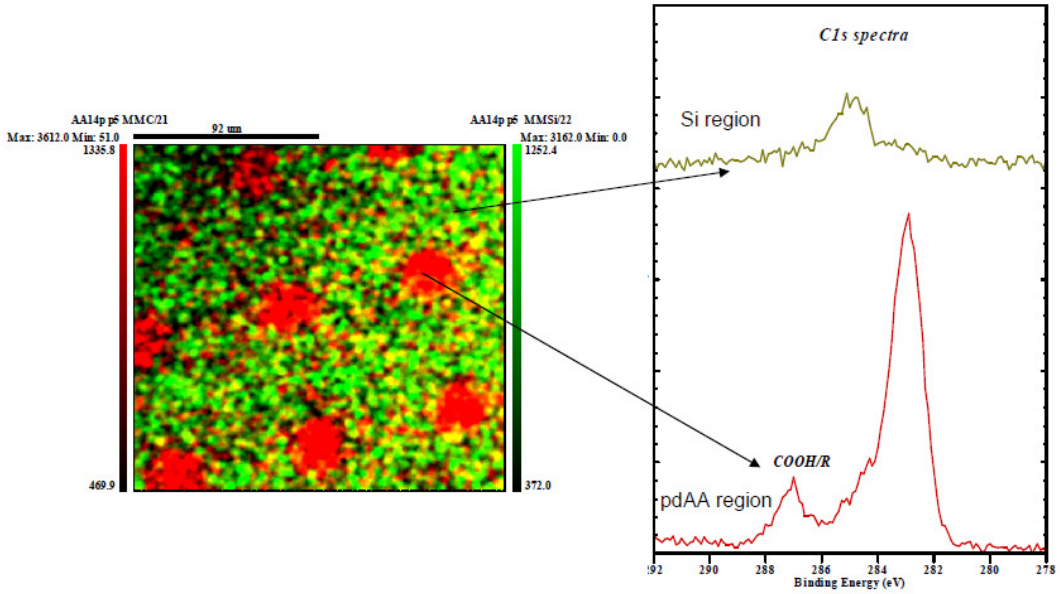

Figure 5.6 a) Photoemission image of Si (green) and exposed pdAA (red) from a pdAA square pattern on Si, b) C1s core level of Si region (top) and exposed pdAA microstructures (bottom). (Image recorded in Low Magnification (LM) mode at 99 eV and 285 eV at 160 eV pass energy; spectra recorded with 27 µm spotsize, LM mode and 40 eV pass energy).

5.2 PEO-pdAA micro-patterning fabrication and characterization

Once the operating conditions of the EBL were established, the fabrication process was carried out on a previously deposited PEO-like film (15 nm) to create a chemical contrast between the non-bioadhesive PEO-like background film and the EBL cross-linked pdAA motives.

In order to assess the possible polymeric residues on the non-irradiated areas after the fabrication process (lift-off with water of the soluble pdAA after the cross-linking of the patterning with the e-beam) XPS study was performed on the PEO-like film.

XPS data showed a similar concentration of COOH moieties in the PEO-like film: 4.46 % as deposited and 4.58 % after the fabrication process (see figure 5.7). These results indicate that the lift-off process was successful also on PEO-like film

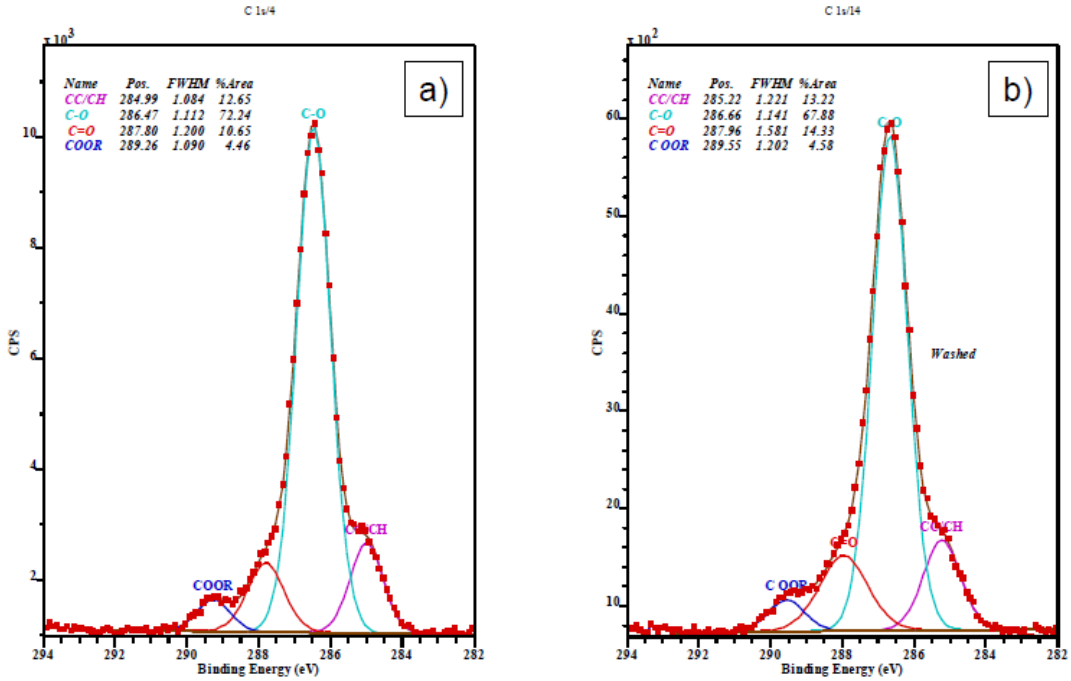

Figure 5.7 C1s core level spectra of a PEO-like film: a) as deposited, b) after pdAA lift-off in ultra pure water

The immobilization of proteins on the bioadhesive structures was studied by means of AFM and X-PEEM. For that purpose, areas of 100 µm x 100 µm were patterned with circles of 5 µm of diameter separated by 20 µm.

The topography of the patterns was analyzed by AFM before and after one hour of immersion in a protein solution. The protein used was IgG and was diluted in a PBS at a concentration of 20 µg/ml. After the immersion in the protein solution, the sample was rinsed with ultra pure water and dried under nitrogen.

The AFM profile showed a thickness increase of about 15 nm of the microstructure after immersion in protein solution, see figure 5.8 b. The changes on the patterned areas were also visible in the AFM phase images, see figure 5.9.

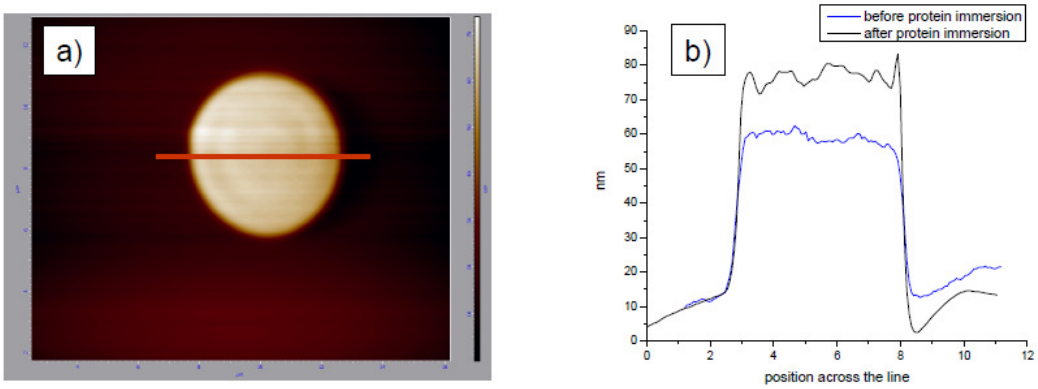

Figure 5.8 a) Topographic image of the patterned surface, b) Profile along the line of surface height before and after immersion in IgG solution.

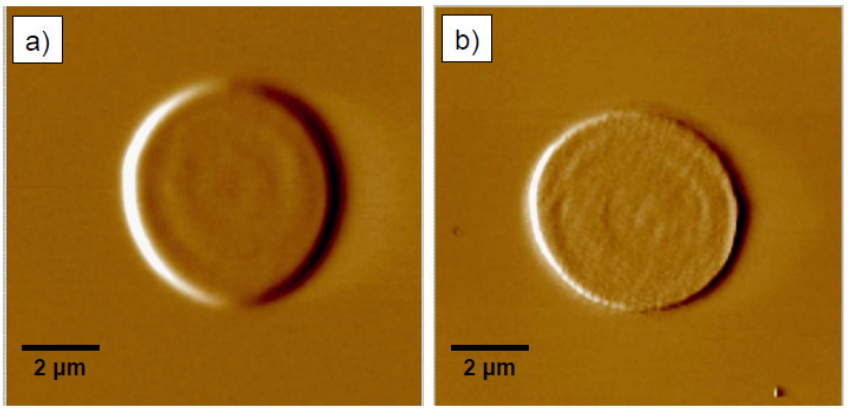

Figure 5.9. Phase image of the patterned surface a) before b) after immersion in IgG solution.

Scanning areas of 12 µm x 12 µm were acquired with AFM. From these images, five areas of 2 µm × 2 µm were selected to get the root mean square (rms) roughness values. Before protein immersion, both ppAA structures and PEO-like matrix present low roughness, with average values of 1.6 ± 0.3 nm and 1.4 ± 0.3 nm, for pdAA and PEO-like areas respectively. After protein immersion, pdAA structure roughness increases to 3.6 ± 1.26 nm, while the PEO-like matrix remains almost unchanged (1.7 ± 0.2 nm). The increase on the thickness (~ 15 nm) and the change in the roughness on the ppAA cross-linked structures suggest that

proteins are preferentially adsorbed onto the pdAA structure. As the increase in thickness is higher than the size of the protein (~ 10 nm) more than a monolayer seems to be adsorbed on the surface.

Regarding the PEO-like matrix, no outstanding roughness modification has been detected with the AFM, which suggests the conservation of the non-bioproperties, since no presence of pdAA residues on the PEO-like matrix was detected.

The protein absorption on the patterned surfaces was also studied by X-PEEM (Ceccone 2010). Ubq diluted in PBS at a concentration of 2 µg/ml was used. The sample was immersed in the protein solution for one hour, then rinsed with ultra pure water and dried under nitrogen.

Spectra of PEO-like film and ppAA layer (deposited in continuous mode at 10W) were previously acquired for the fitting. Images were analyzed by fitting each pixel of the image sequence to a linear combination of the PEO, acrylic acid and HSA as a model for the Ubq reference spectra. In figure 5.10, the spectra of PEO-like film and ppAA layer used for the fitting are shown next to the spectra acquired from the pure monomer in addition the spectra of Ubq is shown next to the HSA model.

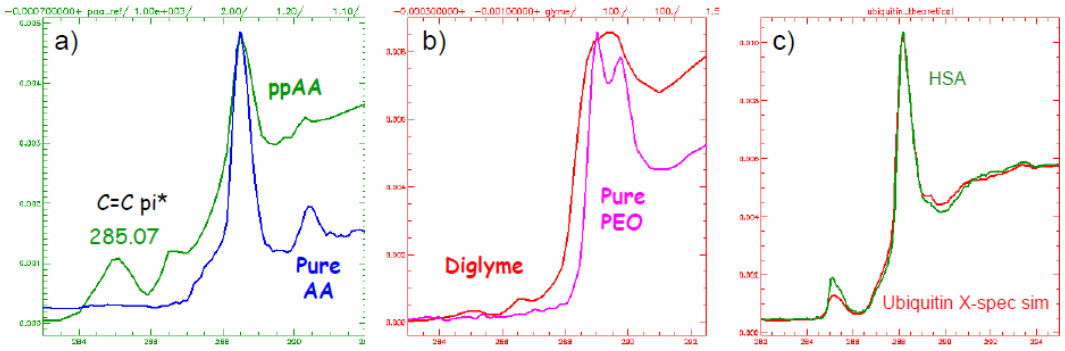

Figure 5.10 Spectra from a) ppAA layer in continuous mode at 10W (green-colored) and pure acrylic acid precursor (blue-colored), b) PEO-like film (red-colored) and pure PEO precursor (pink-colored) and c) HSA (green-colored) as a model for the Ubq reference spectra (red-colored).

The absolute component maps derived from the C1s X-PEEM image sequences (Figure 5.11) were analyzed. In these maps, PEO is color-coded red, pdAA is color-coded green and ubiquitin is color-coded blue. The images reveal that the

matrix is intensely red which indicates it is composed mostly of PEO-like material, whereas the circular pdAA-rich area is purple, from a roughly equal combination of red PEO and blue protein. Only 6% of Ubq was found on the PEO matrix while 32% was found at the pdAA areas.

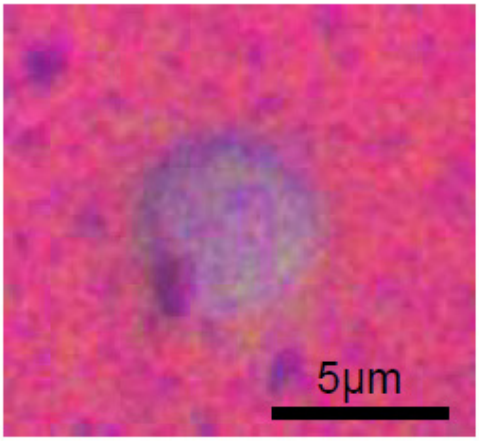

Figure 5.11 Absolute color component maps for 2µg/ml Ubq adsorbed to a PEO-like/pdAA circular structure.

The detection of bioadhesive fragments on the PEO-like matrix by X-PEEM is in agreement with preliminary results of XPS, since a slight increment of carboxylic retention on PEO-like matrix after the lift-off process was determined.

The low adhesion of proteins on the PEO-like film indicates that the matrix is still protein repellent after the fabrication process, and proteins are preferentially adsorbed on the ppAA microstructures (Ceccone 2010).

The interaction of cells with the patterned surfaces was also explored. Arrays of 10 µm width lines separated 20 µm were fabricated in optimized conditions on an indium-tin oxide (ITO) coated glass substrate. Such substrates are transparent and conductive, and can be used as substrates for cells culture.

Optical images, presented in figure 5.12, of the patterned surfaces showed binding of the cells on the entire surface. These results confirm that the low degree of bioadhesive fragments detected on the PEO-like matrix, is responsible for reducing the non-fouling properties of the PEO-like matrix. Since this fabrication method do not show a selective binding of cells, an alternative procedure for the creation of the patterned surfaces has to be proposed.

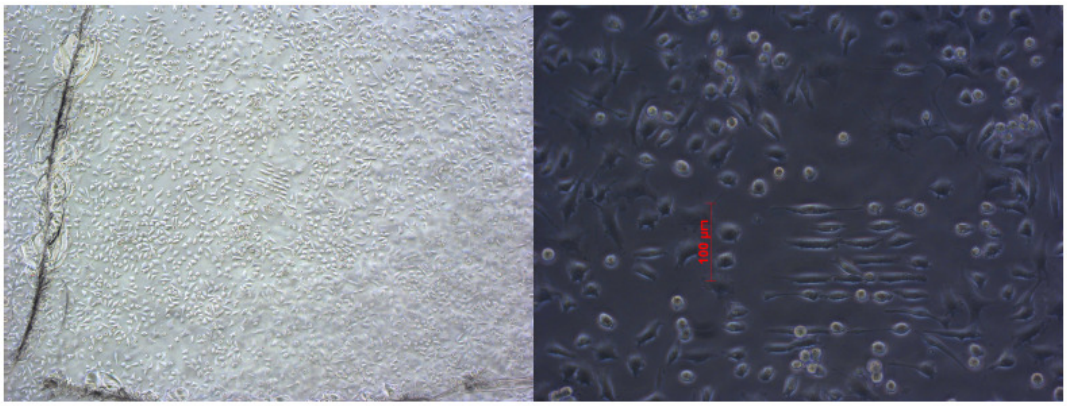

Figure 5.12 Optical images of cells immobilized on the surface

5.3 Discussion and conclusions

Conventional lithography techniques use sacrificial resists for the patterning of surfaces by EBL. The direct cross-linking with the e-beam of a low cross-linked pdAA film with direct developing in water would be a great advantage in terms of reduction of time and costs for biopattern fabrication (fabrication steps and consumables are notably reduced).

The combination of PP and EBL techniques used in our approach allows the fabrication of chemical patterns consisting of bioadhesive structures (pdAA) on a non-bioadhesive matrix (PEO-like film).

The characterization of the structures by AFM revealed an increase in height of approximately 15 nm after immersion in protein solution (IgG), which was associated to the adhesion of proteins on the bioadhesive structure. Such selective binding of protein on the pdAA patterned structures was confirmed by the C 1s X-PEEM images.

In fact, X-PEEM analysis of the surfaces showed a slight increase of carboxylic moieties on the PEO-like film, indicating a modification of the PEO-like film during the fabrication process. Such carboxylic moieties are not soluble in water, though most of the pdAA film dissolves, which suggests that at the first stages of the pdAA deposition process these fragments present a preferential cross-linking. No

presence of pdAA moieties on the PEO-like film was detected by AFM, neither in the images nor in the roughness values, suggesting that this effect is very limited.

Although the presence of bioadhesive moieties on the most top surface of the PEO-like film produced only a small increase of the COOH/R component in the XPS C1s core level spectra, their effect in the biological immobilization is important. Though at protein level the surface reveal a certain degree of selectivity, the immobilization of cells on the whole surface reveals a lack of selectivity at cellular level. Since cell adhesion is a protein mediated process, the low protein adhesion on the PEO-like patterned areas could be responsible of cells adhesion to the non-bioadhesive matrix.

Therefore, the aim of this work, the fabrication of patterned surfaces showing a non- bioadhesive /bioadhesive contrast, is not completely fulfilled and could be only exploited in biomedical devices requiring a low degree of protein contrast. In particular, adsorption assays with labeled oligonucleotides remain to be studied.

Chapter 6

ppAA structures on a PEO-like matrix fabricated by EBL with a PMMA resist

Results presented in Chapter 5 show that direct stabilization of pdAA films by means of EBL has some limitation, since non-bioadhesive properties of the PEO-like film are altered by the presence of bioadhesive fragments on the surface. Such modification can be produced at the first stages of the pdAA deposition process. To avoid it, a conventional resist, PMMA, is included in the fabrication process presented below.

In this chapter, we optimize a micro and nano fabrication method previously reported by Brétagnol *et al*. (Brétagnol 2007 c) in which chemically active nano-patterned surfaces were produced using PMMA as resist. PMMA is a positive tone resist sensitive to the electrons that is commonly used in electron beam lithography. The areas exposed to the e-beam become soluble in solvents, so they can be removed after a proper development. Then a new material can be deposited within the aperture created in the resist and after PMMA lift-off, contrast of materials can be created on the surface. The material deposited in this work will be a plasma polymerized acrylic acid (ppAA) film, which acts as bioadhesive material. For that purpose, the parameters for the ppAA film deposition will be

adjusted to obtain cross-linked films, with good adhesion to the substrate, good stability in water and showing a high retention of carboxylic groups (see chapter 4). The advantage of using the PMMA resist is that it acts as protective layer and preserves the PEO-like film non-bioadhesive properties, since the PEO-like film is not directly exposed to the plasma deposition of the acrylic acid film.

6.1 Fabrication method

The substrates used in this study were ultrasonically cleaned for 5 minutes in ethanol. Then a film of approximately 15 nm of PEO-like film was deposited by plasma polymerization. Then a positive resist layer of a PMMA was deposited as described in chapter 3.

The process of fabrication is illustrated in figure 6.1. For the creation of the structures, the SEM was used in electron mode at 10 KeV (Acceleration voltage that allow the complete exposure of the PMMA resist and minimize possible damages on the PEO-like film). Areas of 100 µm x 100 µm were exposed to the e-beam. After the chemical development, a layer of ppAA was deposited in continuous mode with a peak power of 10 W for 1 minute, which yields to circa 20 nm of ppAA thickness. Finally, the PMMA resist was removed.

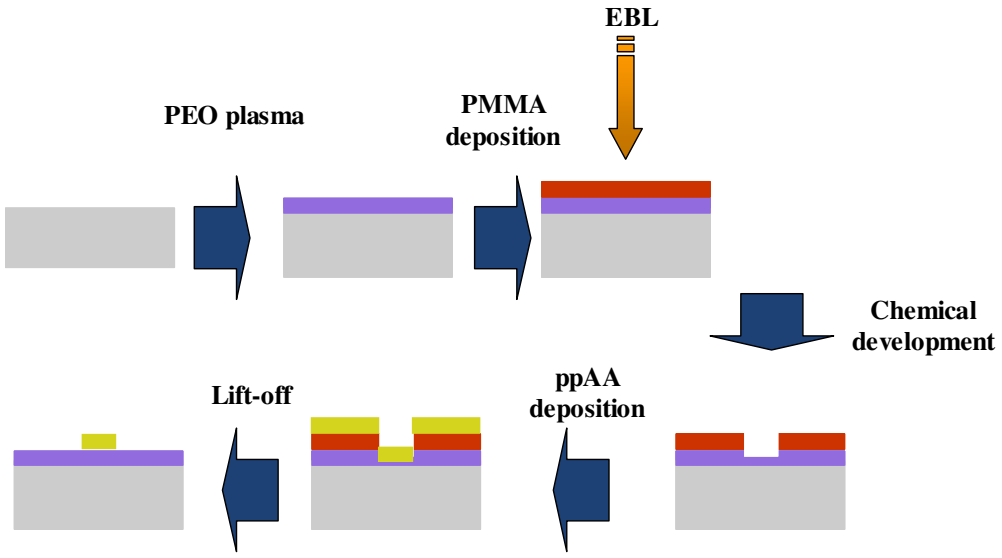

Figure 6.1 Fabrication process

An e-beam dose calibration was performed to optimize the pattern profile, that means, to set the dose that produce a pattern with the same size of the design. The substrate used was a commercial SPR slide, which consists in a high refractive index prism coated with a 50 nm gold film. For that purpose, several areas made up of microstructures were exposed at different doses ranging from 70 to 100 μCcm^{-2}, with steps of 10 μCcm^{-2}.

SEM images of the structures (not shown), after the resist lift-off, were obtained to determine the dose that produces accurately the exposed design. The proper dose was set at 80 μCcm^{-2} working in area exposure mode.

When the pattern is made up of nanostructures, the proximity effect increases as the density of the pattern increases (backscattered electron increased). In order to establish the limits of nano fabrication, patterns formed of lines were exposed in single line exposure mode at different doses varying the pitch from 300 to 500 nm, in steps of 50 nm. The dose was varied from 500 to 1100 $pCcm^{-1}$, in steps of 100 $pCcm^{-1}$. The areas patterned on the resist were then developed and a 20 nm thick film of ppAA was deposited on the substrate. The removal of the resist by immersion in acetone was optimized for the nanostructure: the samples were soaked 5 minutes in acetone followed by 1 minute of ultrasonication. The process was repeated two times.

SEM image of the patterned areas for the calibration dose is shown in figure 6.2. Details at higher magnification of the pattern are also shown: figure 6.2 b shows a SEM image of the final pattern obtained (110 nm width lines of ppAA on a PEO-like matrix) at 500 nm pitch and in figure 6.2 c can be observed an overexposed area (no pattern exist inside the area exposed and some remaining PMMA lines are still stitched to the surface after the lift-off process).

The e-beam calibration dose was repeated several times to test the fabrication repeatability.

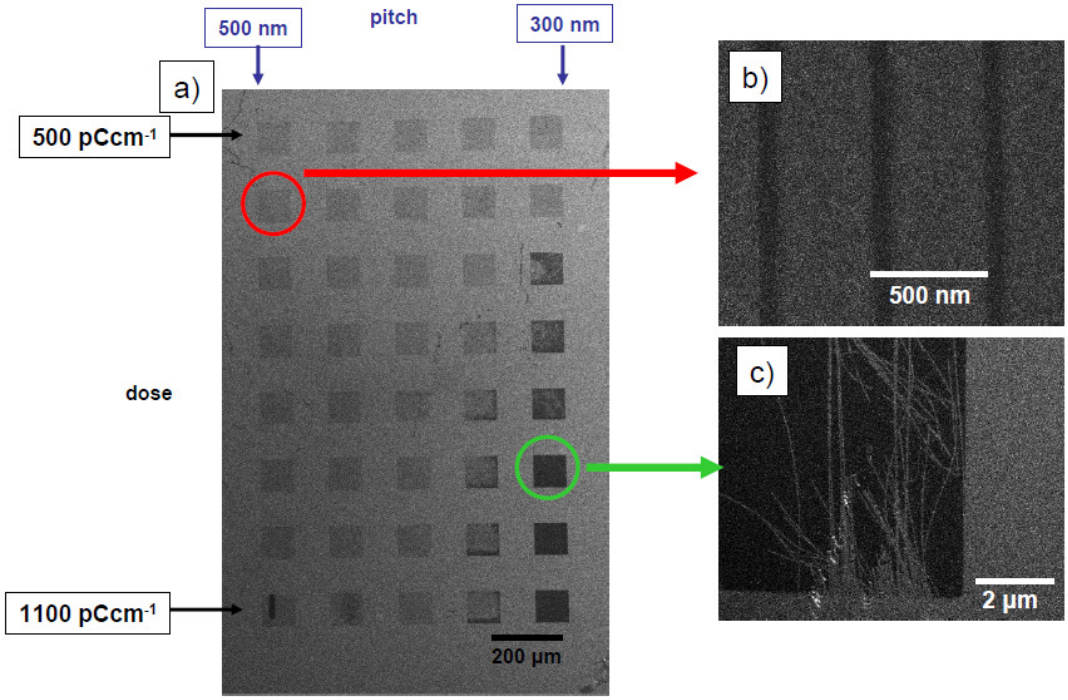

Figure 6.2 SEM image of a) an electron beam calibration dose exposure: 5 x 7 matrix of arrays of 100 µm x 100 µm with doses ranging from 500 to 1100 pCcm^{-1} and a pitch of the lines varying from 500 to 300 nm, b) a detail of the patterns (lines of 110 nm width separated 500 nm) and c) overexposed pattern.

The width of the lines at the different pitches and different doses were obtained by measurements with the SEM, results shown in table 6.1.

These data are indications for next fabrication processes, since small differences on the fabrication process will produce also modifications on the width of the lines. In fact, PEO-like film is an isolating film and small variations on the grounding during the e-beam exposure produce local charges gradients that modify the final result.

In general, lines of around 100 nm width were fabricated at different pitches. The results showed a partial lift-off of the resist for pitches of 350 nm or lower, due to a higher proximity effect. However, excellent results were obtained with pitches between 400 and 500 nm for all the doses applied. By other side, the effect of the dose on the width of the lines is not remarkable, as variations of the dose in the

range of 600 - 1000 $pCcm^{-1}$ result in small changes of the width of the lines, indicating a large plateau of solubility of the PMMA resist.

Pitch (nm)	**Dose ($pCcm^{-1}$)**						
	500	**600**	**700**	**800**	**900**	**1000**	**1100**
500	90	110	125	110	95	117	160
450	100	110	80	105	90	108	125
400	100	110	110	105	100	95	125
350	75	82	110	110	110	110	140
300	Under exposed	70	75	80	108	130	Over exposed
	Line width (nm)						

Table 6.1 Width of the lines obtained on the e-beam calibration dose exposure.

Once the dose limits were determined, some areas were patterned with micro and nanostructures. First, the thickness of the ppAA was optimized to obtain the best quality patterns. With ppAA films over 40 nm thick, we observed that some PMMA resist residues remained attached to the ppAA structures, see figure 6.3. Therefore, the ppAA film thickness was set in the forthcoming samples at 20 nm to guaranty pattern free of PMMA residues.

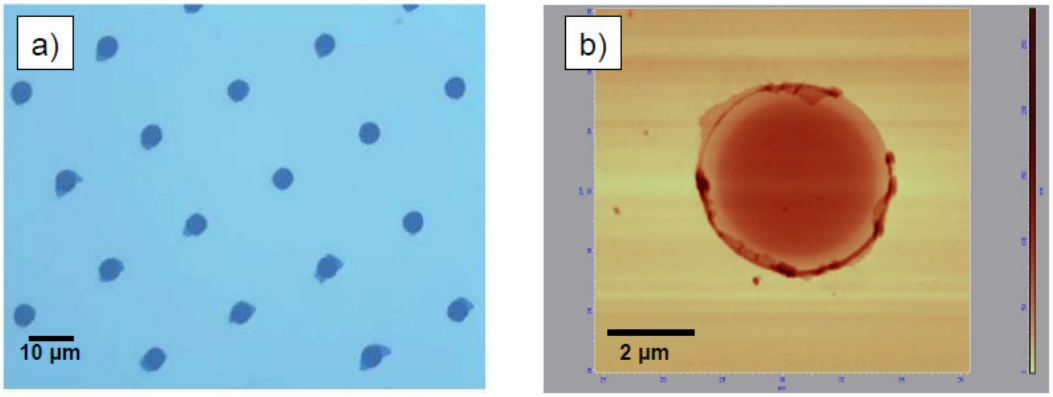

Figure 6.3 PMMA attached on the border of 40 nm thick ppAA circles (5 µm of diameter) on a PEO-like matrix a) Optical image, b) AFM image.

Another crucial factor in the final result is the stability of the PEO-like film during the patterning process. The PMMA resist, and consequently the structures created on it are designed on the PEO-like film. If the PEO-like film is not well cross-linked and not enough adherent, it can become soluble and be removed in contact with the different products used in the fabrication process. In figure 6.4 an example is shown where some areas of the patterning have been dissolved from the surface during the fabrication process due to the PEO-like film partial solubility.

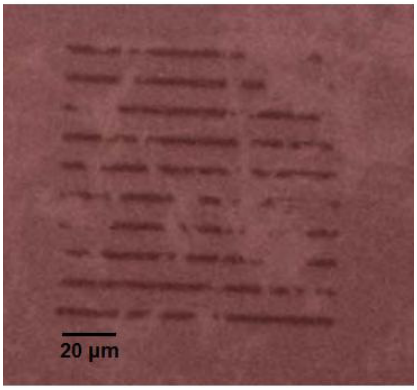

Figure 6.4 Optical image of pattern showing local solubility of the PEO-like films.

In order to avoid this effect, samples are soaked in water one minute and dried with nitrogen before the spin coating of the resist. In such a way, the top fragments of the PEO-like surface, that can show some solubility, are removed before the lithographic process.

6.1.1 PEO-like film characterization by means of XPS.

In chapter 5, a modification of the non-bioadhesive properties of the PEO-like film caused by the plasma process was reported. Therefore, a characterization of the PEO-like film after the removal of the PMMA resist was performed by XPS measurements, in order to verify the PEO-like film anti-fouling properties.
For that purpose, four samples were analyzed:

- PEO as deposited.

- PEO as deposited immersed on BSA (20 µg/ml), rinsed with pure water and dried.
- PEO after a lithography process (we have deposited the PMMA resist as we have described before, and then we have removed the resist sonicating the sample on acetone during one minute).
- PEO after a lithography process immersed on BSA (20 µg/ml), rinsed with pure water and dried with nitrogen.

C1 values from the C1s core level spectra showed a little drop after the fabrication process (66.7 %) compared with the PEO-like coating as deposited (70.7 %) as illustrated in figure 6.5. In such range of values, the PEO-like films show a low protein adsorption (Bretagnol 2006 b), suggesting the anti-fouling properties preservation for protein-surface interactions. By other side, no presence of nitrogen was detected, indicating no binding of proteins on the PEO-like film.

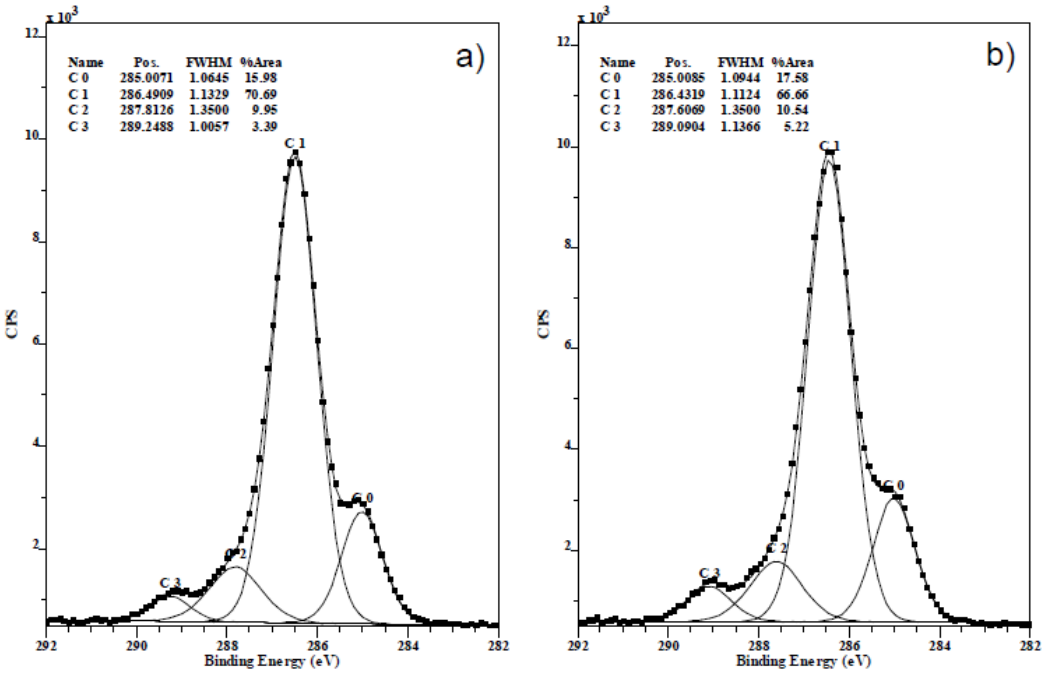

Figure 6.5 C1s core level spectrum of PEO-like film a) as deposited, b) after lithographic process.

6.2 Characterization and interaction with proteins

AFM experiments were carried out to check the protein adhesion on the patterned surfaces. An area of 100 µm x 100 µm was patterned with ellipses separated by 20 µm with a minor and major radius of 2.5 and 3 µm of diameter, respectively (figure 6.6 a). Scanning areas of 20 µm x 20 µm were acquired before and after immersion in a solution containing proteins. The protein used for the characterization was BSA diluted in a PBS solution (pH 7.4) at a concentration of 20 µg/ml. After the immersion in the protein solution, the sample was rinsed with ultra pure water and dried under nitrogen.

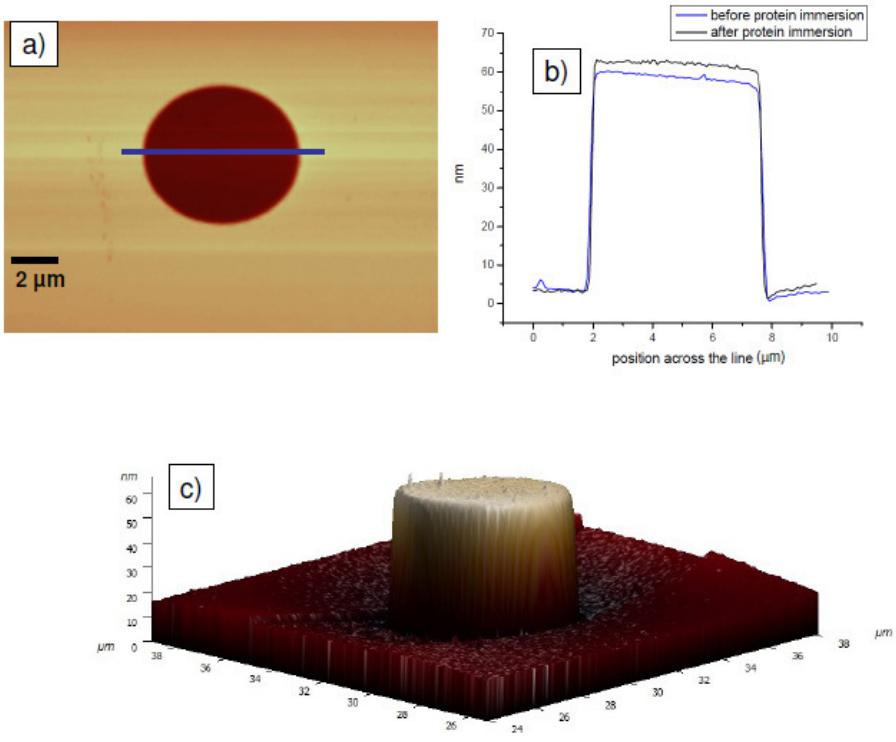

Figure 6.6 a) Topographic image of the patterned surface b) Profile along the blue line before (blue) and after (black) immersion in BSA solution, c) AFM 3D image of ppAA structure on the PEO-lke matrix.

The AFM height profile showed an increase in height (around 5 nm) of the structures after the immersion in protein solution, which suggests a selective

binding of the proteins on the top of the bioadhesive areas of ppAA. As the size of the BSA is circa 14 nm x 4 nm (Gryboś 2004), the increase observed in height can be related with the adhesion of a monolayer of BSA (in the orientation with 4 nm) on the ppAA area.

ToF-SIMS experiments have been performed to confirm the selective binding of proteins on the bioadhesive structure. For that purpose, arrays of 100 µm x 100 µm were patterned with lines (20 µm width and a pitch of 30 µm). The sample was immersed one hour in a solution of Ub-^{15}N diluted in acetate buffer (pH 4) at a concentration of 20 µg/ml, then was rinsed with acetate buffer and finally dried with nitrogen. Ubiquitin enriched with ^{15}N (Ub-^{15}N) was used in order to obtain an isolated signal coming from the C^{15}N ions, in that way the sensitivity of detection with ToF-SIMS is increased. From the ToF-SIMS distribution map of C^{15}N ions on the structured surfaces after immersion in Ub-^{15}N (figure 6.7) can be appreciated a selective binding of the protein on the ppAA structures and the preservation of the PEO-like film anti-fouling properties.

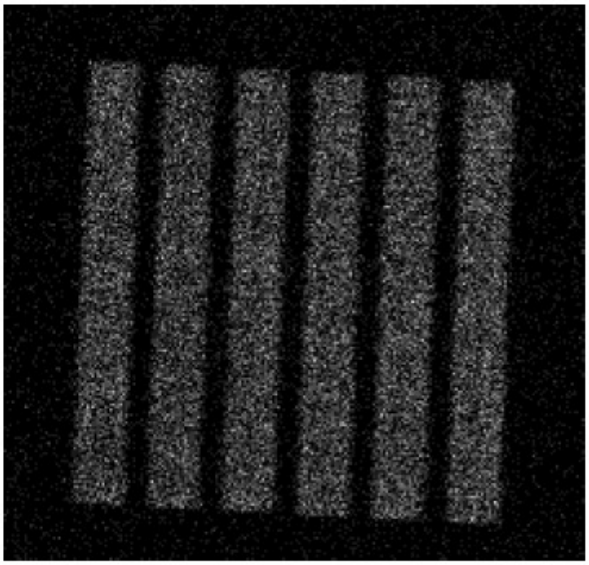

Figure 6.7 ToF-SIMS distribution map of C^{15}N ions on the structured surfaces after immersion in Ub-^{15}N.

6.2.1 pH optimization

Factors that influence the adhesion of proteins on the surface are highly related to the properties of the medium in which the proteins are dissolved. More precisely, the pH has a large influence on the interactions between protein and surface (Li 2008).

In order to determine the better pH condition that favors the adhesion of proteins preliminary SPRi experiments were carried out at two different pH, e.g. 7.4 (PBS buffer) and 4 (acetate buffer). The SPR curves from 4 micrometric structures (lines of 1 µm width, pitch of 5 µm), (figure 6.8 a), and from 4 areas of the bare PEO-like film were selected. The working angle was fixed at 57^{O}. Then PBS was flowed during 20 minutes at a flow rate of 50 µl/min. Then a solution of IgG in PBS (10 µg/ml) was injected and a low adsorption of proteins on the surface was detected (average change in reflectivity of 0.09 %). Then a second flow of IgG in acetate solution (10 µg/ml) was monitored showing a higher immobilization of proteins on the ppAA structures (average change in reflectivity of 0.26 %), (figure 6.8 b). No adhesion of proteins on the bare PEO-like film was monitored for both pH.

Next experiments were carried out with acetate buffer at pH 4 to enhance the protein-surface interaction. In such conditions, the proteins used in this work are positively charged, meanwhile the patterned surfaces show a negative charge, which can promote selective electrostatic interactions between proteins and surface. Besides, the buffer does not contain salts, which could disturb the interactions (Park 2009, Tsumoto 2007).

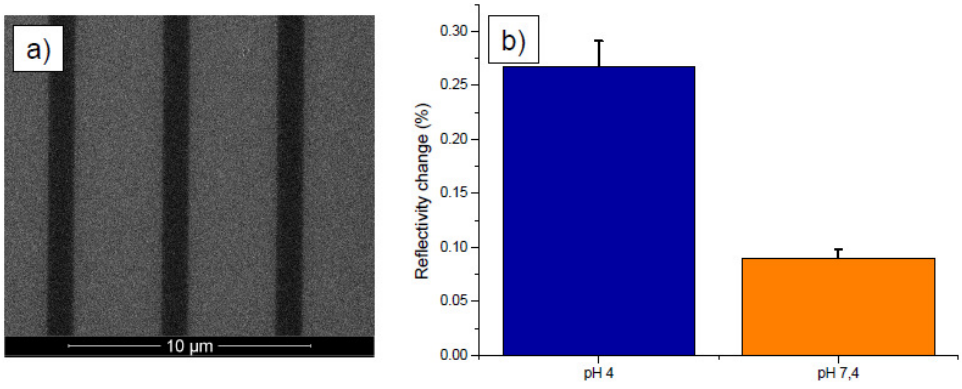

Figure 6.8 a) SEM image of micrometric structures (line of 1 µm width, pitch of 5 µm; black-colour = ppAA; grey-colour = PEO-like film), b) SPR signal from micrometric structures at pH 7.4 and pH 4.

6.2.2 Protein interaction detection at micro and nano patterned areas

SPRi experiments were used for protein-surface characterization. Since the shape of the plasmon curves (amplitude and width) influences the detection sensitivity (Ekgasit 2005) areas patterned with micro and nano features were fabricated in order to study the possible influence of the pattern size on the protein binding detection.

The study started with a theoretical analysis of the SPR plasmon curves at micro and nano scale. Calculations based on Rigorous Coupled Wave Analysis (RCWA) were carried out with GsolverV51 software. The conditions used for the calculations were similar to the ones applied on the experimental assays: substrate consisting in 50 nm of gold on a SF11 prism, measurements performed at a wavelength of 810 nm, refractive index of PEO-like matrix and ppAA of 1.4 and 1.55, respectively. PEO-like film and ppAA structures were designed with a thickness of 25 nm. The pitch of the structures was changed by variation of the grating period (number of lines/mm).

In this way, theoretical SPR curves from micro and nanostructures of ppAA on a PEO like matrix, as well as the bare PEO-like matrix were obtained. Nanostructures were designed with lines of 100 nm separated 450 nm. The design used for the SPR calculation of the nanostructures is illustrated in figure 6.9 a. Microstructures were designed with 20 µm width and a pitch of 35 µm. Theoretical SPR curves are shown in figure 6.9 b.

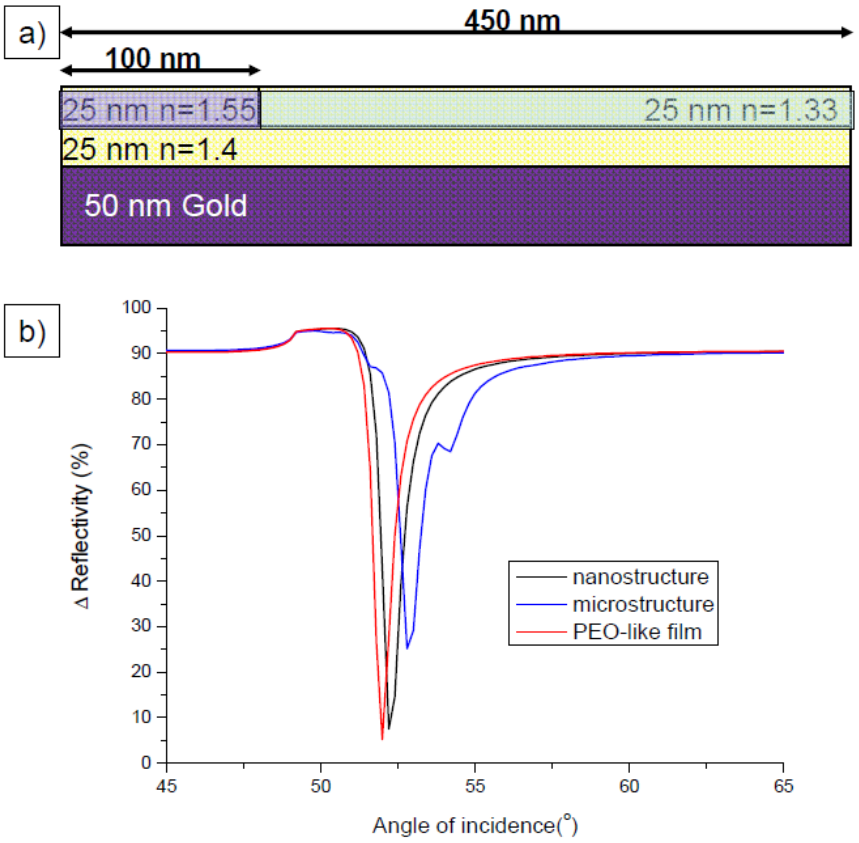

Figure 6.9 a) Design used with GsolverV51 for calculation of SPR curves of nanostructured areas, b) SPR curves of PEO-like film, nano and microstructures of ppAA on a PEO-like film simulated by GsolverV51.

As compared to the bare PEO-like film, the SPR curves show a slight shift of the SPR angle on both micro and nano structures. Such shifts are due to the increase of the refractive index produced by the presence of ppAA, since ppAA has a refractive index around 1.55, which is higher than the refractive index of the water (1.33). Therefore, the structured ppAA area results in an increment on the total refractive index, which depends on the amount of ppAA deposited, that means, on the ppAA thickness and on the filling factor of the patterning.

On the other side, a marked reduction on the amplitude of the SPR curves from the microstructures takes place. Such reduction can be due to the increment of light diffracted from the microstructures, which may increase the total amount of light reaching to the detector (Schueller 1999, Blank 2001).

The theoretical studies were followed by an experimental analysis. Areas of 100 µm x 100 µm were fabricated on a SPR prism at micro and nano scale: 5 nanostructured arrays fabricated with lines of approximately 100 nm width and pitches varying from 300 to 500 nm. Microstructures were fabricated with 4 different designs made up of lines with different width and pitch, as summarized in table 6.2. All the structures had a thickness of approximately 20 nm.

5 µm width 15 µm pitch 33 % active area	10 µm width 30 µm pitch 38 % active area	20 µm width 35 µm pitch 57 % active area	30 µm width 70 µm pitch 57 % active area
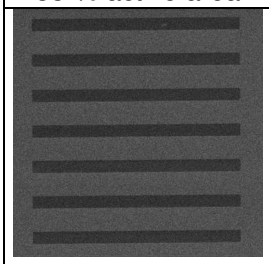	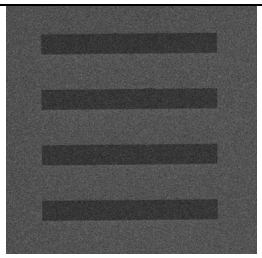	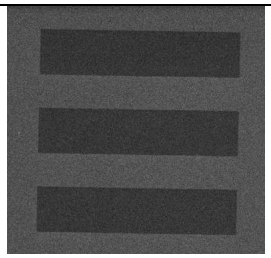	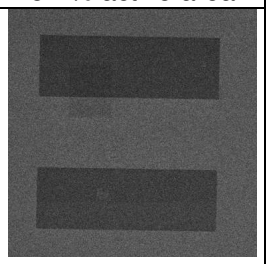

Table 6.2 SEM images of micro structures

Theoretical and experimental plasmon curves from microstructures are shown in figure 6.10 a and b, respectively. Compared to the bare PEO-like film, the depth of the plasmon curves is lower in the experimental curves than in the theoretical calculations, even for the lines with the smaller width (5 and 10 µm). This is probably due to the used SPR light source, which has a non-perfect coherence.
Furthermore, the plasmon curves have the same trend, a reduction in the amplitude as the width of the lines increases, that is, as the ppAA area increases, since the thickness is constant for all of them.

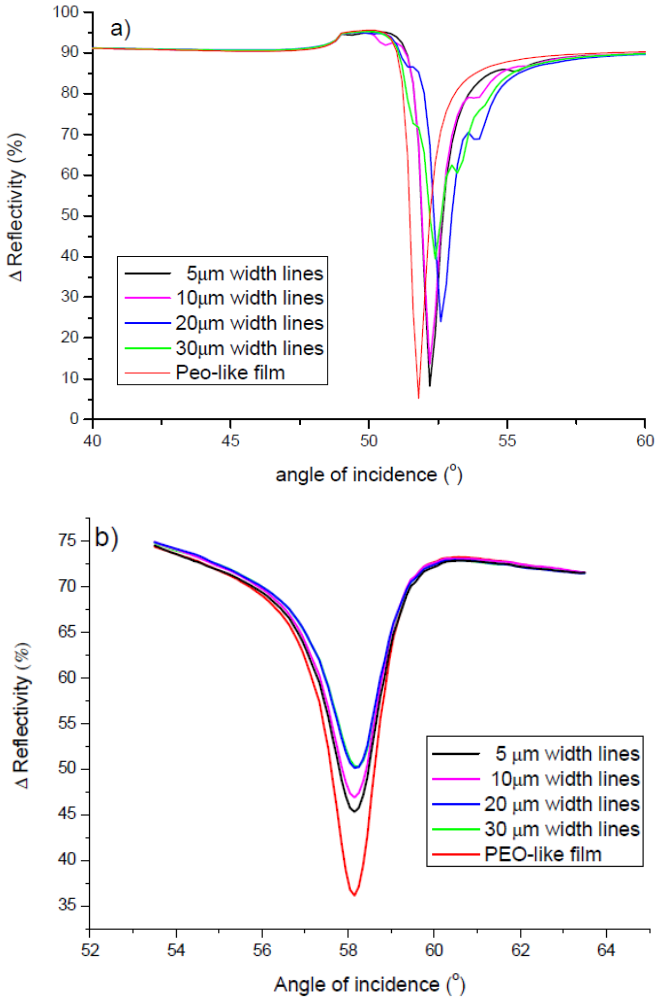

Figure 6.10 Reflectivity curves from bare PEO-like film and micropatterned areas: a) theoretical data, b) experimental data. (The shift to the left on the experimental data is due to the SPRi system that uses a mirror to point the reflected light into the detector)

Regarding the plasmon curves generated on the nanopatterned areas, the trend, compared to the bare PEO-like film, is the same in both theoretical (see figure 6.9 b) and experimental curves (see figure 6.11 a).

It can be noted that for the nanostructured surfaces, SPR measurements are very sensitive to fabrication defects, since SPR curves show a broader dip, with a lower depth and the presence of adjacent dips, as can be seen in figure 6.11 b, which make them not suitable for correct measurements. Consequently, patterns showing such SPR curves will not be considered for the analysis.

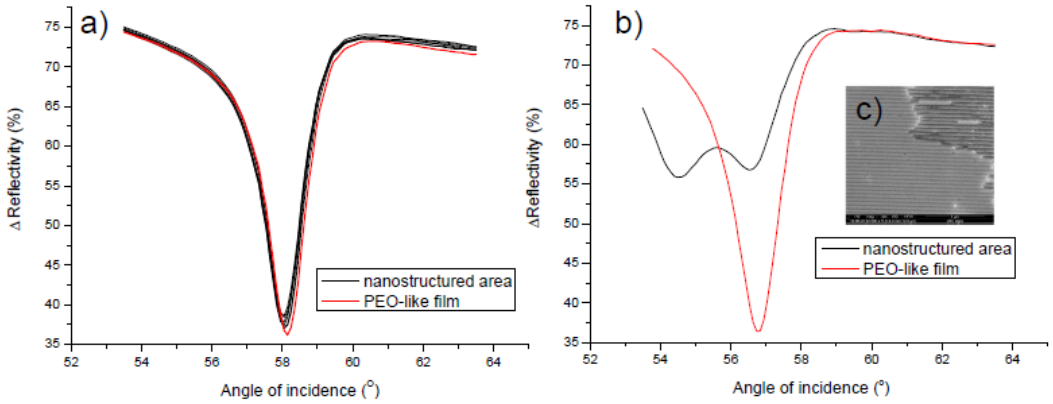

Figure 6.11 Reflectivity curves from PEO-like film and nanostructured areas: a) plasmon curves from well fabricated areas, b) plasmon curves from areas with residues of PMMA on it; c) SEM image of the PMMA faulty nano patterned area.

A characteristic of the SPRi system used in this work is that the light is collected into the detector using mirrors, for that reason, experimental curves are shifted to the left. Note that small variations on the thickness of the ppAA structures (1 – 5 nm) produce noticeable changes on the position of the plasmon curve as compared to the plasmon of the bare PEO-like surface.

After the analysis of the SPR plasmon curves, SPRi protein adsorption assays were carried out. Different micro and nanopatterned areas were fabricated on a gold coated prism: 25 arrays of nano-structures (lines with 450 nm of pitch, 100 nm width) and 10 arrays of microstructures (lines of 2 μm width, pitch of 10 μm). An optical image of the patterned surface on the SPR flow cell is shown in figure 6.13 a. The reflectivity curves were measured from each array and the working angle was set at 57.44^{O}.

A starting flow of acetate buffer (pH 4) was injected for 10 minutes with a flow rate of 20 μl/min, then HSA (100 μg/ml) was injected.

The immobilization of proteins on the patterned surface generated a shift on the plasmon curves proportional to the amount of proteins immobilized. This shift was monitored and its evolution versus time (Figure 6.12 a) shows a higher change in the reflectivity from the nanopatterned areas than from the microstructured areas, confirming the lower sensitivity of detection on the microstructures.

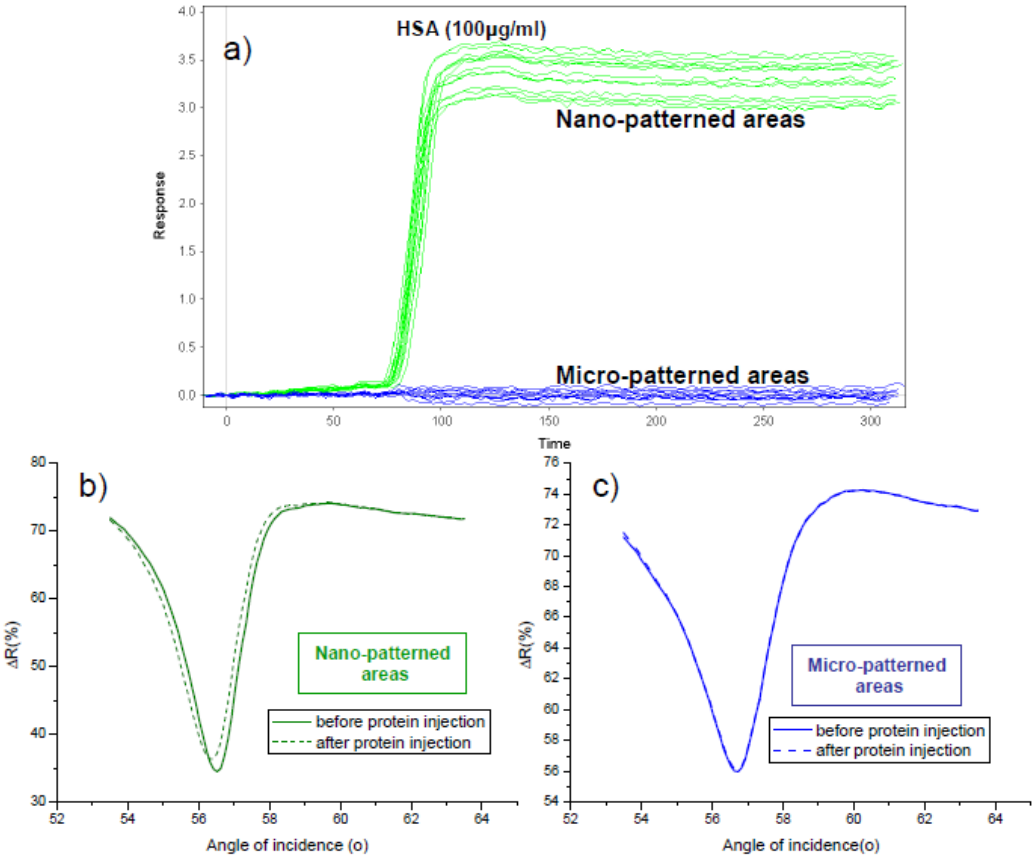

Figure 6.12 a) Sensorgram of proteins immobilization. (Green lines from nanopatterned areas, blue lines from micropatterned areas). Plasmon curves before (solid line) and after (dash line) protein adsorption from b) nano and c) micropatterned areas.

This is confirmed by the SPR difference image after protein immobilization (figure 6.13 b), which shows a brighter color on the nano-patterned areas, indicating that higher protein immobilization took place. The changes on the brightness have been analyzed by an imaging processing software (ImageJ), see Figure 6.13 c. The analysis showed a low intensity from the micro-patterned areas and a high intensity, seven-fold higher, from the nanopatterned arrays.

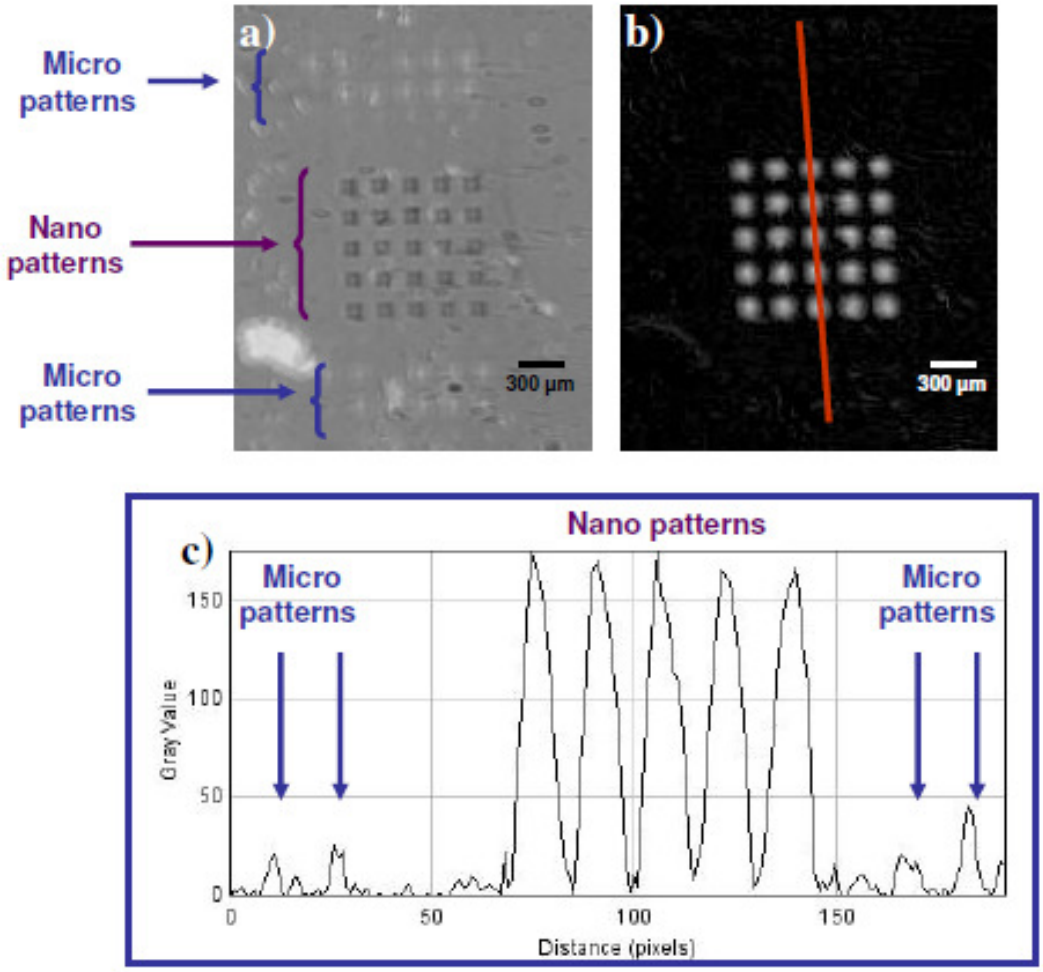

Figure 6.13 a) Optical image of the surface on the flow cell. b) Difference image (before and after protein injection) from the surface. Blue arrows indicate the position of microstructures (5 x 2 matrix), c) Intensity along the red line

As result of the plasmon curve analysis and the SPR protein adsorption assays, we notice a lower sensitivity of detection with the SPRi system for the microstructures due to the reduction of amplitude of the plasmon curves of the microstructures with respect to the nanostructures. This lower detection is not due to a lower protein binding on the microstructured areas (ToF-SIMS experiments showed the selective binding of proteins on the microstructures), it is due to an optical effect: the light is diffracted by the micro grating, so the amount of light that achieves the detector increases. Therefore, the amplitude of the plasmon curve is reduced and as consequence, the sensitivity of detection is reduced. Thus,

gratings at the micro scale are not appropriated for protein detection when SPRi is used as detection platform.

6.2.3 Protein interaction detection at flat and nano patterned areas

In order to evaluate the interaction of proteins on the nanostructured and a non structured surfaces, a prism was fabricated by functionalizing one half of the surface with ppAA (approximately 20 nm thick) and the other half with a PEO-like film (~15 nm). Then, a 5 x 5 matrix of nanopatterned arrays (lines with 450 nm of pitch, 200 nm width) was fabricated on the PEO-like film with the method described previously. A SEM image of the nanopatterned area of the surface is shown in figure 6.14 a. The plasmon curves from the ppAA film and each nanostructured array were obtained (figure 6.14 b). The working angle was set at 56^{O}.

Then, an antibody-antigen recognition experiment was carried out. A flow of acetate buffer (pH 4) was injected for 10 minutes with a flow rate of 20 µl/min, then HSA (20 µg/ml) was injected two times, followed by a blocking step with TTR (10 µg/ml).

Unbound TTR molecules were removed by injection of the buffer solution.

Then Ab-HSA at different concentrations (1, 5, 10, 15, 20, 25, 30 and 50 µg/ml) was injected. All the biomolecular solutions were prepared using the acetate buffer (pH 4).

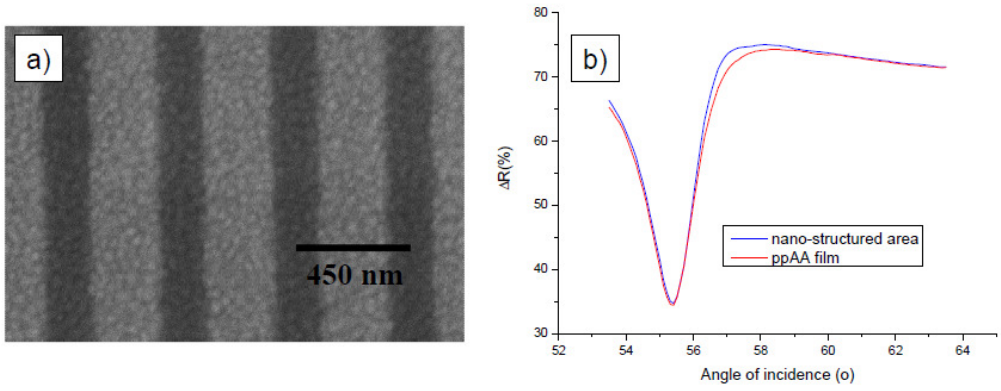

Figure 6.14 a) SEM image of nano-structured area (black: ppAA, grey: PEO-like film) b) Reflectivity curves from ppAA film and nano-structured areas.

The detection sensitivity (S) of the nanopatterned surface and the flat surface, calculated by the slope of the calibration curve in the linear regime, see figure 6.15, are respectively 0.1227 ua*ml/µg and 0.1893 ua*ml/µg. The sensitivity is lower for the nanostructured surface since the bio-active area is smaller than for the flat ppAA surface (44 %).

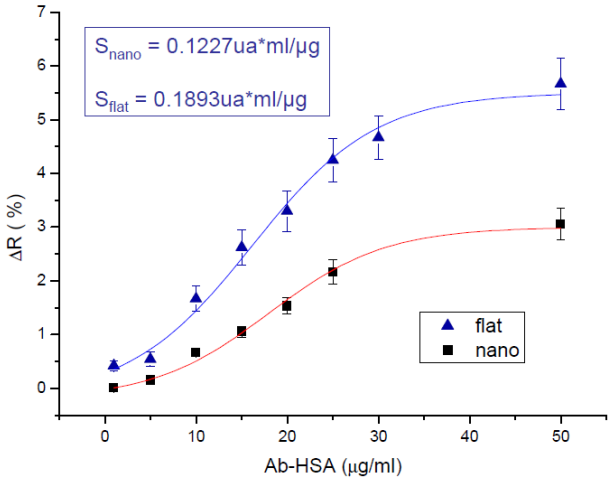

Figure 6.15 Calibration curve from nanostructures and flat surface.

Nevertheless, if the SPR signal is normalized to the ppAA active area on the surfaces (that means, a 100 % on the flat surface and a 44 % on the nanopatterned areas), see figure 6.16, the binding results obtained at low concentrations are similar, whereas a higher binding efficiency of Ab-HSA is observed at concentrations higher than 20 µg/ml.

A better efficiency as the concentration is increased could be explained by a higher surface-protein interaction inside the nanostructured channels (areas of approximately 200 nm width). As the space inside the channels is reduced as compared to a flat surface, the proteins have more probability of interaction with the surface or with other proteins (forming aggregation of proteins) giving place to a higher immobilization.

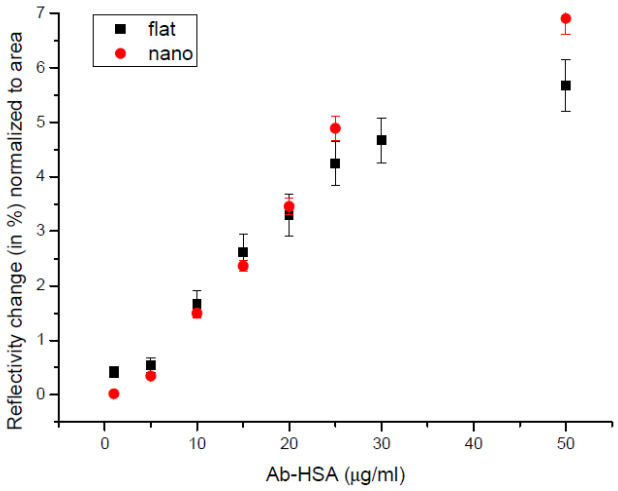

Figure 6.16 Calibration curve from nanostructures and flat surface normalized to the area.

Additional experiments were carried out to study the effect of the pH on the HSA/ Ab-HSA recognition efficiency. For that purpose, a 5 x 5 matrix of nanopatterned arrays (lines with 450 nm of pitch, 200 nm width) was fabricated on the PEO-like film.

HSA (20 µg/ml) was injected two times at pH 4 for immobilization. Then Ab-HSA was injected in PBS solution (pH 7.4) resulting in a desorption of the HSA previously bonded to the surface.

In figure 6.17 a, SPR responses for four injections of Ab-HSA diluted in pH 4 at different concentrations are shown. The increase of reflectivity reflects the adhesion of proteins on the surface. However, when the Ab-HSA is diluted at pH 7.4, a negative signal is observed, see figure 6.17 b, indicating the gradual desorption of the proteins previously bounded (HSA).

Such desorption of proteins when the pH is varied indicates that surface-protein interactions are driven by electrostatic forces, as a weak interaction between protein and surface is established and the pH variation can unbind the immobilized proteins (Müller 2005).

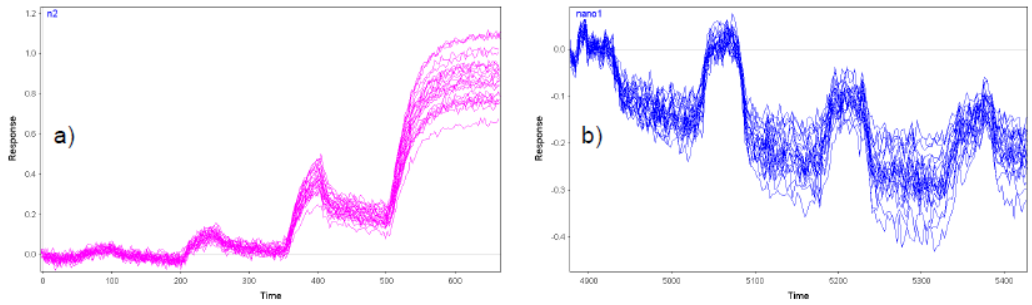

Figure 6.17 Sensorgram of Ab-HSA injections at a) pH 4, b) pH 7.4

6.3 Cellular interaction

The interaction of cells with the patterned surfaces was also explored. An area of 500 x 500 μm^2, made up of of lines of 10 µm width separated 40 µm was patterned, as we described before, on an Indium-tin oxide (ITO) coated glass substrates. Human stem cells were seeded on these substrates in order to check the interaction with the patterned areas. The optical image showed a selective binding of the cells on the ppAA structures, see figure 6.18.

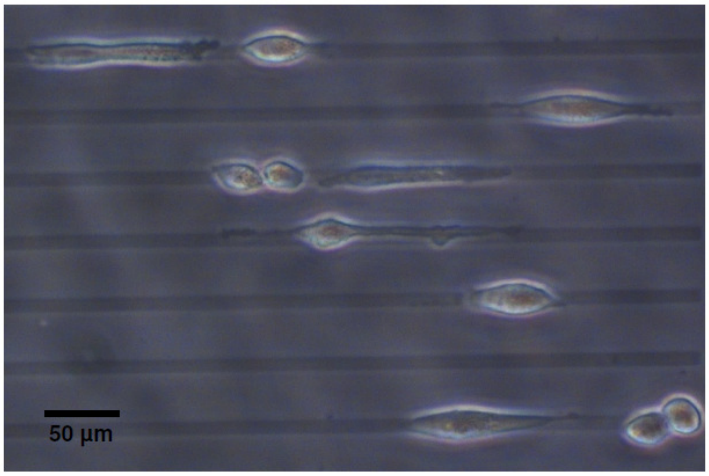

Figure 6.18 Optical image of cells immobilized on the ppAA structures.

The selective binding of cells on the patterned areas confirms the preservation of the non-bioadhesive properties of the PEO-like film during the fabrication process

and shows the capacity of this chemical contrast to tailor the immobilization of cells.

6.4 Discussion and conclusions

Fabrication of patterns in isolating conditions was studied with EBL. Chemical patterns at micro and nano scale (approximately 100 nm width lines) were created at different pitches by combination of EBL and plasma processes. The lithographic process was performed on a PMMA resist spin coated on an isolating layer (PEO-like film), which conferred to the process an added difficulty in the fabrication at nanometric scales due to charging effects. In such demanding conditions, the fabrication with EBL of well patterned arrays at sub-micro scale is a remarkable result (Lussi 2005).

The use of a resist on the fabrication process preserved the non-bioadhesive properties of the PEO-like surfaces allowing the fabrication of chemical contrasts by means of ppAA structures on a PEO-like matrix. Both micro and nanostructures were produced after a proper optimization of the EBL process.

Every fabrication step had a critical influence in the final result, specially working at the nano scale. The use of polymers determines also the final result as they limit the height of the structures, since the possibility of a bad lift-off increases as the amount of polymer deposited increases.

The characterization of the structures with the AFM was carried out analyzing the surfaces before and after being in contact with a protein solution of BSA. The AFM height profile on the ppAA structures showed an increase of height after the immersion in protein solution, which was associated to the adhesion of proteins on the bioadhesive structure. ToF-SIMS and SPRi experiments confirmed not only such selective binding of protein on the ppAA-patterned structures, but also the preservation of the non-bioadhesive properties of the PEO-like film on the fabrication process.

Regarding SPRi experiments, has been checked that the geometry of the pattern has a high influence on the sensitivity of detection. Gratings produced at the micro scale give place to diffraction phenomena that reduce the detection performance,

therefore nano patterned areas are more appropriated when the biointerface is applied in an SPRi detection system.
In addition, SPRi experiments showed a higher binding detection of proteins on surfaces structured at the nano scale than on flat surfaces when high concentration of protein was used. Such higher change in the reflectivity signal from the nanopatterned areas suggests an enhancement of surface-protein interaction due to the nanostructured geometry. A factor to study is the protein transport inside the nanochannels (200 nm width), since a lower diffusion of the proteins could promote protein-protein interactions (creating agglomeration of proteins) and surface-protein interactions.
The immobilization of cells only on the ppAA structures confirms the validity of such surfaces for the selective immobilization of cells.

Therefore, the aim of this work (fabrication of patterned surfaces showing a bio/non bio-adhesive contrasts) is fulfilled with this fabrication process, since the non-bioadhesive properties of the PEO-like matrix are preserved. The drawback of the fabrication process is the number of steps required to obtain a satisfactory pattern. This makes it difficult to determine the origin of faulty steps whenever a discarded sample is produced. However, the microstructures created for cells attachments show an outstanding result, and their application for studying the mechanisms governing the cell shape in response to the pattern geometry (Théry 2006).

Chapter 7

Nanopatterning by EBL exposure of a PEO-like film

The objective of this work is to produce micro and nanopatterned areas on a PEO-like matrix by means of direct exposure of the areas of interest by the e-beam. Brétagnol et *al.* (Brétagnol 2007 a) reported a chemical modification of PEO-like films by exposure to the e-beam. Such exposure produces a decrease on the concentration of the ether bonds that turns the exposed surfaces into bioadhesive films. The importance of this process is that, on one hand, it reduces the conventional lithography steps, and on the other hand it produces a chemical contrast on the surface by direct writing with the EBL. This chapter presents the optimization of the process and the application of the produced nano patterned surfaces as biointerfaces for further SPRi detection system.

The characterization of the micro patterned areas has been performed by ToF-SIMS, AFM and ellipsometry.

7.1 Method of Fabrication

The substrates used in this study were ultrasonically cleaned for 5 minutes in ethanol. Then a film of approximately 15 nm of PEO was deposited on the substrate. Finally, the structures were produced on the surface by direct exposition

of the patterned areas to the electron beam. The fabrication process is described in figure 7.1.

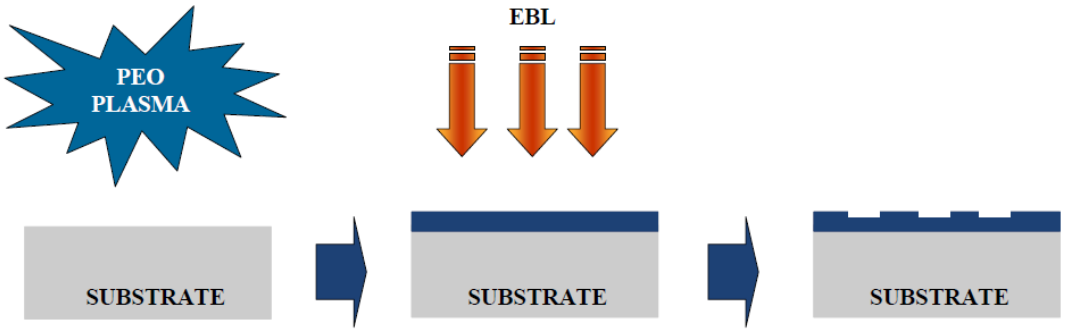

Figure 7.1 Fabrication process by direct e-beam irradiation of PEO-like film.

The dose required to create a pattern depends on the electron energy applied in the lithographic process. As the electron energy is reduced the dose required to make a pattern is also reduced, since the penetration of the electrons into the substrate is reduced as well, resulting in a higher deposited electron energy near the surface and in an increase of the forward scattering, i.e. a broadening of the beam diameter (Mohammad 2010).

The reduction on the energy does not only allow optimizing the exposure time, but also produces a reduction of the backscattered electrons generated during the process, which leads to a better confinement of the electrons on the patterned area. Such reduction can be modeled with the Monte Carlo method by using the software CASINO. Electron penetration in a multilayer made up of a PEO-like film (Diethylene Glycol Dimethyl Ether $(CH3OCH2CH2)_2O$ with a thickness of 20 nm) on silicon has been modeled with CASINO v2.42and the results (electron trajectories and energy distribution) are presented in figure 7.2 . The results show that the reduction of electron energy from 10 to 1 keV results in the reduction of the backscattered electrons (in red) and of the penetration of the electrons (in blue).

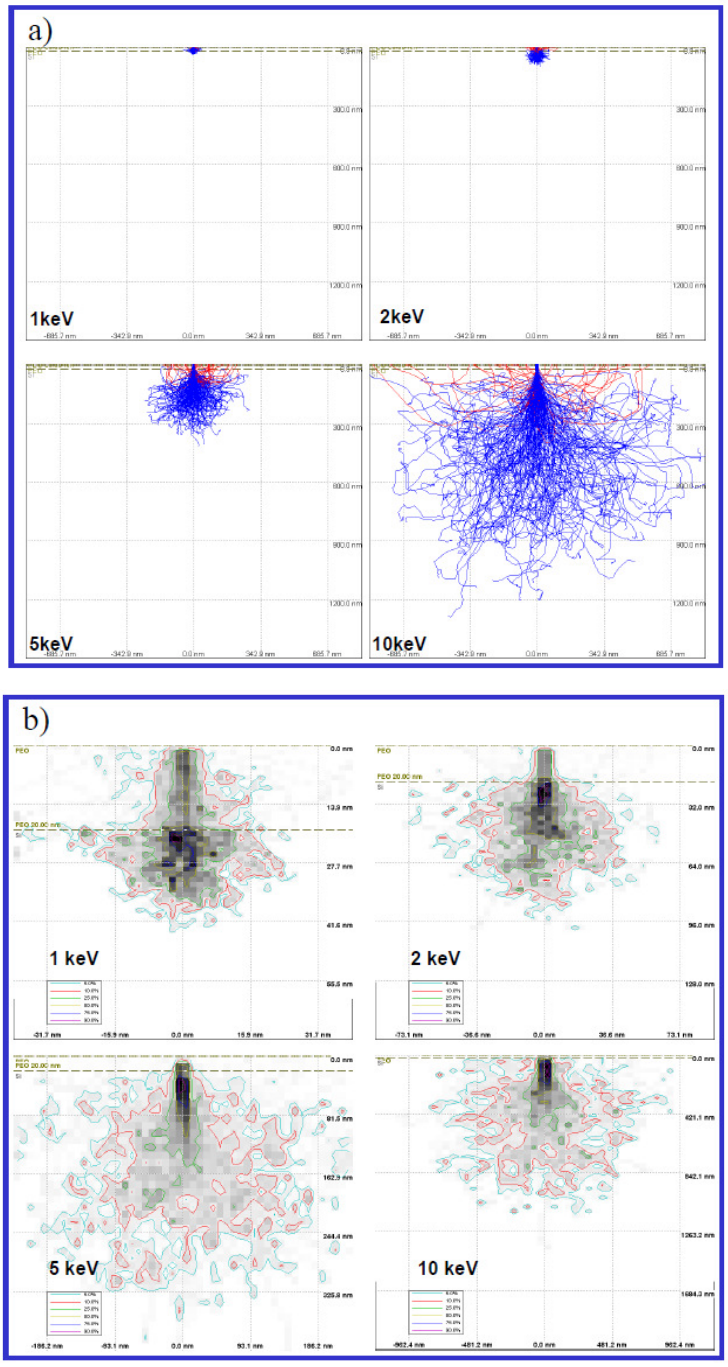

Figure 7.2 a) Simulation with CASINO v2.42 of 200 electron trajectories with an incident beam of 10 nm into a 20 nm layer of PEO deposited on a silicon substrate, b) energy distribution by position.

This result shows that an optimization of the fabrication parameters is necessary to produce bioadhesive nano features. This study will be done in parallel to the

biological characterization of the structured areas. Such optimization has as objective a reduction on the exposure time, that is, a decrease in the energy and the dose applied in the fabrication process to obtain a good immobilization of proteins on the exposed areas.

7.2 Characterization and interaction with proteins

Brétagnol et *al.* (Brétagnol 2007 a) reported the adhesion of BSA on the e-beam irradiated PEO-like film. Fragments of proteins measured by ToF-SIMS analysis increased as the dose applied was increased, reaching a plateau at an irradiation dose of 5000 μCcm^{-2} at 20 keV. Such parameters have been used as reference for the present study. Nevertheless, to improve the protein adhesion (Brétagnol 2007 a), we have reduced the energy of the electrons to 10 keV and have set the irradiation dose to 3000 μCcm^{-2}, which correspond to 6000 μCcm^{-2} at 20 keV.

7.2.1 Characterization by AFM.

The bioadhesive properties of the surfaces patterned at 10 keV of energy and a dose of 3000 μCcm^{-2} were analysed with AFM measurements. Areas of 100 µm x 100 µm were patterned with circles of 500 nm of diameter, separated 5 µm of distance. The sample was analyzed before and after immersion in a solution with proteins (BSA, 20 µg/ml, diluted in PBS solution pH 7.4).

Scanning areas of 25 µm x 25 µm were obtained before and after immersion in proteins. Areas of 15 µm x 15 µm cropped from these images are shown in figure 7.3. AFM profiles along the pattern showed a decrease on height of circa 4 nm on the exposed areas (see figure 7.3 c). After immersion in the protein solution the surface profile is characterized by an increase on height of about 7 nm only on the patterned areas (see figure 7.3 d), indicating a selective adhesion of proteins on the irradiated areas. This result that confirms the modification of the PEO-like film into a bioadhesive area by exposition to the e-beam. As the size of the BSA is circa 14 nm x 4 nm, the increase observed in height (4 plus 7 nm) can be related to the adhesion of a monolayer (in the orientation with 14 nm) or several layers in the opposite orientation.

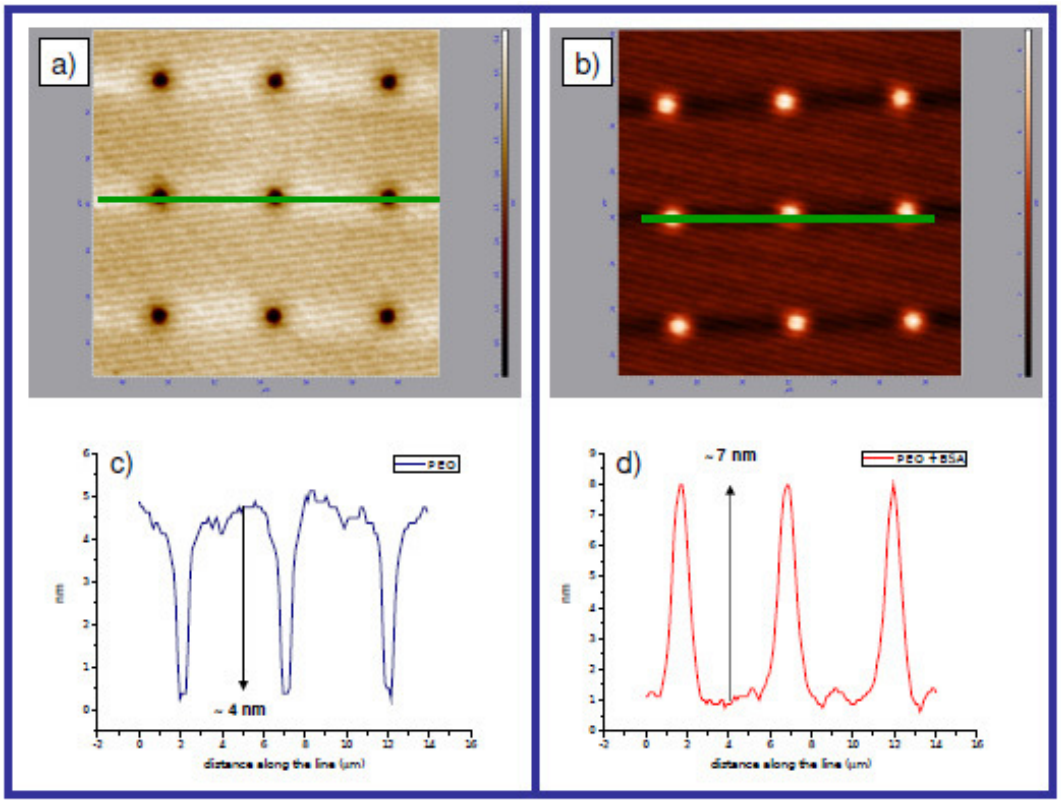

Figure 7.3 a) Topographic image of the patterned surface a) before b) after immersion in proteins (BSA 20 µg/ml). Profile along the green line c) before, d) after immersion in proteins.

7.2.2 Microstructure characterization by Ellipsometry.

Ellipsometry measurements have been performed to study the effect of the radiation exposure on the PEO-like film properties (thickness and refractive index). The measurements have been performed on PEO irradiated at 2 keV.

The thickness of the PEO-film as deposited was determined by ellipsometry (18 nm). Then, the film was patterned with areas of 200 µm x 200 µm with doses ranging from 200 to 1400 µCcm^{-2}, in steps of 400 µCcm^{-2}. The height of the areas exposed to the electron beam was determined by AFM measurements. Finally, the refractive index of the patterned areas was obtained by ellipsometry.

Figure 7.4 a shows an increase of the refractive index together with a reduction of the thickness as the dose applied on the EBL process was increased. The relative index of refraction of irradiated areas versus the bare PEO-like film is shown in figure 7.4 b. Such changes indicate a densification of the film produced by the

exposure to the electrons and confirm the reduction on height detected by AFM experiments due to the e-beam exposure (figure 7.3). Such densification on the exposed areas due to an increment of energy delivered on the area indicate a higher cross-linking of the PEO-film after the exposure to the e-beam.

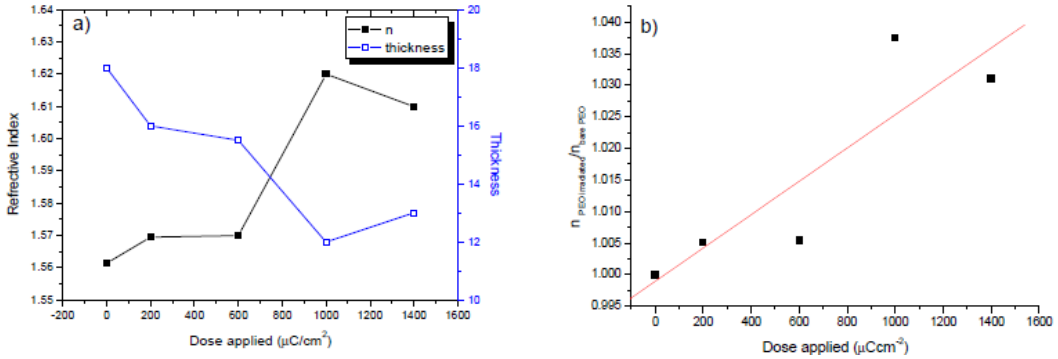

Figure 7.4 a) Variation of thickness (right axis, blue color) and refractive index (left axis, black color) as a function of the exposure dose, b) Relative index of refraction of irradiated areas versus bared PEO-like film. The lines are just a visual guide.

7.2.3 Buffer pH optimization

The influence of the pH in the biological medium is a crucial factor for the immobilization of proteins as previously presented in chapter 6. In order to determine the best pH conditions for promoting the interaction of proteins with the surface, a commercial SPR prism was patterned with arrays of 100 μm x 100 μm squares and an SPR experiment was carried out with proteins diluted in buffers at different pH.

First, a flow of PBS buffer (pH 7.4) was injected for 10 minutes. Then the IgG diluted in PBS buffer (10 μg/ml) was injected. The change of reflectivity measured was very low showing that a very low protein binding occurred (average change in reflectivity of 0.003 %). Then the buffer solution was changed to an acetate solution (pH 4) and was flown for 10 minutes. Finally, the diluted IgG in acetate buffer (10 μg/ml) was subsequently injected, the a change in the SPR signal was monitored on the patterned areas (average change in reflectivity of 0.08 %), see figure 7.5. The low SPR response obtained with this test can be related with the

concentration used in the assays. In the next experiments, higher concentrations were used in order to differentiate better the signal from the noise.

No adhesion of proteins on the bare PEO-like film was monitored for both pH: such result indicates a selective binding of proteins only on the irradiated areas and a better interaction with the surface at low pH (pH 4). For that reason, forthcoming experiments were carried out with acetate buffer. The proteins used in this work (BSA, IgG, Fb, Ubq and HSA) have an isoelectric point of approximately 5.5. Consequently, they exhibit a positive global charge at the pH conditions in which the experiments were performed.

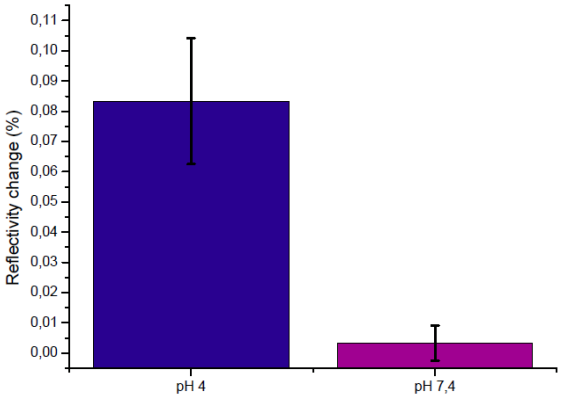

Figure 7.5 SPR signals after injection of IgG (20 µg/ml) at different pH.

7.2.4 Optimization of EBL parameters

Once the pH conditions for protein immobilization were determined, SPR experiments have been carried out in order to optimize the EBL parameters that ensure the best bioadhesive properties of the patterned surfaces.

The first objective was to determine the minimum exposure energy enabling the production of bioadhesive features on the PEO-like surface. Squared arrays of 100 x 100 μm^2 were patterned on a SPR prism at different energies, see figure 7.6 a). Eight different doses were applied for each energy, as detailed in table 7.1.

Energy (keV)	Dose applied (μCcm^{-2})
10	500 / 1000 / 2000 / 3000 / 4000 / 5000 / 6000 / 7000
5	250 / 500 / 1000 / 1500 / 2000 / 2500 / 3000 / 3500
2	100 / 200 / 400 / 600 / 800 / 1000 / 1200 / 1400

Table 7.1 Summary of energy and doses applied in the e-beam process.

The SPR experiment was carried with acetate buffer (pH 4). The plasmon curves from each patterned area and from 2 areas of the PEO-like film were selected. The working angle was fixed at 56.6^{O}. First, a flow of buffer was injected for 10 minutes at a flow rate of 50 μl/min. Then HSA (100 μg/ml) was injected until saturation of the surface. Images taken before and after injection of proteins, as well as the SPR dynamic response were analyzed. The difference image (subtraction of the images obtained before and after the injection of proteins) provided by the SPRi software presents a brighter color on the irradiated areas indicating a selective binding of HSA just on the patterned areas, see figure 7.6 b.

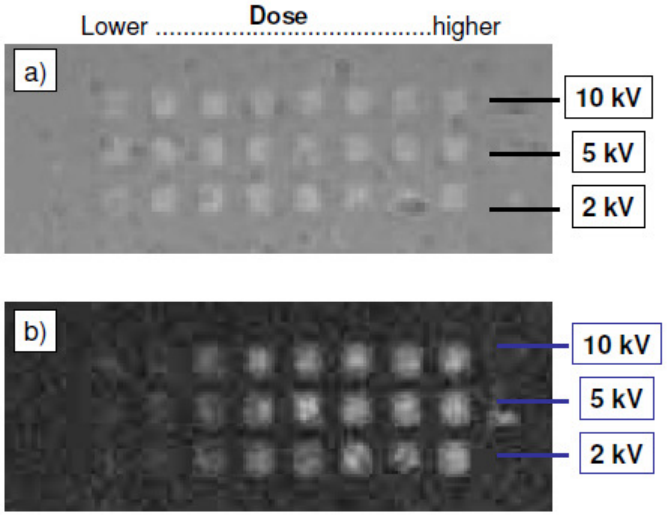

Figure 7.6 a) Optical image of patterned surface in the flow cell, b) difference image (before and after protein injection). Patterned areas were exposed at three different energies: 10, 5 and 2 keV

The change in the plasmon curves of each array and from the bare PEO-like film was monitored. The results show the same trend for the different energies, i.e. protein adhesion is low at low doses (100 and 200 μCcm^{-2} at 2 keV, 250 and 500 μCcm^{-2} at 5 keV, 500 and 1000 μCcm^{-2} at 10 keV) with a gradual increase as the dose increases to reach a plateau at high doses (1000 - 1400 μCcm^{-2} at 2 keV, 2500 - 3500 μCcm^{-2} at 5 keV, 5000 - 7000 μCcm^{-2} at 10 keV) were the adhesion presents the maximum values as shown in figure 7.7. No binding of proteins was monitored on the bare PEO-like film. Additional experiments carried out in areas patterned with an energy of 1 keV at different doses (50, 100, 200, 300, 400, 500, 600 and 700 μCcm^{-2}) showed non binding of proteins in a range of doses of 50 - 400 μCcm^{-2} and a very slight adhesion (around 0.1%) for higher doses.

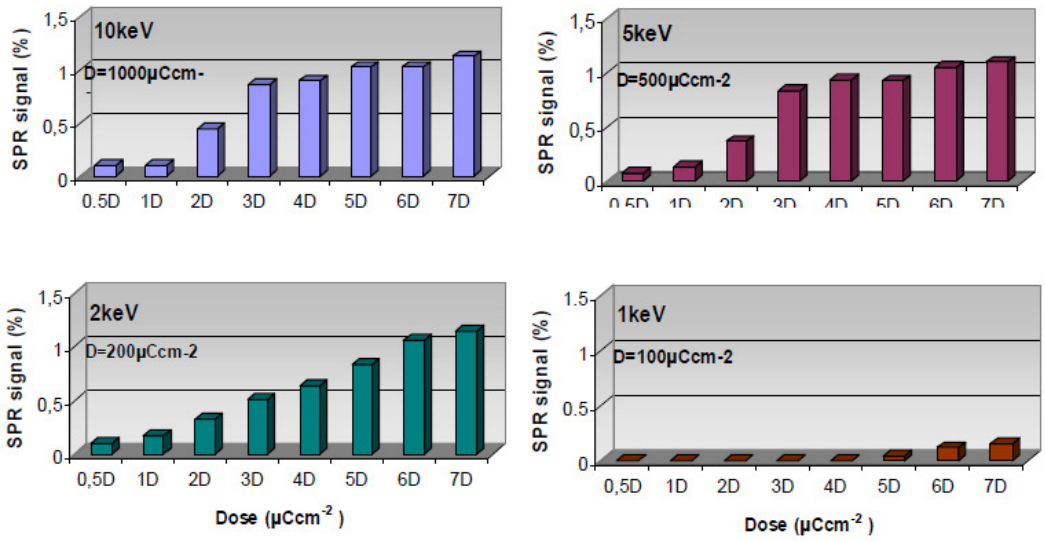

Figure 7.7 SPR response from patterned areas at 10 keV, 5 keV, 2 keV and 1 keV.

The results indicate that 2 keV is the minimum dose required to generate bioadhesive areas on the PEO-like film by exposure to the e-beam. This energy level was used to produce the following samples, in view of the advantages in reduce the fabrication time and enhance electrons confinement on the designed areas (reduced backscattered electrons).

Once the energy on the EBL process has been fixed to 2 keV, experiments to determine the dose in which the adhesion is enhanced were performed. For that purpose, samples were patterned and analyzed by SPR and ToF-SIMS. For SPR experiments, an SPR prism covered with 15 nm of PEO-like film was patterned with squared arrays of 100 x 100 μm^2 with doses ranging from 100 to 1400 μCcm^{-2} (100, 200, 400, 600, 800, 1000, 1200 and 1400 μCcm^{-2}). For ToF-SIMS experiments a silicon substrate was covered with 15 nm of PEO-like film and squared arrays of 200 x 200 μm^2 with doses ranging from 200 to 1200 μCcm^{-2}, in steps of 100 μCcm^{-2} were patterned.

The SPR experiments were initiated with a flow of acetate buffer (pH 4) injected for 10 minutes. Then HSA (50 µg/ml) was injected twice to achieve the saturation of the surface. Images taken before and after injection of proteins, as well as the SPR dynamic response were analyzed. The SPR difference image before and after protein immobilization, see Figure 7.8 a), shows a brighter color on the patterned areas. This brightness increases progressively as the dose used in the fabrication is increased, indicating a higher immobilization of proteins at higher doses.

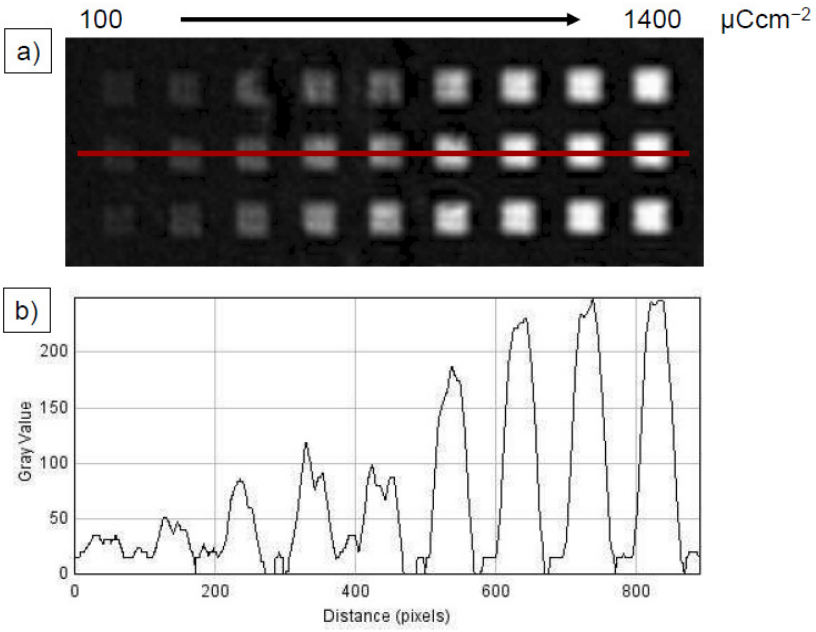

Figure 7.8 a) Difference image (before and after injection of HSA), b) Intensity along the line. Red line is just a visual guide.

The change on the brightness of the difference image was analyzed by an imaging processing software (ImageJ). The intensity on the profile along the pattern (red line on fig 7.8 a) can be seen in figure 7.8 b.

The analysis showed a low intensity at low doses (100 - 200 μCcm^{-2}), followed by a gradual increase of the intensity for doses greater than 200 μCcm^{-2}. At high doses (1000 - 1400 μCcm^{-2}), a plateau in the intensity is achieved, indicating a similar binding of proteins in these areas.

In the SPRi assay, the surface has been saturated of proteins to get the maximum bio-activity achievable at the different doses. The plateau in the intensity at high doses indicates that the maximum bio-activity is achieved in that range of energies.

ToF-SIMS experiments have been performed to confirm this result. Ubiquitin enriched with ^{15}N (Ub-^{15}N) was used in order to obtain an isolated signal coming from the $C^{15}N$ ions, in that way the sensitivity of detection with ToF-SIMS is increased.

The sample was immersed one hour in a solution of Ub-^{15}N diluted in acetate buffer (pH 4) at a concentration of 20 µg/ml, then was rinsed with acetate buffer and finally dried with nitrogen. The intensity of the characteristic $C^{15}N$ was obtained, confirming a higher binding of proteins on the patterned areas as the dose applied in the EBL process was increased. From figure 7.9 it can be seen the low intensity of $C^{15}N$ ions at low doses (200 - 400 μCcm^{-2}). Meanwhile the intensity gradually increases for doses higher than 400 μCcm^{-2} as the dose applied increases. In these results, in contrast to the SPR results, no plateau is reached with doses higher than 1000 μCcm^{-2}: this it is due to the concentration of proteins used in the experiments. In SPRi assays, a high concentration was used to achieve the saturation on the bio-active areas whereas in ToF-SIMS experiments, no saturation of the bio-active areas was achieved.

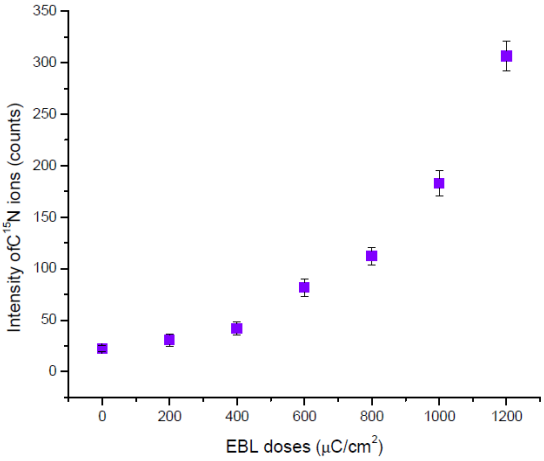

Figure 7.9 ToF-SIMS intensity of the $C^{15}N$ ions versus dose applied

Nevertheless, SPRi and ToF-SIMS data indicate a good immobilization of proteins at 1000 μCcm^{-2} or higher doses. To promote the surface-protein interaction a dose of 1200 μCcm^{-2}, obtained at an energy of 2 keV, was selected for the fabrication of the next samples.

7.2.5 Electrostatic interaction of gold nanoparticles with the patterned surface at low pH

In order to simulate the electrostatic binding between protein and structures, the PEO-like film was patterned with bioadhesive circles of 1 μm of diameter separated 5 μm. A sample was immersed into a solution containing negatively charged gold nanoparticles (-2.5mV, pH 2.5) and other sample into positively charged gold nanoparticles solution (28 mV, p H4). After one hour of immersion, the surfaces were rinsed with acetate buffer (pH 4) and dried with nitrogen.

AFM and SEM images were acquired from the patterned areas. From the SEM image was observed an attachment of negatively charged gold nanoparticles on the patterned surface (figure 7.10 a). However, no significant differences were observed with SEM analysis on samples immersed in positively charged nanoparticles. Nevertheless, AFM image of the surface (see figure 7.10 b) showed no attachment of positively charged nanoparticles on the exposed areas. These results indicate a modification of the electric charge distribution of the patterned

areas, i.e. a higher positive charge on the irradiated than on the non-irradiated areas. In fact, figure 7.10 c shows the interaction of negatively charge nanoparticles on the PEO-like film and on the irradiated area, showing a homogeneous distribution of gold nanoparticles on the exposed area. Meanwhile on the PEO-like film the distribution is not homogeneous. Such results confirm the electric charge modification on the exposed areas.

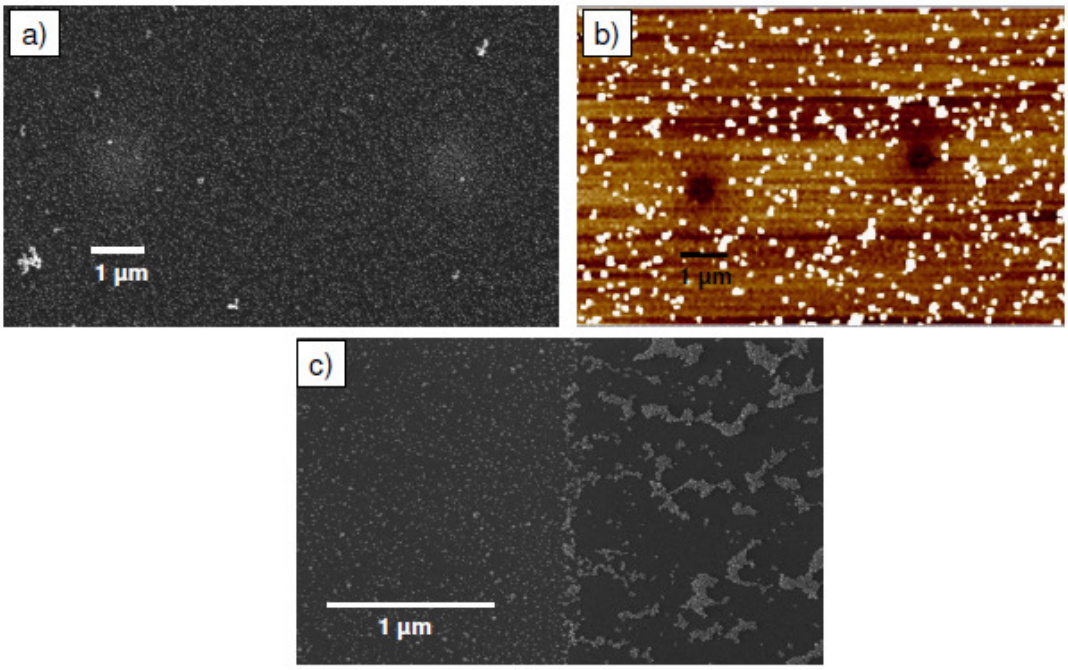

Figure 7.10 a) SEM image of irradiated areas after immersion in a solution of negatively charged gold nanoparticles, b) AFM height image after immersion of the sample in a solution of positively charged gold nanoparticles, c) SEM image showing the homogeneous distribution of negatively charge nanoparticles on the exposed area and their agglomeration on the PEO-like areas.

The characterization with the gold nanoparticles showed and enhanced interaction of negatively charged gold nanoparticles with the irradiated PEO-like film. However, most of the proteins used in this work have an isoelectric point of approximately 5.7 and they show a global positive charge at pH 4. This suggests that the electrostatic interaction of proteins with the patterned surface is not enhanced in these working conditions. Nevertheless, the electrostatic interaction can take place even in the condition tested, since the proteins can show domains on their surface with negative charge even if their global charge is positive. This is

particularly interesting because it might mean that proteins could be immobilized by specific domains on their surface.

7.2.6 Protein nanostructure interaction characterization

The goal of this study was to optimize the EBL conditions to enhance protein binding on nanostructured surface. A set of EBL parameters was used and surfaces were tested with different proteins (HSA, IgG).

SPR prism surfaces with micro and nanostructured areas (100 µm x 100 µm) have been fabricated with a dose of 1200 μCcm^{-2} at 2 keV. The patterning was made of 16 arrays of squares (an area of 100 µm x 100 µm) fabricated in the area exposure mode and 14 arrays of lines at nano scale (500 nm of pitch, 170 nm width) fabricated also in the area exposure mode (vertical step size of 500 nm, horizontal step size of 30 nm). Figure 7.13 b shows a SEM image of the nanostructures obtained after SPRi experiments.

The SPRi experiment started by injecting an acetate buffer (pH 4) for 10 minutes. Then the working angle was fixed at 57.45^{O}. The first step was the immobilization of the protein on the exposed areas. HSA (50 µg/ml) was injected two times in the flow cell followed by an injection of TTR (10 µg/ml), in order to saturate the unbound binding side of the surface. Unbound TTR molecules were removed by injection of the buffer solution. The process was carried out with a flow rate of 25 µl/min.

The immobilization of proteins on the exposed areas generated a shift on the plasmon curves proportional to the amount of protein immobilized. The shift observed was higher on the micro patterned areas, see figure 7.11. In fact, the change in the reflectivity indicates a signal six-fold higher on the micro patterned areas than on the nano patterned ones (SPR response of 6.4 and 1 from micro and nano patterned areas respectively). The result was confirmed by analysis of the difference image, before and after protein adsorption, see figure 7.12, which showed more than five-fold amplified brightness for the micro patterned areas.

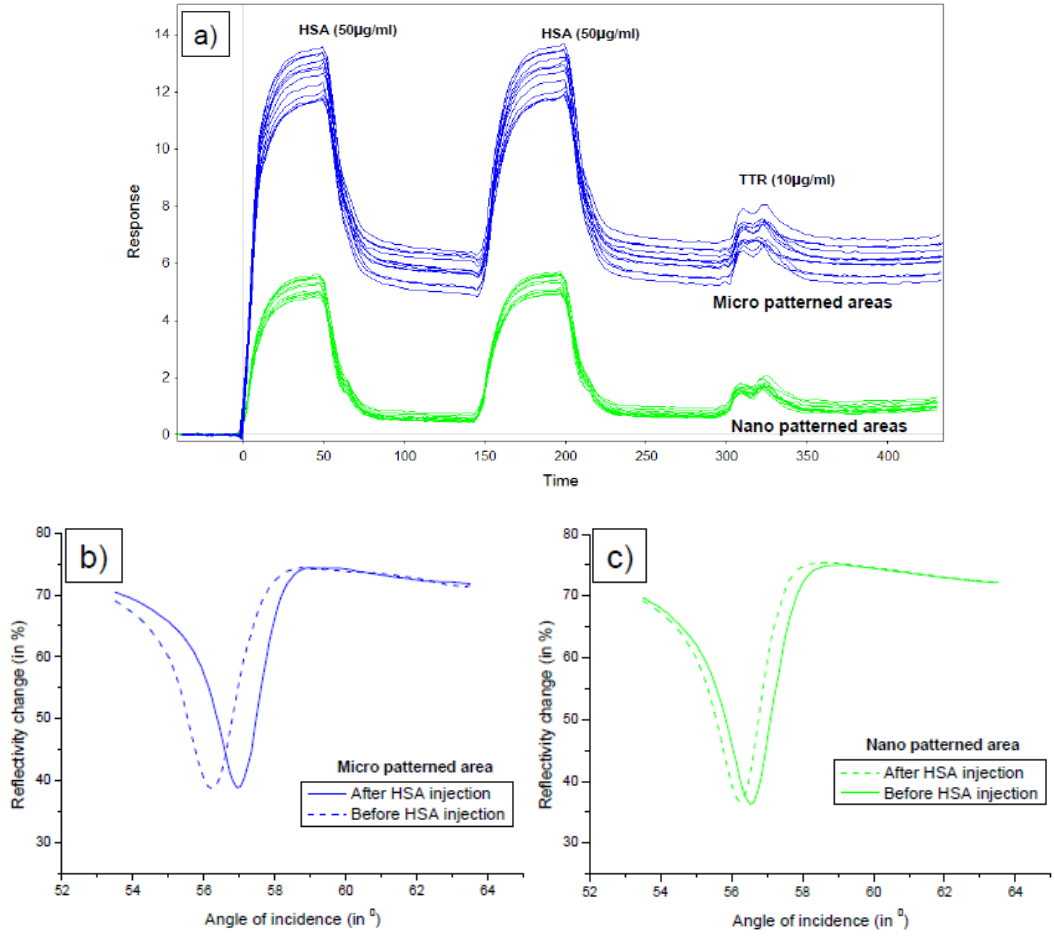

Figure 7.11 a)Sensorgram of protein immobilization. (Blue lines from micro patterned areas; green lines from nano patterned areas). Plasmon curves before (solid line) and after (dash line) protein adsorption from b) micro and c) nano patterned areas.

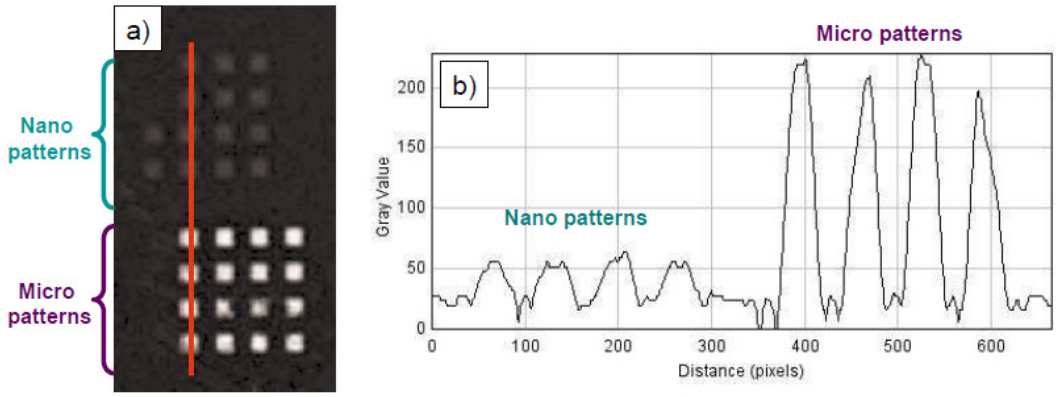

Figure 7.12 a) Difference image after protein injection (Nano patterned areas at top, micro patterned areas on bottom) b) Intensity along the red line.

After the immobilization of proteins on the patterns, an antibody-antigen recognition assay was carried out. Ab-HSA at different concentrations (1, 5, 10, 15, 20, 25, 30 and 50 µg/ml) was injected. The process was performed using the PBS buffer (pH 7.2) with a flow rate of 25 µl/min.

The recognition of the Ab-HSA is higher on the flat-patterned areas. In fact the sensitivity in the micro patterned area (0.1478 a.u.*ml/µg) is three times higher than the obtained for the nano patterned areas (0.052 a.u.*ml/µg), as can bee seen in figure 7.13 a. Considering that the active area in the nano patterning is almost three times lower than the area from the micro patterned area (a 34% of active area) the amount of proteins immobilized per area is the same in both areas, nano and micro patterned, see figure 7.14.

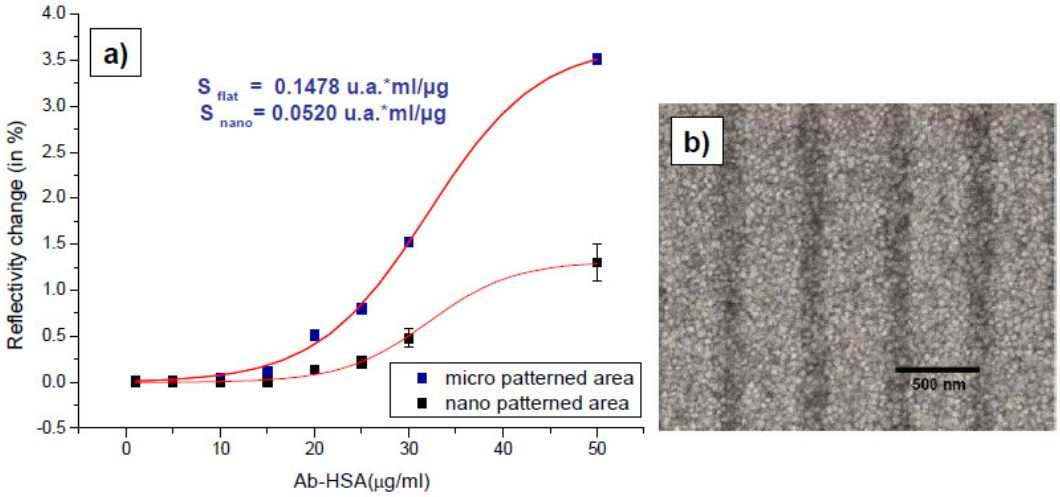

Figure 7.13 a) SPR Calibration curve of micro and nano patterned areas b) SEM image of nanostructures.

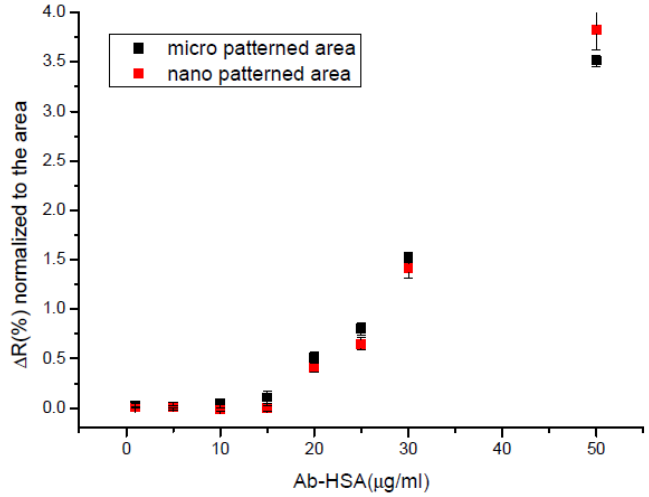

Figure 7.14 SPR Calibration curve of nano and micro patterned areas normalized to the area

During the experiment, no desorption of proteins was observed due to a change on the pH of the buffer (immobilization was done at pH 4, meanwhile the Ab-HSA was injected at pH 7.4) which indicates that the immobilization of the HSA is not due to electrostatic interactions.

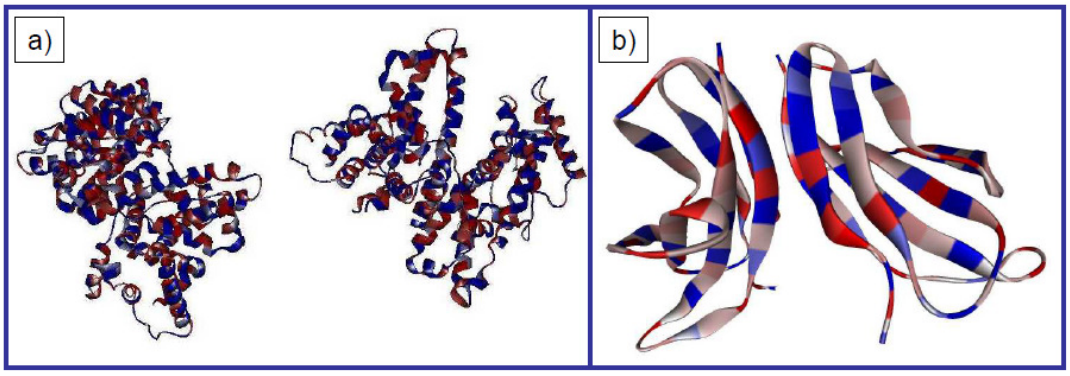

Figure 7.15 High (red) and low (blue) hydrophobic fragments on a) HSA and b) Fibronectin

At pH 4 the hydrophobic interaction of protein with the surface can be promoted (Nardella 1978, Silva 2010) in fact, the HSA protein is rich in hydrophobic fragments (areas in red in figure 7.15 a)) and they are also distributed by all the protein which promotes the hydrophobic interaction with the surface. However, fibronectin is a protein showing a low amount of hydrophobic fragments on the

protein. SPR experiments were carried out injecting fibronectin (20 µg/ml) at pH 4 and no binding of protein on the patterned surface was detected. Such results, together with the electrostatic interaction of gold nanoparticles with the surface and the lack of desorption changing the pH on the SPR experiments indicate a promotion of hydrophobic bonding on the patterned surfaces.

7.3 Cellular characterization

The interaction of cells with the patterned surfaces was also explored. Arrays of lines of 5 µm width separated 20 µm were patterned on an Indium-tin oxide (ITO) coated glass substrate covered with 20 nm of PEO-like film. Stem cells were incubated on these substrates in order to check the interaction with the patterned areas. The optical images showed in most of the samples (93 %) no binding of cells on the surfaces. However, in some samples, a selective binding of cells on the exposed areas was observed.

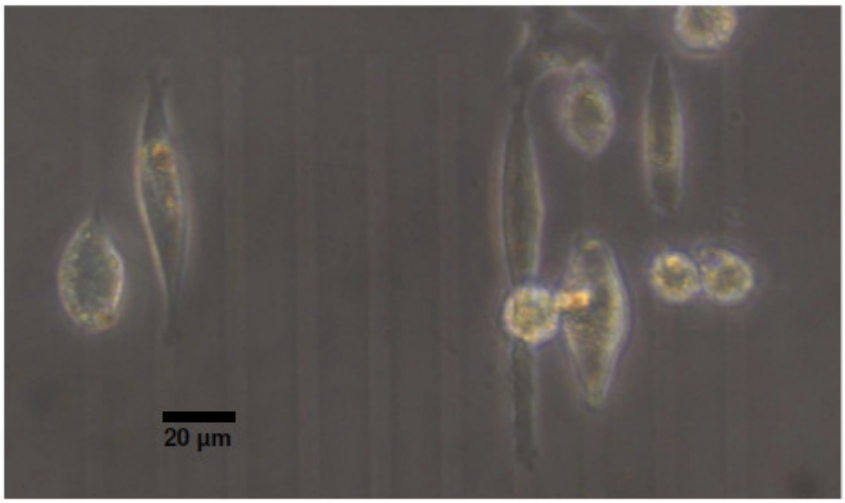

Figure 7.16 Optical image of cells immobilized on the e-beam modified PEO-like film.

7.4 Discussion and conclusions:

Several research groups are currently exploring the direct writing on polymers by electron beam, in order to produce patterns avoiding the use of additional materials, as chemical developers or sacrificial resist (Della Giustina 2009,

Weimann 2001, Balaur 2004). In this chapter, the fabrication of chemical patterns by means of direct writing with EBL was performed.

The fabrication method presented is a simple and direct process, which turns the non bioadhesive properties of the PEO-like film on bioadhesive, allowing a selective binding of proteins on the patterned areas, as was observed by AFM analysis.

The characterization of the exposed areas by SPR and ToF-SIMS showed the dependence of the bioadhesive character on the dose applied on the fabrication. The fabrication process was optimized to reduce the exposure time and enhance the bioadhesive properties of the exposed areas. Such parameters have been applied on SPRi assays showing a selective immobilization of proteins only on the exposed areas and allowing the application of such surfaces for bio-recognition assays. The SPR signal obtained from nano-patterned and flat areas showed no enhancement due to the nano-patterning, in fact, the signal obtained was proportional to the active area.

The electrostatic interaction of gold nanoparticles with the exposed areas indicated a change in the physico-chemical properties of the surface, as the charge distribution was modified. The e-beam modification of the surface enhanced the interaction of negatively charged nanoparticles on the exposed areas at pH around 4. As the proteins show a global positive charge at such pH, and no desorption of proteins was observed when the pH of the buffer was modified (SPR assays), it was concluded that binding of proteins on the irradiated surfaces was promoted essentially by hydrophobic interactions.

Chapter 8

Patterning of gold structures on a non bioadhesive matrix

This chapter is divided into two main sections according to the lithography process used in the fabrication. In the first section, EBL is used for the patterning process, meanwhile FIBL was employed on the second section. PEO plasma and PEO thiol monolayers have been used as non-bioadhesive substrates in both sections.

For the fabrication of patterns using PEO-like films as non-bioadhesive matrix, EBL and plasma processes have been combined. In the process, PMMA has been used to create the patterns and to preserve the non-bioadhesive properties of the PEO-like film during the plasma process. The preparation conditions (spin coating, chemical development and lift-off) of the PMMA resist were described in chapter 6. PEO-thiols chemisorbed on the gold surface are alternatively used as anti-fouling layer in a full thiol based pattern configuration.

8.1 Fabrication of patterns by means of EBL

In this section, patterned gold areas were functionalized by chemisorption of thio-glucose. Immobilization assays were carried out with MBP and anti-MBP Protein.

8.1.1 Gold/PEO-like film chemical contrasts

8.1.1.1 Fabrication process

The complete fabrication process of Au/PEO-like structures was as follows: a thin film of approximately 15 nm of PEO-like film was deposited on an SPR prism, followed by the spin-coating of PMMA. Then, the patterned structures were generated with a SEM equipped with an external beam controller working in electron mode at 10 keV.

The exposed regions of the resist were chemically removed, and then an oxygen plasma was used for removal of the PEO from the opened areas of the PMMA resist. The pattern was in this way transferred to the gold substrate.

The parameters of plasma etching were fixed at a flow rate of 25 sccm of oxygen, a power of 100 W and an exposure time of 75 seconds. The etching rate of the PEO-like plasma (30 nm/min) and the PMMA resist (60 nm/min) was obtained by ellipsometry measurements of the thickness of the PEO-like film and the PMMA layer, before and after a treatment with oxygen plasma at different times (15, 30 and 45 seconds).

For the stripping of the PMMA resist, the sample was immersed in acetone. A scheme of the complete fabrication process is shown in figure 8.1.

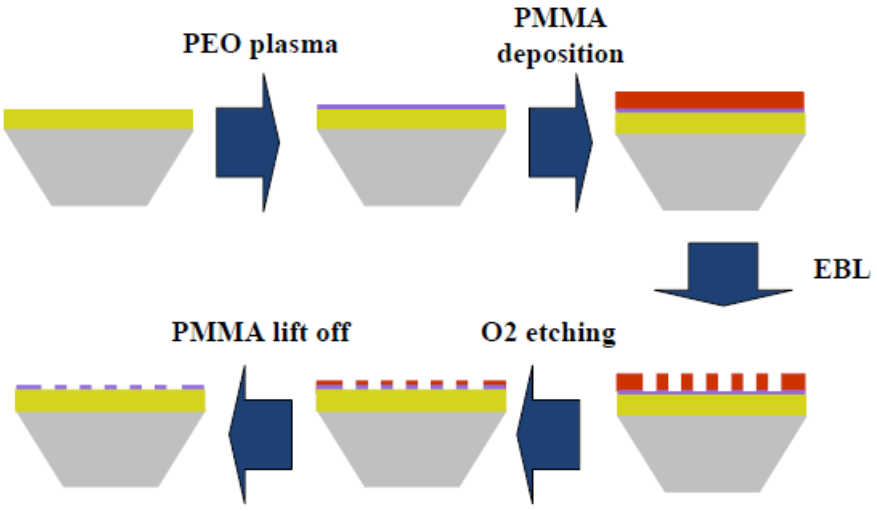

Figure 8.1 Scheme of fabrication process of gold/PEO-like film contrasts by means of a PMMA resist.

8.1.1.2 Characterization of Protein-nanostructure interaction

The immobilization of proteins on the patterned surface was analysed by means of SPRi. For the experiment, 12 arrays of 100 µm x 100 µm were fabricated. Each array was made up of lines with a pitch of 350 nm and a width of 168 nm (48 % of active area). The dose applied on the fabrication was of 675 $pCcm^{-1}$, in single line exposure mode. SEM image of the patterns is shown in figure 8.2.

The experiment started with a flow of PBS (pH 7.4) during 20 minutes at a flow rate of 20 µl/min. The plasmon curves were obtained from every array and from the bare PEO-like film. The working angle was set at 57.83^{O}.

Then PBS buffer was injected for 10 minutes at a flow rate of 20 µl/min, followed by injection of HSA (100 µg/ml) to check the specific binding on the surface (HSA can bind to the bare gold surface but not to a thio-glucose functionalized surface). No binding of HSA was detected, neither on the patterned area nor on the bare PEO-like matrix. This confirms the complete fuctionalization of the gold surface by the thio-glucose.

Then, a solution containing a mix of MBP (50 µg/ml) and anti-MBP (5 µg/ml) was injected.

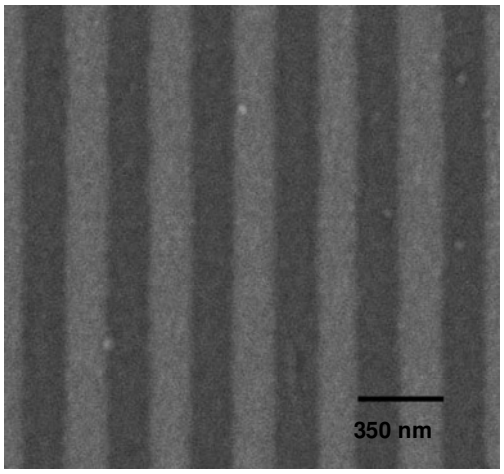

Figure 8.2 SEM image of nano patterned area (black line = PEO-like film, grey line = gold)

The shift on the plasmon curves generated by the immobilization of the biomolecules was monitored and its evolution versus time (figure 8.3 a) showed a change in reflectivity of 1.26 % ± 0.13. Such shift on the plasmon curves can be appreciated on figure 8.3 b) where the plasmon curves of the PEO-like film before and after the protein interaction show no change; this indicates that the anti-fouling properties of the PEO-like film are preserved. However, the plasmon curves of the nano structured areas after the experiment show a shift on the angle position that is related to the binding of proteins.

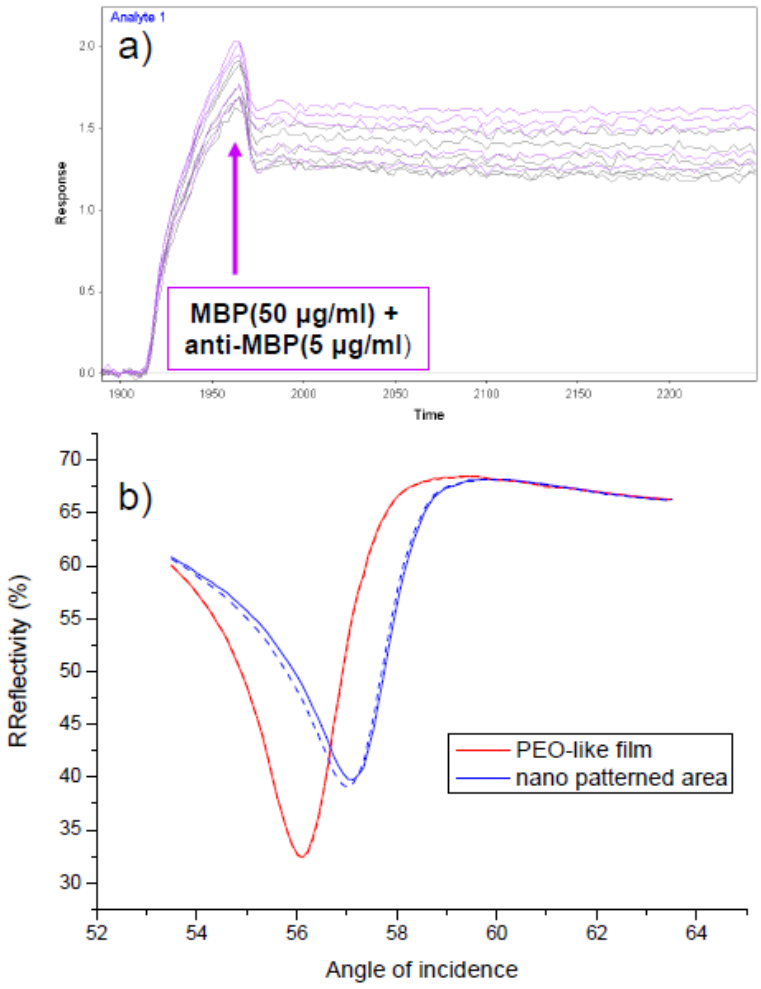

Figure 8.3 a) Sensorgram showing the injection of proteins and b) plasmon curves of PEO-like film (red) and nano patterned areas (blue) before (solid line) and after (dash line) injection of proteins.

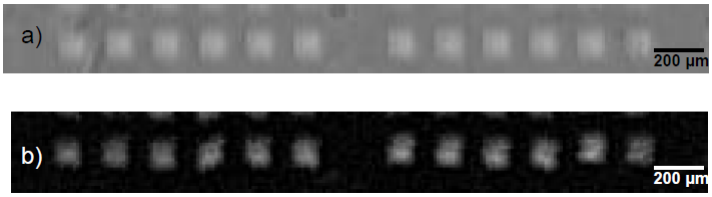

Figure 8.4 a) Optical image of patterned surface on the SPR flow cell, b) SPR difference images (before and after protein injection) of 100 x 100 μm^2 arrays.

The optical image of the patterned areas on the flow cell can be seen in figure 8.4 a). The difference image before and after injection of the proteins (figure 8.4 b) shows a higher brightness on the patterned areas, meanwhile the PEO-like matrix is not altered, confirming a selective binding of proteins on the functionalized gold areas.

The results obtained with the SPRi (sensorgram, position of plasmon curves and difference image before and after the injection of proteins) show a selective binding of proteins on the functionalized gold areas and the preservation of the non-bioadhesive properties of the PEO-like film with this fabrication process.

8.1.2 Gold PEO-thiol chemical contrasts

In this section, the fabrication of chemical contrast of gold with a starting PEO-thiol monolayer was explored. As in the previous section, a PMMA resist was used.

The preservation of the non-fouling properties of the PEO-thiol after the fabrication process with the PMMA resist were first studied by XPS. For that aim, a commercial SPR slide (previously cut into four pieces) was functionalized by chemisorption of PEO thiols. The samples were treated as follows:

Sample type1: Gold surface functionalized with PEO-thiols.

Sample type2: Gold surface functionalized with PEO-thiols, immersed one hour into a solution containing MBP (50 µg/ml diluted in PBS), then rinsed with PBS and dried with nitrogen.

On samples type 3 and 4, a PMMA layer was spin-coated. The samples were baked during 15 minutes at 50 degrees and finally the resist was removed with acetone.

Sample type 3 was analyzed just after the fabrication process and sample type 4 was immersed one hour into the protein solution (50 µg/ml MBP diluted in PBS), rinsed with PBS and dried with nitrogen.

XPS analysis was carried out on the four samples. C1s core level spectra of PEO-thiols before and after the fabrication process shows two major components attributable to alkyl chains and the ether carbon atoms at 285.0 and 286.8 eV, respectively, see Figure 8.6.

The presence of alkyl chains responsible of the non-bioadhesive properties of the PEO-thiols (component at 285.0 eV) is only slightly modified after the fabrication process, showing a reduction from 48.6 % to 47.4 % after the treatment. No presence of nitrogen was detected on the samples immersed in MBP for one hour, indicating the non adhesion of proteins on the surface and consequently the preservation of the anti fouling properties of the PEO-thiol after the fabrication process.

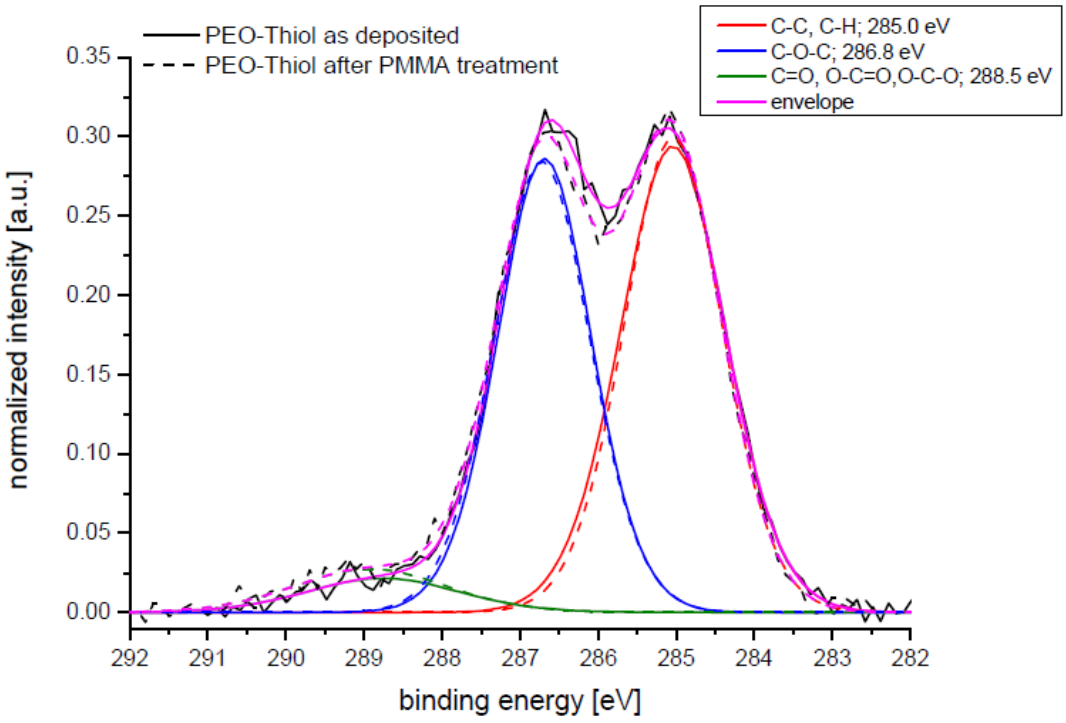

Figure 8.6 C1s core level spectra of PEO-thiol before (solid line) and after (dash line) the PMMA treatment.

8.1.2.1. Fabrication process

The interaction of the patterned surfaces with the proteins was analyzed by SPRi. A SPR prism was created as follows after the chemisorption of the PEO-thiol on the gold surface: a positive resist layer of PMMA was deposited as described previously. 51 arrays of 100 µm x 100 µm were fabricated on the prism working at 10 keV. One square and 50 arrays made up of lines with a pitch of 500 nm and a width of 200 nm (40 % of active area). The dose applied on the fabrication was 900 $pCcm^{-1}$, in single line exposure mode.

The exposed regions of the resist were removed by chemical development as described before. Next step was a plasma oxygen etching (same parameters used in section 8.1) for the transfer of the pattern on the substrate by removing of PEO on the opened areas of the PMMA resist. As the contamination of the surface by fragments of PEO-thiol or PMMA can reduce the binding of the thiol-glucose to the gold surface, a thin film of gold of circa 5 nm was deposited on the sample. Finally, the PMMA resist was removed by immersion in acetone, as described before.

A scheme of the complete fabrication process is shown in figure 8.7 and a SEM image of the pattern is shown in figure 8.8.

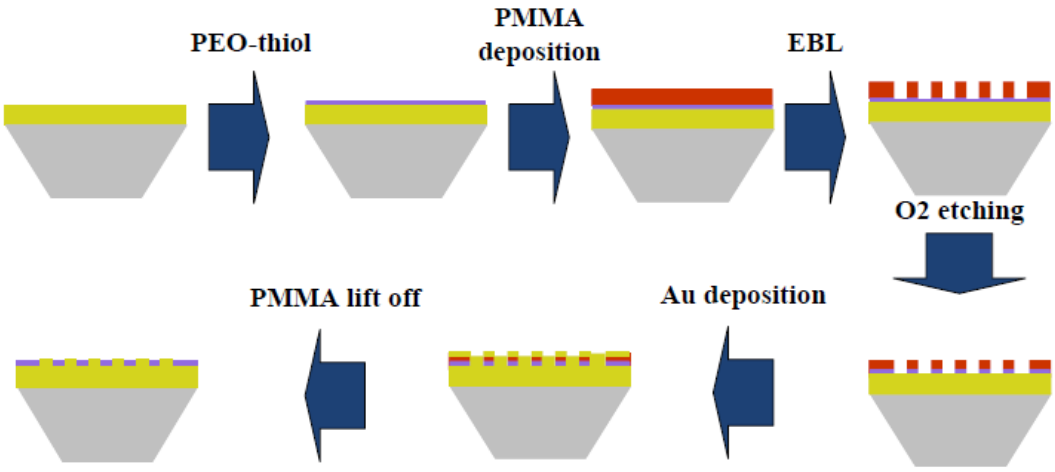

Figure 8.7 Scheme of fabrication process of gold/ PEO-thiol contrasts by means of PMMA resist.

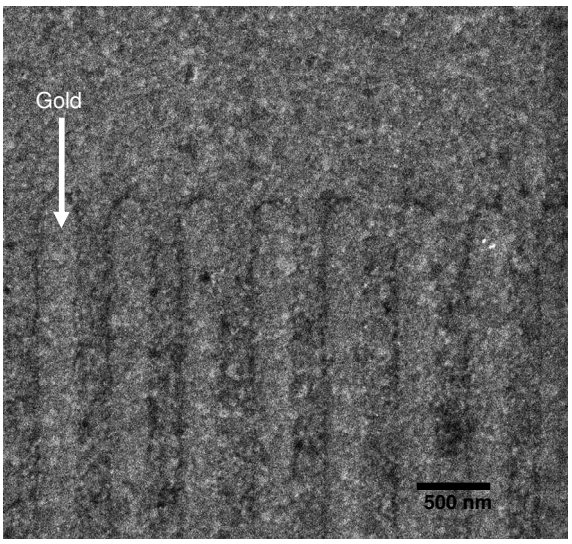

Figure 8.8 SEM image of patterned area. White line in the image indicates the position of gold structures on the pattern.

8.1.2.2 Characterization of protein-nanostructure interaction

The prism described previously was used in the following SPRi experiment. The optical image of the patterns on the SPR flow cell can be seen in figure 8.10 a. First, the surface was exposed to a flow of PBS buffer (pH 7.4) injected for 10 minutes at a flow rate of 20 µl/min. Then, the plasmon curves from the PEO-thiol, the nano structured areas and the square were obtained. The working angle was set at 57.44^{O}. Then MBP was injected at different concentrations (1, 5, 10, 25 and 50 µg/ml) followed by the injection of 5 µg/ml of anti-MBP. All the solutions were made with PBS.

The variation of the SPR signal after every injection of protein can be seen in figure 8.9. A small immobilization of protein take place on the bare PEO-thiol (0.2 % of change in reflectivity) and the signal obtained on the non-structured areas is slightly higher than on the nano patterned area.

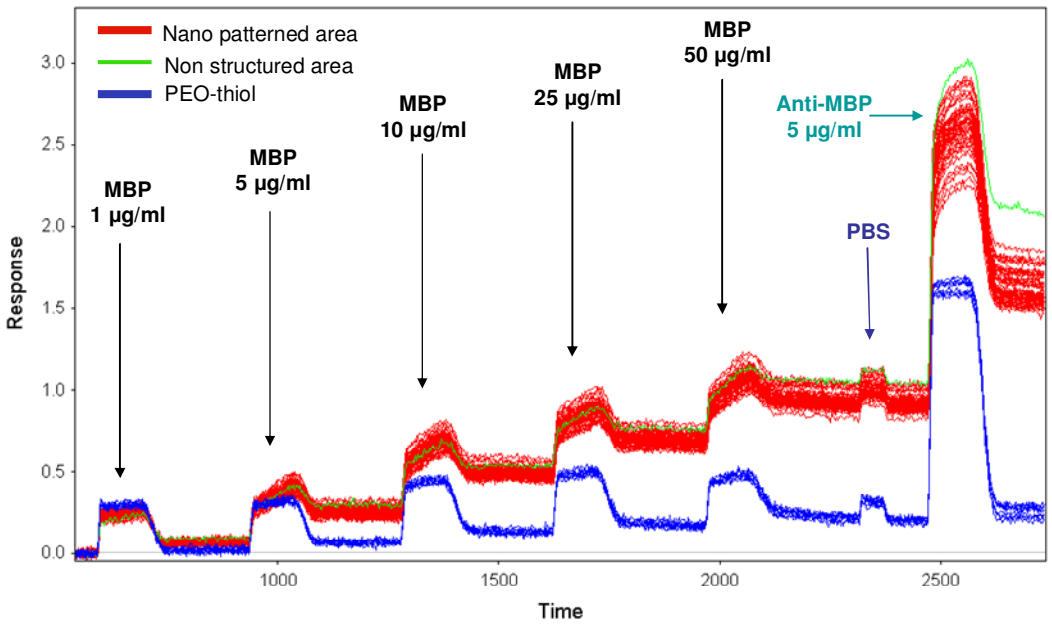

Figure 8.9 SPR Sensorgram showing the protein injections.

The immobilization of proteins on the exposed areas was also detected by an increase in the brightness in the difference image (before and after injection of proteins), see figure 8.10 b.

Binding of proteins on the bare PEO-thiol is also noticeable in the SPR difference image as the brightness of the background is increased (see image before injection of proteins in chapter 3, figure 3.11 a. However, a remarkable result is the detection of the lowest concentration of MBP (1 µg/ml) used in the assay.

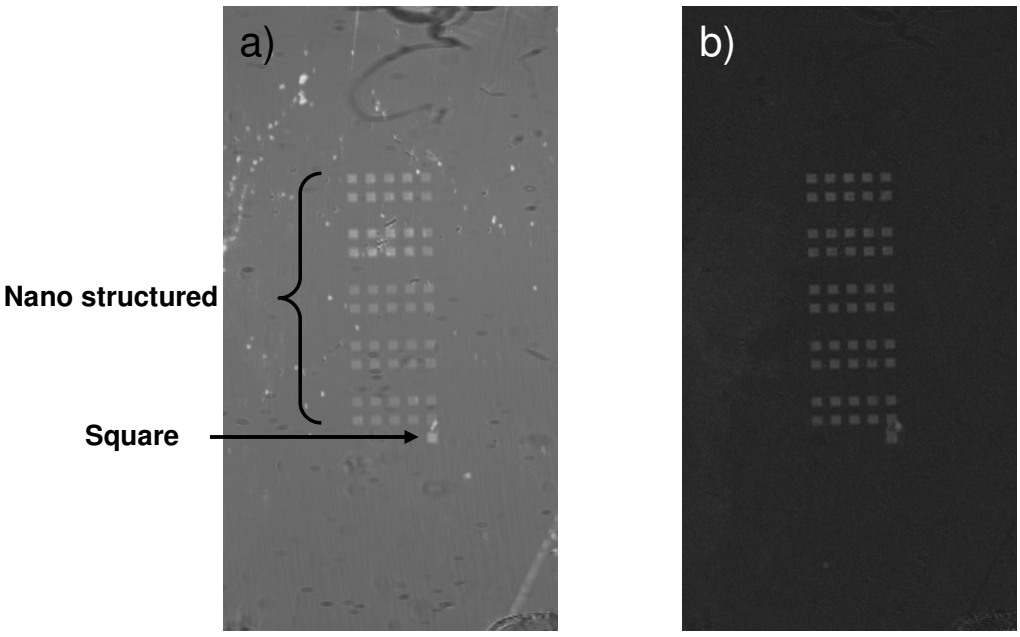

Figure 8.10 a) Optical image of patterns on the SPR flow cell, b) difference image after protein injection. All the arrays had a patterned area of 100 µm x 100 µm.

The higher SPR signal from the non-patterned areas becomes more evident once the background signal (bare PEO-thiol) is subtracted, and especially in the anti-MBP injection, see figure 8.11. The protein binding was also confirmed by the shift in the plasmon curves before and after the final injection of proteins, see figure 8.12.

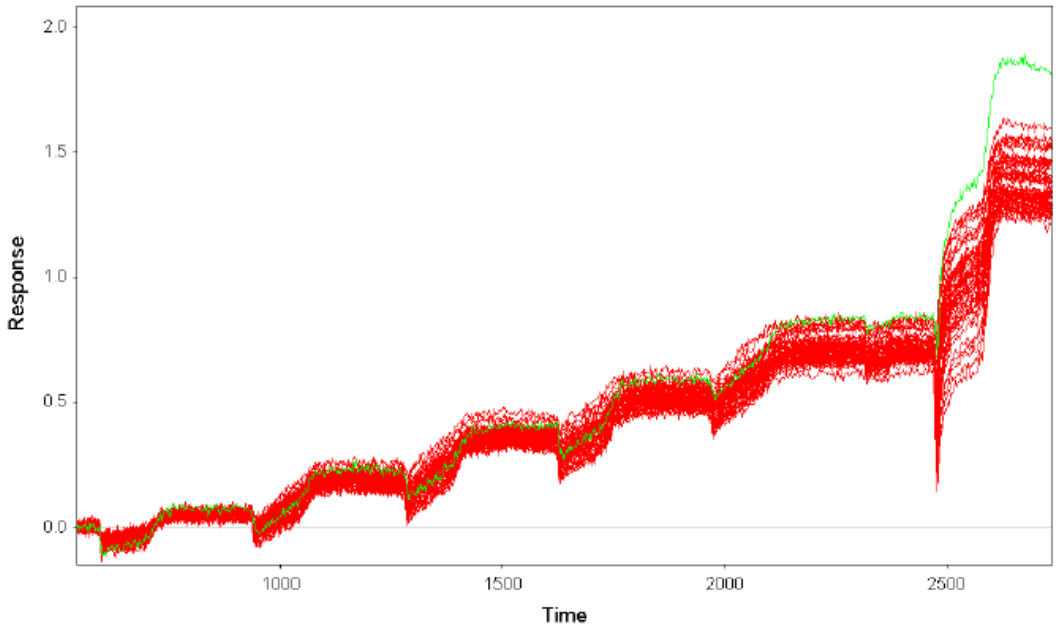

Figure 8.11 Sensorgram of gold surface functionalized with thio-glucose after background (bare PEO-thiol signal) subtraction (red-colour lines from nano patterned areas; green-colour line from non structured area).

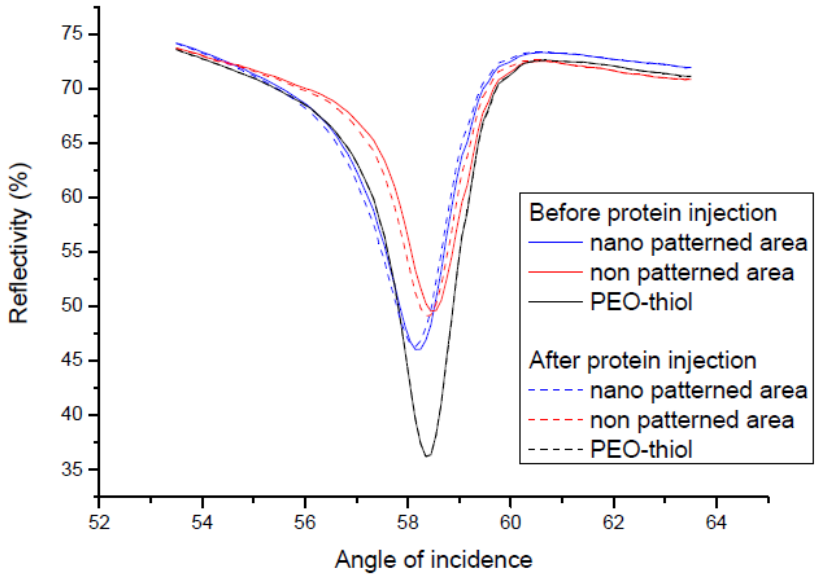

Figure 8.12 SPR plasmon curves before (solid line) and after (dash line) protein injection.

The sensitivity of detection of the MBP on the surface had similar values for the non structured area (0.030 a.u.*ml/µg) and for the nano structured areas (0.032

a.u.*ml/µg), see figure 8.13 a. However, the sensitivity normalized to the active area is more than double in the nano structured areas, see figure 8.13 b.

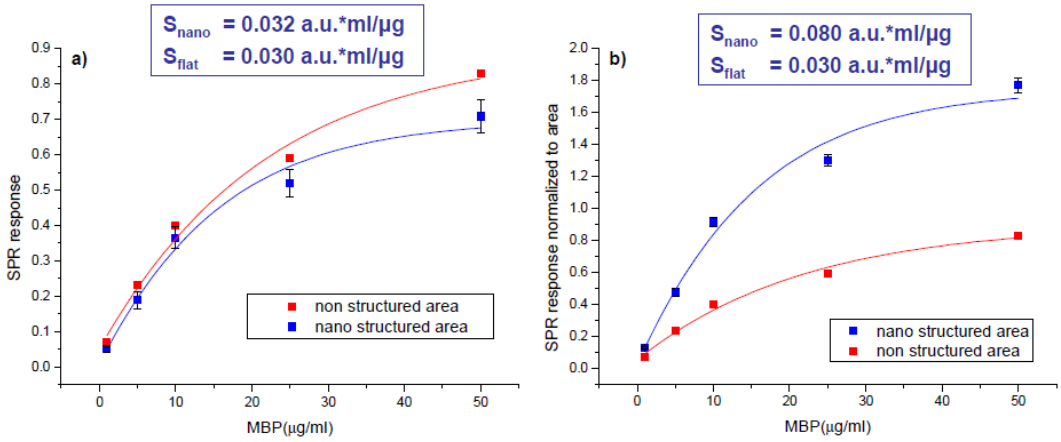

Figure 8.13 a) Calibration curve of the MBP binding to the surface b) Calibration curve of the MBP binding to the surface normalized to the active area.

Regarding the SPR signal obtained from the anti-MBP interaction with the MBP immobilized on the surface a higher response was obtained on the nano patterned areas when the signal is normalized to the active area, as can be seen in figure 8.14.

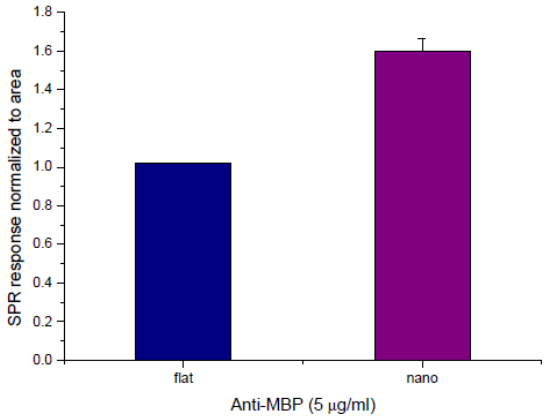

Figure 8.14 SPR response of anti-MBP binding from flat and nano pattern normalized to the active area

The SPRi results obtained in this experiment indicate that the chemical contrast created with this method allow not only the application of the patterned surface as biointerface for biomolecular recognition assays, but also enhance the functional immobilization on the nano-structured areas with respect to flat homogeneous substrates.

8.2 Fabrication of patterns by means of EBL

In this section, the creation of chemical contrasts by the direct removal of the non-fouling film by exposure to the focused ion beam was explored. An scheme of the fabrication process is shown in figure 8.15.

Figure 8.15 Pattern fabrication by means of FIBL

8.2.1 Direct writing on PEO-like film

In this section, the creation of chemical contrasts by the direct removal of the PEO-like film by exposure to the ion beam was explored. For the creation of the patterning, the sample was tilt 52^{O} to position the sample perpendicular to the ion beam. SEM was working on ion mode at 30 keV with a current of 45 pA.

The dose used in the fabrication was 9600 $pCcm^{-1}$ in single line exposure mode.

The arrays created were made up of lines with a pitch of 500 nm and 66 nm width (13 % of active area) as can be seen in the SEM image of figure 8.16.

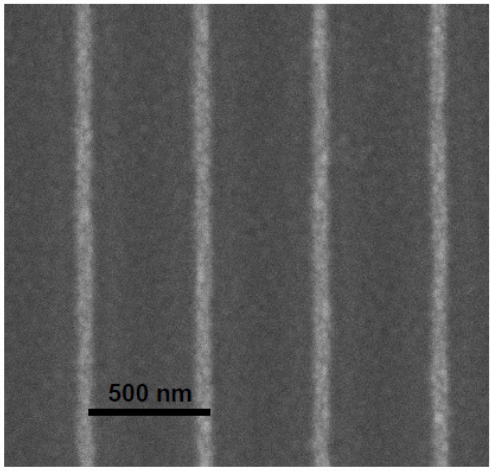

Figure 8.16 SEM images of areas patterned with FIBL.

8.2.1.1 Characterization of protein-nanostructure interaction

For SPRi experiments, 6 arrays of 100 µm x 100 µm were fabricated on an SPR prism. Figure 8.17 shows an optical image of the patterned surface on the flow cell. The patterned prism was left overnight covered by the thio-glucose solution to functionalize the gold surfaces, rinsed with water and dried with nitrogen.

The SPRi experiment started with a flow of PBS for 10 minutes at a flow rate of 20 µl/min. The plasmon curves from the bare PEO-like film and the nano structured areas were obtained. The working angle was set at 57.44^{O}.

Then, HSA was injected to check the specific binding, followed by an injection of 50 µg/ml of MBP and a subsequent injection of anti-MBP (5 µg/ml) at a flow rate of 20 µl/min.

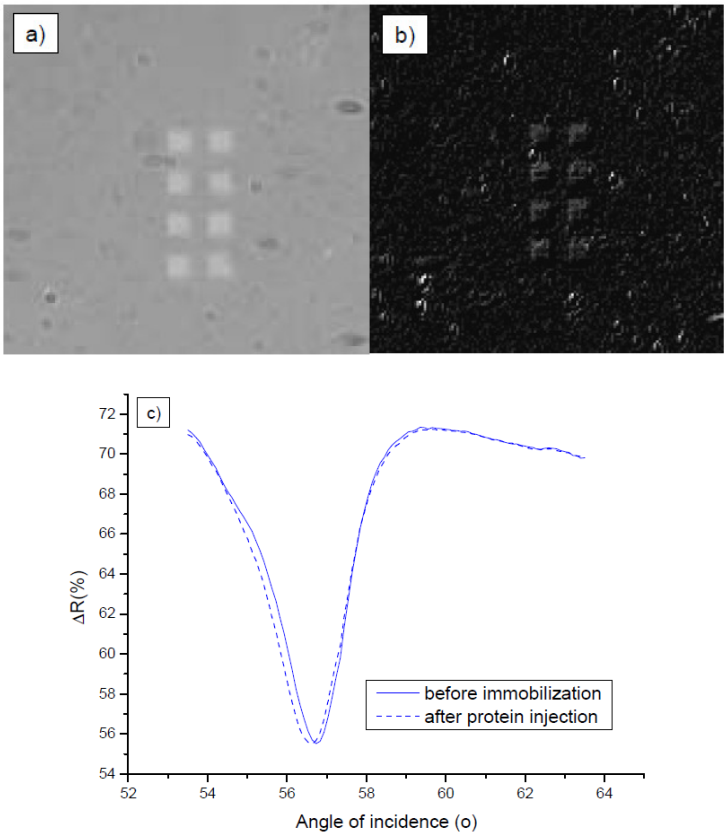

Figure 8.17 a) Optical image of the pattern on the flow cell, b) Difference image after protein injection **c)** Plasmon curves of nano structured areas before (solid line) and after (dash line) protein injection

The SPR difference image, before and after protein immobilization (figure 8.17 a and b) showed a brighter color on the nano patterned areas indicating the binding of proteins on the structures. The binding of proteins was confirmed by the shift in the angle in which the plasmon curves of the nano structured areas are placed after the protein immobilization, see figure 8.17 c), and corroborates the ability of the FIBL as technique for the fabrication of such chemical contrasts.

The difference in brightness in the SPR difference image is not high. This result is in agreement with the low binding detected in the sensorgram (figure 8.18) that showed a change in percent reflectivity of 0.08 % after injection of MBP. Remark that no binding of HSA was detected on the patterned areas, indicating a full coverage of the gold surface by the thio-glucose.

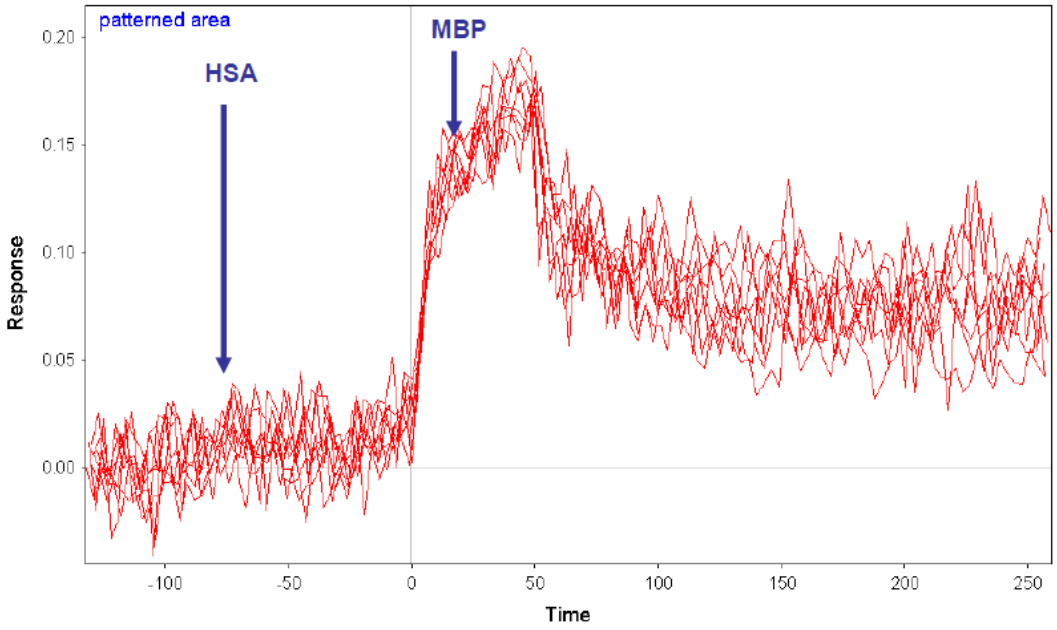

Figure 8.18 Sensorgram from nano patterned surfaces after HSA and MBP injection

As reference data for the surface-protein interaction with the nano patterns, an SPRi experiment was carried out with a non-patterned prism functionalized with thio-glucose. The SPR response from the flat surface after injection of 50 µg/ml of MBP showed a change in reflectivity of 1.17 %.

Regarding the SPR signal obtained in this experiment, a total change in reflectivity of 0.08 %, is low compared with the signal obtained from the non-patterned surface. However, this sample has a low active area (13 %) and when the SPR response is normalized to the active area the immobilization of proteins on the nano patterned areas (1.23 %) results to be higher than on the flat surface (1.17 %).

However, the SPR signal normalized to the patterned area in this experiment does not show a high difference with respect to the flat surface as occurred in the previous chapter with surfaces functionalized with PEO-thiols. A reason that can justify the lower immobilization is the size of the structures created with this technique and the behavior of the PEO-like film in liquid.

To have an input on the most probable origin of this behavior, ellipsometry measurements were carried out in a liquid cell. The results showed the increment on the thickness of the PEO-like film when it is immersed in water, see figure 8.19. Such increase in thickness could be responsible of making the PEO-like film cover part of the gold functionalized surface (lines with 66 nm width), reducing in this way the total active area.

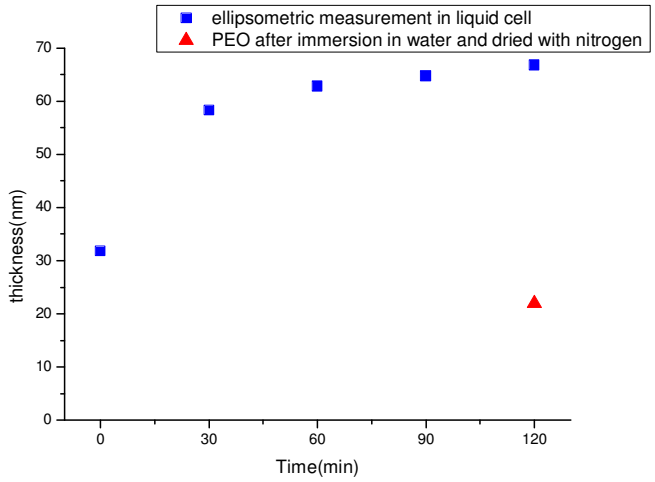

Figure 8.19 Thickness measurements of PEO-like film in water versus time.

8.2.2 Direct writing on PEO-thiols

The creation of patterns by means of the ion beam on a surface functionalized with PEO-thiols was carried out in this section. The aim of this work is the removal of the PEO-thiols from the surface to allow a subsequent functionalization with another thiol, or the direct immobilization of analytes on the patterned area. As the PEO-thiols bind to the gold surface by a sulfur-gold bond, the first study carried out was the analysis of the area exposed to the ion beam in order to determine the presence of the sulfur on the surface after the exposition.

Si substrates covered with 30 nm of gold were used in a ToF-SIMS analysis. Arrays of 25 x 25 μm^2 were fabricated with the ion beam using two acceleration voltages were (5 and 30 keV) and dose ranges between 20 and 5120 μCcm^{-2} with an exponential increment (20, 40, 80, 160, 320, 640, 1280, 2560 and 5120 μCcm^{-2}).

From the ion distribution maps of different fragments of PEO-thiols, gold and gallium in the samples (see figure 8.20) no presence of the Au binding group of the PEO-thiols (HS^- ion) on the exposed areas was revealed (fig 8.20.a). Other components of the PEO-thiols, as the glycol related group ($C2H3O^-$ ion) were also absent in the bombarded areas (fig 8.20.b). Meanwhile, the gold signal (Au^-) is more intense in the surface of the exposed area (fig 8.20.c). These data strongly suggest the removal of PEO-thiols by the ion beam, creating in this way a chemical contrast.

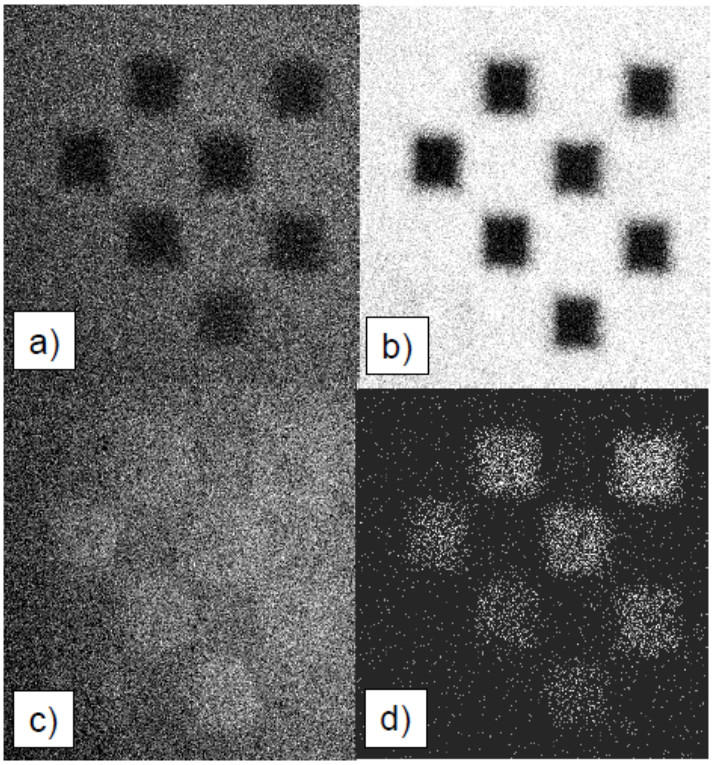

Figure 8.20 ToF-SIMS ion distribution maps of a) HS^-, b) $C2H3O^-$, c) Au^- and d) GaO^- in sample exposed at 30 KeV. Squared patterns have an area of 25 x 25 μm^2

The chemical map showing the GaO^- content on the sample indicates a significant contribution in the patterned surface coming from the ion beam source. Ga may be considered as a potential contaminant, and for this reason we explored different exposure parameters to avoid it as much as possible.

Monte Carlo calculations were generated with the software SRIM-2008.04 in a multilayer made up of a PEO-thiol (CH_2-CH_2-O with a thickness of 10 nm) on gold (50 nm thick). The trajectory of 1000 ions of Ga was consideraded in the calculations.

Results suggest that the amount of Ga in the surface depends mainly in the acceleration voltage. Figure 8.21 illustrates the distribution of the Ga ions at different acceleration voltages, 5 keV (Figure 8.21 a) and 30 keV (Figure 8.21 b). As the removal of the PEO-thiol from the gold substrate is not considered in the calculations, the ion distributions on the bare gold at 5keV and 30 keV (figures 8.21 c and 8.21 d, respectively) were also calculated. In this way the initial and ideal final thickness of the PEO-thiol film were considered.

At 30 KeV, there are more ions implanted in the gold layer than at 5 KeV, however the total amount of Ga present in the surface (2 - 3 nm) is reduced using higher voltages due to an enhanced penetration depth of the ions.

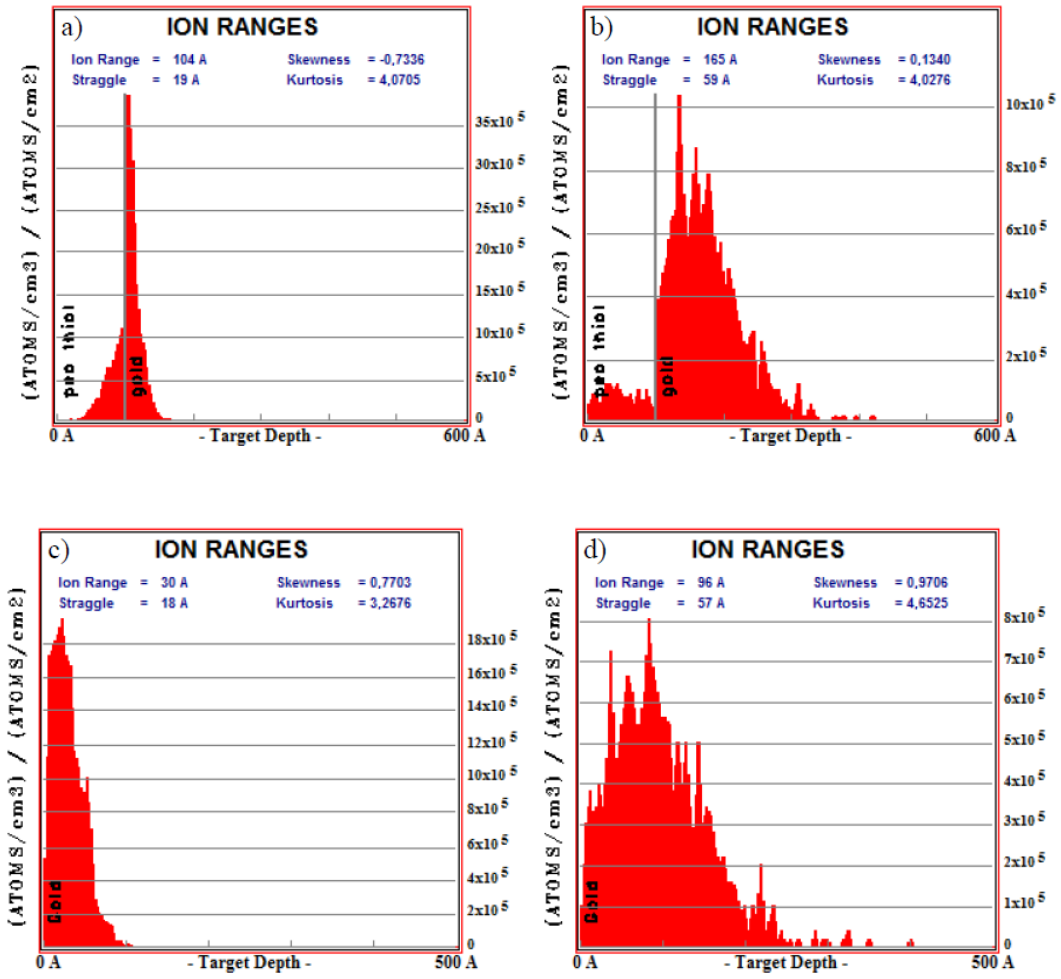

Figure 8.21 Monte Carlo calculation generated with SRIM-2008 software. Calculations were based on the trajectory of 1000 ions of Ga. Ga ions distributions of the initial state: a multilayer of 10 nm of PEO-thiol on a gold substrate at a) 5 keV and b) 30 keV. Ga ions distribution of the ideal final state: at c) 5 keV and d) 30 keV.

The ToF-SIMS data from GaO^- and PEO-thiol fragments normalized to gold are shown in figure 8.22 a) and b), respectively. The background was subtracted from all the data using the minimum of each data set. The experimental data are consistent with the Monte Carlo simulation, since the amount of Ga is higher in the surface at 5 KeV than at 30 KeV. In order to avoid excess of damage to the surface and an unnecessary implantation of Ga, we monitored the removal of the PEO-thiol fragments with the dose that showed saturation for both ions, HS- and C2H3O-, around 160 $\mu C/cm^2$.

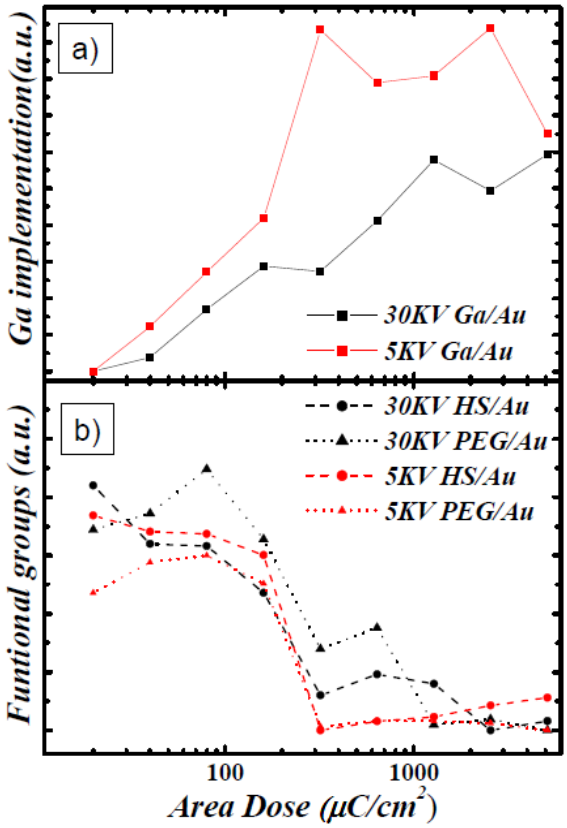

Figure 8.22 a) Relative presence of Ga normalized to Au. b) Relative presence of HS^- and $C2H3O^-$ fragments normalized to Au.

8.2.2.1 Characterization of protein-nanostructure interaction

For SPRi measurements squared arrays of 75 µm x 75 µm were fabricated on a SPR glass slide. The ion beam lithography was performed at 30 KeV and 160 μCcm^{-2}.

SPR experiments were carried out setting the working angle at 58.55°, as determined by working in PBS.

Figures 8.23 a) and b) present optical images of the ion patterned surfaces on the flow cell before and after the protein injection (10 µg/ml of IgG diluted in PBS) respectively.

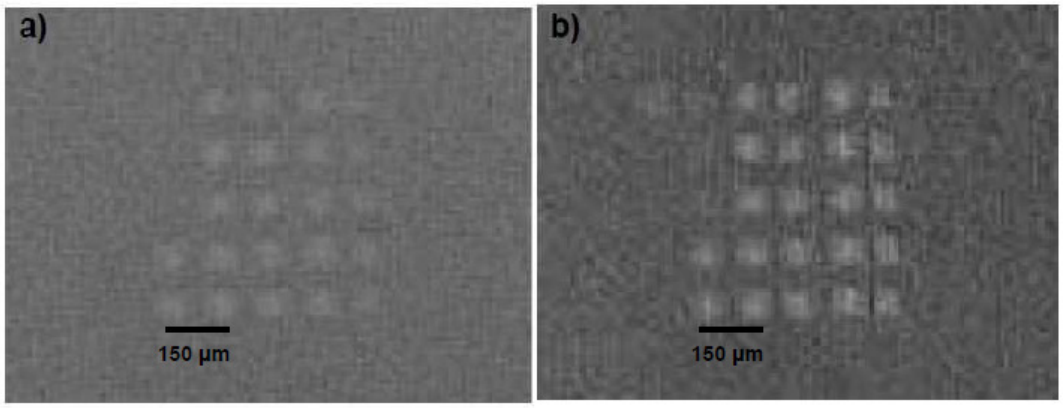

Figure 8.23 Optical image of ion patterned surfaces on the flow cell a) before and b) after IgG injection. 75 µm x 75 µm squared arrays were patterned at 30 keV.

Form figure 8.23, an increase of brightness on the ion patterned areas after protein injection can be observed; it indicates the selective binding of proteins directly on gold areas and confirms the ability of ion beam for the creation of chemical contrasts.

8.3 Discussion and conclusions:

The strategy of this work was the production of contrasts of gold on a non-fouling matrix by means of EBL and FIBL. PEO plasma and PEO thiol were used as non-fouling films.

The gold areas patterned with EBL were functionalized with thio-glucose and the immobilization of protein on the bound thiol showed excellent results for both functionalization methods. Indeed, SPR experiments carried out with PEO-thiols showed that the sensitivity normalized to the active area was higher on the nano patterned areas than on flat functionalized surfaces. Results that are in agreement with published works reporting an enhancement on surface-protein interactions using nanostructured surfaces (Valsesia 2008 a, Valsesia 2008 b).

As no binding enhancement has been detected in previous chapters, when the patterns were fabricated at nanometric scale, a factor to consider as “binding promoter” is that the binding sites were placed below the non-bioadhesive matrix

(approximately 15 nm). Meanwhile in the other chapters the structures were above the PEO matrix or almost at the same level.

Regarding the PEO layers, a better preservation of the non-fouling properties on the PEO-like films after the fabrication process was detected by SPRi experiments, since no binding of protein was observed on them. Meanwhile, a small amount of protein was bound on PEO-thiols (0.2 % change in percent reflectivity). This result can be due to the small reduction of the non-fouling character of the film after the resist treatment as indicated by XPS. In any case, the anti-fouling character of the PEO-thiol on the samples was enough to create chemical contrasts within the gold areas.

Regarding patterns fabricated by means of FIBL, we have to remark the high potential of this fabrication method on biomolecular detection

Although this fabrication method is very time consuming (12-folds than with EBL exposure for the creation of a squared area of 100 μm x 100 μm), reduces tremendously the fabrication steps, avoiding in this way surface contamination, and produce features of reduced dimensions (lines of 60 nm width were produced). Apart from treatment duration, one drawback of the technique is contamination by Ga ions, which has to be minimized.

In conclusion, both fabrication methods can be applied for the creation of chemical patterns and have excellent perspectives for being applied for the fabrication of biointerfaces, as prove the SPR results obtained in this work.

Chapter 9

General conclusions

The necessity of analytical devices for biomolecular recognition guarantying a good performance has opened up an important research area in the last decades. Since the efficiency of interaction between biomolecules and surfaces has a crucial role to achieve high performance detection, a lot of efforts have been done in order to improve the characteristic of the biointerface (the place where the biomolecule immobilization take place). Such efficiency can be influenced by different factors, among them the chemistry or the topographical properties of the surface. For that reason, we have explored the fabrication of surfaces with both a controlled topography and a specific chemistry by using a multidisciplinary approach, in order to produce biointerfaces able to perform reliable biorecognition assays.

In this thesis, new methods for the fabrication of patterns with chemical contrasts were explored. Their application of these new biointerfaces as biosensing platforms was performed by SPRi.

Patterns were created by means of EBL and FIBL processes using a CAD software, avoiding in this way the use of additional physical masks and giving to the process a high flexibility for creating a broad variety of features with a total control of the geometry and the size of the pattern.

Both EBL and FIBL processes can create features at nano scale (around 20 nm) with high repeatability, which makes them to ideal techniques for the pattern fabrication. The disadvantage of these techniques is the speed of fabrication, which was compensated by a reduction of the total area patterned on the surface.
The lithographic methods have been applied to a combination of functional surfaces (bioadhesive and anti-fouling) obtained by plasma polymerization or self-assembled monolayers, in order to obtain a localized immobilization of proteins or cells on the patterned surfaces.
Such combination of functionalization techniques and lithographic processes has been reported if few works in the past years (Brétagnol 2007b, Brétagnol 2007c). The main drawbacks that have to be faced with this fabrication methodology are:

- The lithographic process (and materials employed in the process, e.g. solvents) must preserve the chemical properties of the films for their ulterior application.
- The stitching properties of the polymers reduce the reproducibility of the pattern when the structures are fabricated at sub-micro and nano scale.
- The high number of steps involved in the fabrication process can influence in the final result and increase the fabrication time.

However, these processes show properties not achievable with other techniques, such as a total control on the geometry, size and spatial distribution of the patterned areas. These unique capabilities have motivated the optimization of the fabrication process to use the patterned surfaces as platforms for the study of protein-surface interactions, i.e. as biointerfaces on biodetection systems.

According to the different approaches followed in this work, we can underline the following specific conclusions:

- The plasma conditions for the deposition of acrylic acid films were optimized in order to get a high retention of carboxylic groups and control the stability of the films in water (high retention with low stability and lower retention for high stability for respectively low and high RF power). Such

conditions conferred bioadhesive properties to the acrylic acid plasma deposited films.

- The direct cross-linking with the e-beam of a poorly cross-linked pdAA film was investigated and optimized. The main advantage of this method is that it avoids the use of polymeric resists i.e. simplifying the whole patterning process. The patterns can be developed by using water, which eliminated the need of organic solvents in the lift-off process. Patterns made of e-beam cross-linked pdAA on a PEO-like matrix were successfully created with this method. Characterization of the patterns with proteins showed their preferential binding on the PAA cross-linked areas. However, the presence of bioadhesive residues on the top surface of the PEO-like film was detected by XPS and X-PEEM. These residues can be a consequence of a direct exposure of the PEO to plasma during the PAA deposition. It results in a reduction of the qualities of the chemical contrast, i.e. adhesive-non adhesive, obtained on the surface.
- ppAA structures on a PEO-like matrix were produced by means of EBL using PMMA resists. The preservation of the non-fouling properties of the PEO-like film was fulfilled with the use of the PMMA resist, since the PEO-like film was not exposed to the plasma deposition of the acrylic acid films. In this way, striped patterns with a width down to 100 nm and showing a high chemical contrast were obtained. Moreover, the bioactivities of these surfaces have been studied by SPRi. Localization of proteins adhesion can be controlled at nanoscale. SPRi results indicated a better relative sensitivity on nanopatterned than on micropatterned areas, since the presence of diffraction effects due to the micrometric grating that tends to reduce the reflectivity. In addition, cellular characterization presented a selective binding of cells on the bioadhesive structures.

- PEO-like films were successfully modified by means of EBL turning the non- bioadhesive surface into bioadhesive. Such process reduces considerably the fabrication steps and eliminates the need of resist

processing chemicals. To enhance protein surface interactions, the EBL process required limiting backscattered electrons by reducing electron energy and optimizing the dose applied.

- Chemical contrast made of gold and non-bioadhesive background layers have been produced by means of EBL and FIBL. In particular, gold exposed areas have been successfully functionalized by chemisorption of a thiol. Selected patterning schemes (plasma PEO-like exposed to FIBL and PEO-thiol contrasts created with EBL) showed increased sensitivity per surface area towards protein binding than the micro functional counterparts as derived from SPRi assays.

The different fabrication methods exposed in this work have produced successfully patterns with controlled chemical contrast. A common property these techniques are the controlled custom-made reduction of the active area on the biointerface in order to lower the quantity of the immobilized analyte, which reduces considerably the costs in biological assays.

This study shows that the accurate control of the geometry, size, shape and spatial distribution of the surface patterns is an interesting tool for studying protein-surface interactions on areas patterned at micro, sub-micro and nanoscale. Therefore, the fabrication of patterns at micro and nano scale has allowed studying a possible enhancement of the protein binding detection as a function of the scale. The protein-surface characterization has been carried out by SPRi experiments showing an excellent binding detection on nanostructured areas, phenomenon that has been previously reported in some works (Valsesia 2008 a, Valsesia 2008 b).

SPRi results have shown the influence of the pattern on the detection response: micropatterned areas can result in low detection due to diffraction effects and a better detection was achieved when the patterned areas where placed at a lower level than the non-bioadhesive matrix (15 nm in height from the patterning to the top non-bioadhesive layer). These results indicate that the performance of SPR detection systems can be improved by a proper design of the patterned

biointerface. Therefore, the developed methods represent a very good tool to study the influence of different geometries (lines, circles, triangles,…) at different distribution and sizes on the binding capacity of surface and subsequent detection performance.

Evidently, future work is needed to explore the compatibility of the patterning processes with new materials and characterize the patterned surfaces with different biomolecules and cells are complementary studies that can open an alternative applicability of these surfaces for biosensing applications.

References

Adams, T. M. and R. A. Layton (2010). Creating and transferring patterns—Photolithography. Introductory MEMS, Springer US: 65-94.

Ajay, A. K. and D. N. Srivastava (2007). "Microtubular conductometric biosensor for ethanol detection." Biosensors and Bioelectronics 23(2): 281-284.

Ashwell, G. J. and M. P. S. Roberts (1996). "Highly selective surface plasmon resonance sensor for NO2." Electronics Letters 32(22): 2089-2091.

Balaur, E., T. Djenizian, et al. (2004). "Electron beam-induced modification of organic monolayers on Si(1 1 1) surfaces used for selective electrodeposition." Electrochemistry Communications 6(2): 153-157.

Barnes, W. L., A. Dereux, et al. (2003). "Surface plasmon subwavelength optics." Nature 424(6950): 824-830.

Belkin, S., M. B. Gu, et al. (2009). Surface Functionalization for Protein and Cell Patterning. Whole Cell Sensing Systems I, Springer Berlin / Heidelberg. 117: 109-130.

Bilitewski, U. (2006). "Protein-sensing assay formats and devices." Analytica Chimica Acta 568(1-2): 232-247.

Blanc, D. and S. Pelissier (2001). "Fabrication of sub-micron period diffraction gratings in self-processing sol–gel glasses." Thin Solid Films 384(2): 251-253.

Bobacka, J., A. Ivaska, et al. (2003). "Potentiometric Ion Sensors Based on Conducting Polymers." Electroanalysis 15(5-6): 366-374.

Bonroy, K., F. Frederix, et al. (2006). "Comparison of random and oriented immobilisation of antibody fragments on mixed self-assembled monolayers." Journal of Immunological Methods 312(1-2): 167-181.

Boyan, B. D., T. W. Hummert, et al. (1996). "Role of material surfaces in regulating bone and cartilage cell response." Biomaterials 17(2): 137-146.

Brétagnol, F., A. Valsesia, et al. (2006 a). "Surface Functionalization and Patterning Techniques to Design Interfaces for Biomedical and Biosensor Applications." Plasma Processes and Polymers 3(6-7): 443-455.

Brétagnol, F., M. Lejeune, et al. (2006 b). "Fouling and non-fouling surfaces produced by plasma polymerization of ethylene oxide monomer." Acta Biomaterialia 2(2): 165-172.

Brétagnol, F., O. Kylián, et al. (2007 a). "Micro-patterned surfaces based on plasma modification of PEO-like coating for biological applications." Sensors and Actuators B: Chemical 123(1): 283-292.

Brétagnol, F., A. Valsesia, et al. (2007 b). "Direct Nanopatterning of 3D Chemically Active Structures for Biological Applications." Advanced Materials 19(15): 1947-1950.

Brétagnol, F., A. Valsesia, et al. (2007 c). "Fabrication of functional nano-patterned surfaces by a combination of plasma processes and electron-beam lithography." Nanotechnology(13).

Buzanska, L., M. Zychowicz, et al. (2010). "Neural stem cells from human cord blood on bioengineered surfaces--Novel approach to multiparameter bio-tests." Toxicology 270(1): 35-42.

Bühlmann, P., E. Pretsch, et al. (1998). "Carrier-Based Ion-Selective Electrodes and Bulk Optodes. 2. Ionophores for Potentiometric and Optical Sensors." Chemical Reviews 98(4): 1593-1688.

Catalona, W. J., D. S. Smith, et al. (1991). "Measurement of prostate-specific antigen in serum as a screening test for prostate cancer." New England Journal of Medicine 324(17): 1156-1161.

Ceccone, G., B. O. Leung, et al. (2010). "X-ray spectromicroscopy study of ubiquitin adsorption to plasma polymerized microstructures." Surface and Interface Analysis 42(6-7): 830-834.

Chadwick, et al. (1993). An optical temperature sensor using surface plasmons. Tokyo, JAPON, Japanese journal of applied physics.

Cho, D. L., P. M. Claesson, et al. (1990). "Structure and surface properties of plasma polymerized acrylic acid layers." Journal of Applied Polymer Science 41(7-8): 1373-1390.

Choi, D.-G., H. K. Yu, et al. (2004). "Colloidal Lithographic Nanopatterning via Reactive Ion Etching." Journal of the American Chemical Society 126(22): 7019-7025.

Cooper, M. A. and V. T. Singleton (2007). "A survey of the 2001 to 2005 quartz crystal microbalance biosensor literature: applications of acoustic physics to the analysis of biomolecular interactions." Journal of Molecular Recognition 20(3): 154-184.

Curtis, A. and C. Wilkinson (1997). "Topographical control of cells." Biomaterials 18(24): 1573-1583.

Della Giustina, G., M. Prasciolu, et al. (2009). "Electron beam lithography of hybrid sol-gel negative resist." Microelectronic Engineering 86(4-6): 745-748.

de Silva, A. P., H. Q. N. Gunaratne, et al. (1997). "Signaling Recognition Events with Fluorescent Sensors and Switches." Chemical Reviews 97(5): 1515-1566.

Detomaso, L., R. Gristina, et al. (2005). "Stable plasma-deposited acrylic acid surfaces for cell culture applications." Biomaterials 26(18): 3831-3841.

Drummond, T. G., M. G. Hill, et al. (2003). "Electrochemical DNA sensors." Nat Biotech 21(10): 1192-1199.

Dupas, C., P. Houdy, et al. (2007). Lithography and Etching Processes. Nanoscience, Springer Berlin Heidelberg: 3-40.

Ekgasit, S., C. Thammacharoen, et al. (2005). "Influence of the metal film thickness on the sensitivity of surface plasmon resonance biosensors." Applied Spectroscopy 59(5): 661-667.

Elimelech, M., W. H. Chen, et al. (1994). "Measuring the zeta (electrokinetic) potential of reverse osmosis membranes by a streaming potential analyzer." Desalination 95(3): 269-286.

Falconnet, D., G. Csucs, et al. (2006). "Surface engineering approaches to micropattern surfaces for cell-based assays." Biomaterials 27(16): 3044-3063.

Fan, X., I. M. White, et al. (2008). "Sensitive optical biosensors for unlabeled targets: A review." Analytica Chimica Acta 620(1-2): 8-26.

Ferrari, M., R. Bashir, et al. (2007). Biosensors and Biochips. BioMEMS and Biomedical Nanotechnology, Springer US: 1-20.

Fintschenko, Y. and G. S. Wilson (1998). "Flow injection immunoassays: A review." Microchimica Acta 129(1): 7-18.

Fischer, D., Y. Li, et al. (2003). "In vitro cytotoxicity testing of polycations: Influence of polymer structure on cell viability and hemolysis." Biomaterials 24(7): 1121-1131.

Gates, B. D., Q. Xu, et al. (2004). "UNCONVENTIONAL NANOFABRICATION." Annual Review of Materials Research 34(1): 339-372.

Gerard, M., A. Chaubey, et al. (2002). "Application of conducting polymers to biosensors." Biosensors and Bioelectronics 17(5): 345-359.

Giannuzzi, L. A., F. A. Stevie, et al. (2005). Ion - Solid Interactions. Introduction to Focused Ion Beams, Springer US: 13-52.

Ginger, D. S., H. Zhang, et al. (2004). "The Evolution of Dip-Pen Nanolithography." Angewandte Chemie International Edition 43(1): 30-45.

Grieshaber, D., R. MacKenzie, et al. (2008). "Electrochemical Biosensors - Sensor Principles and Architectures." Sensors 8(3): 1400-1458.

Gryboś, J., M. Marszałek, et al. (2004). "PAC Studies of BSA Conformational Changes." Hyperfine Interactions 159(1): 323-329.

Homola, J. (2003). "Present and future of surface plasmon resonance biosensors." Analytical and Bioanalytical Chemistry 377(3): 528-539.

Homola, J., S. S. Yee, et al. (1999). "Surface plasmon resonance sensors: review." Sensors and Actuators B: Chemical 54(1-2): 3-15.

Jafari, R., M. Tatoulian, et al. (2006). "Stable plasma polymerized acrylic acid coating deposited on polyethylene (PE) films in a low frequency discharge (70 kHz)." Reactive and Functional Polymers 66(12): 1757-1765.

Jurga, M., A. W. Lipkowski, et al. (2009). "Generation of functional neural artificial tissue from human umbilical cord blood stem cells." Tissue engineering. Part C, Methods 15(3): 365-372.

Kasemo, B. (2002). "Biological surface science." Surface Science 500(1-3): 656-677.

Katz, E., I. Willner, et al. (2004). "Electroanalytical and Bioelectroanalytical Systems Based on Metal and Semiconductor Nanoparticles." Electroanalysis 16(1-2): 19-44.

Kelly, J. M., R. D. Short, et al. (2003). "Experimental evidence of a relationship between monomer plasma residence time and carboxyl group retention in acrylic acid plasma polymers." Polymer 44(11): 3173-3176.

Lecuit, T. and P. F. Lenne (2007). "Cell surface mechanics and the control of cell shape, tissue patterns and morphogenesis." Nature Reviews Molecular Cell Biology 8(8): 633-644.

Lejeune, M., F. Brétagnol, et al. (2006). "Microstructural evolution of allylamine polymerized plasma films." Surface and Coatings Technology 200(20-21): 5902-5907.

Lejeune, M., A. Valsesia, et al. (2005). "Structural characterization of nanopatterned surfaces." Surface Science 583(1): L142-L146.

Li, A. P. Hitchcock, et al. (2008). "X-ray Microscopy Studies of Protein Adsorption on a Phase Segregated Polystyrene/Polymethylmethacrylate Surface. 2. Effect of pH on Site Preference." The Journal of Physical Chemistry B 112(7): 2150-2158.

Li, L., S. Chen, et al. (2005). "Protein Adsorption on Oligo(ethylene glycol)-Terminated Alkanethiolate Self-Assembled Monolayers:â€‰ The Molecular Basis for Nonfouling Behavior." The Journal of Physical Chemistry B 109(7): 2934-2941.

Lisboa, P., A. Valsesia, et al. (2007). "Thiolated polyethylene oxide as a non-fouling element for nano-patterned bio-devices." Applied Surface Science 253(10): 4796-4804.

Liu, Y., J. Lei, et al. (2008). "Amperometric sensor for hydrogen peroxide based on electric wire composed of horseradish peroxidase and toluidine blue-multiwalled carbon nanotubes nanocomposite." Talanta 74(4): 965-970.

Livage, J. (1999). "Sol-gel synthesis of hybrid materials." Bulletin of Materials Science 22(3): 201-205.

Lofas, S. (1995). "Dextran modified self-assembled monolayer surfaces for use in biointeraction analysis with surface plasmon resonance." Pure and Applied Chemistry 629: 829-834.

Lord, M. S., M. Foss, et al. (2010). "Influence of nanoscale surface topography on protein adsorption and cellular response." Nano Today 5(1): 66-78.

Love, J. C., L. A. Estroff, et al. (2005). "Self-Assembled Monolayers of Thiolates on Metals as a Form of Nanotechnology." Chemical Reviews 105(4): 1103-1170.

Luong, J. H. T., K. B. Male, et al. (2008). "Biosensor technology: Technology push versus market pull." Biotechnology Advances 26(5): 492-500.

Luppa, P. B., L. J. Sokoll, et al. (2001). "Immunosensors--principles and applications to clinical chemistry." Clinica Chimica Acta 314(1-2): 1-26.

Lussi, J. W., C. Tang, et al. (2005). "Selective molecular assembly patterning at the nanoscale: A novel platform for producing protein patterns by electron-beam lithography on SiO 2/indium tin oxide-coated glass substrates." Nanotechnology 16(9): 1781-1786.

Marrazza, G., I. Chianella, et al. (1999). "Disposable DNA electrochemical biosensors for environmental monitoring." Analytica Chimica Acta 387(3): 297-307.

Marx, K. A. (2003). "Quartz Crystal Microbalance: A Useful Tool for Studying Thin Polymer Films and Complex Biomolecular Systems at the Solutionâ^'Surface Interface." Biomacromolecules 4(5): 1099-1120.

Mohammad, M. A., T. Fito, et al. (2010). "Systematic study of the interdependence of exposure and development conditions and kinetic modelling for optimizing low-energy electron beam nanolithography." Microelectronic Engineering 87(5-8): 1104-1107.

Moharram, M. A., S. M. Rabie, et al. (2002). "Infrared spectra of γ-irradiated poly(acrylic acid)–polyacrylamide complex." Journal of Applied Polymer Science 85(8): 1619-1623.

Mrksich, M. (2002). "What can surface chemistry do for cell biology?" Current Opinion in Chemical Biology 6(6): 794-797.

Mrksich, M. and G. M. Whitesides (1996). "Using Self-Assembled Monolayers to Understand the Interactions of Man-made Surfaces with Proteins and Cells." Annual Review of Biophysics and Biomolecular Structure 25(1): 55-78.

Müller, U. R., D. V. Nicolau, et al. (2005). Biomolecules and Cells on Surfaces — Fundamental Concepts. Microarray Technology and Its Applications, Springer Berlin Heidelberg: 23-44.

Nardella, F. A. and M. Mannik (1978). "Nonimmunospecific Protein-Protein Interactions of IgG: Studies of the Binding of IgG to IgG Immunoadsorbents." The Journal of Immunology 120(3): 739-744.

Nelson, B. P., T. E. Grimsrud, et al. (2000). "Surface Plasmon Resonance Imaging Measurements of DNA and RNA Hybridization Adsorption onto DNA Microarrays." Analytical Chemistry 73(1): 1-7.

Ogaki, R., M. Alexander, et al. (2010). "Chemical patterning in biointerface science." Materials Today 13(4): 22-35.

Oh, B.-K., W. Lee, et al. (2005). "Surface plasmon resonance immunosensor for the detection of Yersinia enterocolitica." Colloids and Surfaces A: Physicochemical and Engineering Aspects 257-258: 369-374.

Owen, G. (1985). "Electron lithography for the fabrication of microelectronic devices." Reports on Progress in Physics 48(6): 795-851.

Park, Y. and G. Choi (2009). "Effects of pH, salt type, and ionic strength on the second virial coefficients of aqueous bovine serum albumin solutions." Korean Journal of Chemical Engineering 26(1): 193-198.

Plowman, T. E., J. D. Durstchi, et al. (1999). "Multiple-Analyte Fluoroimmunoassay Using an Integrated Optical Waveguide Sensor." Analytical Chemistry 71(19): 4344-4352.

Podgorsek, R. P., T. Sterkenburgh, et al. (1997). "Optical gas sensing by evaluating ATR leaky mode spectra." Sensors and Actuators, B: Chemical 39(1-3): 349-352.

Ravindra, N., C. Prodan, et al. (2007). "Advances in the manufacturing, types, and applications of biosensors." JOM Journal of the Minerals, Metals and Materials Society 59(12): 37-43.

Rogers, J. A. and R. G. Nuzzo (2005). "Recent progress in soft lithography." Materials Today 8(2): 50-56.

Rolland, J. P., E. C. Hagberg, et al. (2004). "High-Resolution Soft Lithography: Enabling Materials for Nanotechnologies." Angewandte Chemie International Edition 43(43): 5796-5799.

Roman, G. and et al. (2003). "Block copolymer micelle nanolithography." Nanotechnology 14(10): 1153.

Romano-Rodríguez, A. and F. Hernández-Ramírez (2007). "Dual-beam focused ion beam (FIB): A prototyping tool for micro and nanofabrication." Microelectronic Engineering 84(5-8): 789-792.

Rossini, P., P. Colpo, et al. (2003). "Surfaces engineering of polymeric films for biomedical applications." Materials Science and Engineering: C 23(3): 353-358.

RüÌdel, U., O. Geschke, et al. (1996). "Entrapment of Enzymes in Electropolymers for Biosensors and Graphite Felt Based Flow-Through Enzyme Reactors." Electroanalysis 8(12): 1135-1139.

Salaita, K., Y. Wang, et al. (2007). "Applications of dip-pen nanolithography." Nat Nano 2(3): 145-155.

Sardella, E., P. Favia, et al. (2006). "Plasma-Aided Micro- and Nanopatterning Processes for Biomedical Applications." Plasma Processes and Polymers 3(6-7): 456-469.

Sato, S. and M. T. Swihart (2006). "Propionic-acid-terminated silicon nanoparticles: Synthesis and optical characterization." Chemistry of Materials 18(17): 4083-4088.

Scarano, S., M. Mascini, et al. (2010). "Surface plasmon resonance imaging for affinity-based biosensors." Biosensors and Bioelectronics 25(5): 957-966.

Sergeyeva, T. A., N. V. Lavrik, et al. (1996). "Polyaniline label-based conductometric sensor for IgG detection." Sensors and Actuators B: Chemical 34(1-3): 283-288.

Shankaran, D. R. and N. Miura (2007). "Trends in interfacial design for surface plasmon resonance based immunoassays." Journal of Physics D: Applied Physics 40(23): 7187-7200.

Schueller, O. J. A., D. C. Duffy, et al. (1999). "Reconfigurable diffraction gratings based on elastomeric microfluidic devices." Sensors and Actuators, A: Physical 78(2): 149-159.

Shvarev, A. E., D. A. Rantsan, et al. (2001). "Potassium-selective conductometric sensor." Sensors and Actuators B: Chemical 76(1-3): 500-505.

Siegers, C., M. Biesalski, et al. (2004). "Self-Assembled Monolayers of Dendritic Polyglycerol Derivatives on Gold That Resist the Adsorption of Proteins." Chemistry – A European Journal 10(11): 2831-2838.

Silva, R. A., M. D. Urzúa, et al. (2010). "Protein adsorption onto polyelectrolyte layers: Effects of protein hydrophobicity and charge anisotropy." Langmuir 26(17): 14032-14038.
Siow, K. S., L. Britcher, et al. (2006). "Plasma Methods for the Generation of Chemically Reactive Surfaces for Biomolecule Immobilization and Cell Colonization - A Review." Plasma Processes and Polymers 3(6-7): 392-418.

Smith, H. I. and M. L. Schattenburg (1993). "X-ray lithography from 500 to 30 nm: X-ray nanolithography." IBM Journal of Research and Development 37(3): 319-329.

Swaraj, S., U. Oran, et al. (2005). "Study of influence of external plasma parameters on plasma polymerised films prepared from organic molecules (acrylic acid, allyl alcohol, allyl amine) using XPS and NEXAFS." Surface and Coatings Technology 200(1-4): 494-497.

Th. Wink, S. J. v. Z., A. Bult and W. P. van Bennekom (1997). "Self-assembled Monolayers for Biosensors." Analyst, 1997, 122, 43R - 50R, DOI: 10.1039/a606964i.

Théry, M., A. Pépin, et al. (2006). "Cell distribution of stress fibres in response to the geometry of the adhesive environment." Cell Motility and the Cytoskeleton 63(6): 341-355.

Thierry, B., M. Jasieniak, et al. (2008). "Reactive Epoxy-Functionalized Thin Films by a Pulsed Plasma Polymerization Process." Langmuir 24(18): 10187-10195.

Trnkova, L., V. Adam, et al. (2008). "Amperometric sensor for detection of chloride ions." Sensors 8(9): 5619-5636.

Tsumoto, K., D. Ejima, et al. (2007). "Effects of salts on protein–surface interactions: applications for column chromatography." Journal of Pharmaceutical Sciences 96(7): 1677-1690.

Ulbricht, M. (2006). "Advanced functional polymer membranes." Polymer 47(7): 2217-2262.

Urban, G., T. Nann, et al. (2006). Bio–Nano-Systems. BioMEMS, Springer US. 16: 351-373.

Valsesia, A., I. Mannelli, et al. (2008 a). "Protein Nanopatterns for Improved Immunodetection Sensitivity." Analytical Chemistry 80(19): 7336-7340.

Valsesia, A., P. Colpo, et al. (2008 b). "Use of Nanopatterned Surfaces To Enhance Immunoreaction Efficiency." Analytical Chemistry 80(5): 1418-1424.

Vieu, C., F. Carcenac, et al. (2000). "Electron beam lithography: resolution limits and applications." Applied Surface Science 164(1-4): 111-117.

Weimann, T., W. Geyer, et al. (2001). "Nanoscale patterning of self-assembled monolayers by e-beam lithography." Microelectronic Engineering 57-58: 903-907.

Weiss, M. N., R. Srivastava, et al. (1996). "Experimental investigation of a surface plasmon-based integrated-optic humidity sensor." Electronics Letters 32(9): 842-843.

Werner, C. and A. García (2006). Interfaces to Control Cell-Biomaterial Adhesive Interactions. Polymers for Regenerative Medicine, Springer Berlin / Heidelberg. 203: 171-190.

Wnuk, J. D., S. G. Rosenberg, et al. (2011). "Electron beam deposition for nanofabrication: Insights from surface science." Surface Science 605(3-4): 257-266.

Wouters, D. and U. S. Schubert (2004). "Nanolithography and Nanochemistry: Probe-Related Patterning Techniques and Chemical Modification for Nanometer-Sized Devices." Angewandte Chemie International Edition 43(19): 2480-2495.

Xia, Y. and G. M. Whitesides (1998). "SOFT LITHOGRAPHY." Annual Review of Materials Science 28(1): 153-184.

Xie, X. N., H. J. Chung, et al. (2006). "Nanoscale materials patterning and engineering by atomic force microscopy nanolithography." Materials Science and Engineering: R: Reports 54(1-2): 1-48.

Xu, C., K. Ohno, et al. (2008). "Dispersion of polymer-grafted magnetic nanoparticles in homopolymers and block copolymers." Polymer 49(16): 3568-3577.

Yang, S.-M., S. G. Jang, et al. (2006). "Nanomachining by Colloidal Lithography." Small 2(4): 458-475.

Yao, N., Z. L. Wang, et al. (2005 a). Focused Ion Beam System—a Multifunctional Tool for Nanotechnology. Handbook of Microscopy for Nanotechnology, Springer US: 247-286.

Yao, N., Z. L. Wang, et al. (2005 b). Electron Beam Lithography. Handbook of Microscopy for Nanotechnology, Springer US: 287-321.

Yasuda, H. and T. Hirotsu (1978). "Critical evaluation of conditions of plasma polymerization." J Polym Sci Polym Chem Ed 16(4): 743-759.

List of acronyms

AFM	Atomic Force Microscopy
ALS	Advanced Light Source
ATR	attenuated total reflection
BCPL	block copolymers Lithography
BE	Binding energy
BSA	Bovine Serum Albumin
CCD	charge-coupled-device
CL	Colloidal Lithography
CW	continuous discharge plasma
DC	duty cycle
DEGDME	diethylene glycol dimethyl ether
EBL	Electron Beam Lithography
ECM	extra cellular matrix
EKA	electrokinetic analyzer
Fb	Fibronectin
FIBL	Focused Ion Beam Lithography
FTIR	Fourier Transform Infra-Red Spectroscopy
HSA	Human Serum Albumin
HUCB-NSC	Human Umbilical Cord Blood Neural Stem Cells
Ig	immunoglobulin
IPA	isopropyl alcohol
ITO	indium-tin oxide
LM	Low Magnification
malEFGK	maltose membrane transport system
MaPE-ICP	Magnetic Pole Enhanced-Inductive Coupled Plasma
MBP	Maltose Binding Protein
MIBK	methyl isobutyl ketone
OEG	oligo (ethylene glycol)
PBS	Phosphate buffered saline
pdAA	plasma deposited acrylic acid
PDB	protein data bank
PDMS	polydimethilsiloxane
PEG	Poly (ethylene glycol)

PEO	polyethylene oxide
PMMA	Poly(methyl methacrylate)
PP	plasma polymerization
ppAA	plasma polymers from acrylic acid
PW	pulsed discharge plasma
RSF	Relative Sensitivity Factors
SAMs	self-assembled monolayers
SBL	Scanning Beam Lithography
SEM	Scanning Electron Microscopy
SL	Soft Lithography
SPL	Scanning Probe Lithography
SPM	scanning probe microscopy
SPR	Surface Plasmon Resonance
SPRi	Surface Plasmon Resonance imaging
SVD	singular value decomposition
TIR	total internal reflectance
ToF-SIMS	Time-of-flight secondary ion mass spectroscopy
TTR	Transthyretin
Ubq	Ubiquitin
X-PEEM	X-ray photoemission electron microscopy
XPS	X-ray Photoelectron Spectroscopy
XRL	X-ray Lithography

Publications 2009-2011

* “X-ray spectromicroscopy study of ubiquitin adsorption to plasma polymerized microstructures”, G. Ceccone, B. O. Leung, M. J. Perez-Roldan, A. Valsesia, P. Colpo, F. Rossi, A. P. Hitchcock and A. Scholl, Surf. Interface Anal. 2010, 42, 830–834.

* “Preparation, modification and cellular evaluation of PEG–PEGd supports with titania nanoparticle loads”, Vanessa Sánchez Vaquero, Alvaro Muñoz Noval, Nuria Tejera Sánchez, María Jesus Pérez Roldán, Andrea Valsesia, Giaccomo Ceccone, Josefa Predestinación García Ruiz, Miguel Manso Silván and Francois Rossi, Surf. Interface Anal. 2010, 42, 481–485.

* “Chemical modification and patterning of self assembled monolayers using scanning electron and ion beam lithography”, María Jesús Pérez Roldán, Cesar Pascual Garcia, Gerardo Marchesini, Douglas Gilliland, Ceccone Giacomo, Dora Mehn, Pascal Colpo, Rossi Francois, (submitted).

Abstract

The performance of devices for molecular detection and advanced cell culture rely on the efficiency of interaction between biomolecules or cells and the surface. Consequently, a crucial part of the device is the interface in which the immobilization takes place. Therefore, a multidisciplinary research activity endeavors in their fabrication and optimization.
The factors that influence biomolecule immobilization on solid surfaces are namely their chemistry and the topography, which are the main parameters selected in this work for the design of a diversity of devices..

In this thesis we propose different methods of fabrication of patterned surfaces showing a controlled topography and a specific chemistry. The fabrication was carried out combining different materials and different techniques for the functionalization and patterning of the surface. The surfaces were functionalized with materials selected by their bio or non-bioadhesive properties that were obtained by plasma polymerization or thiol self-assembly. Patterns were created by means of electron or ion beam lithographic methods and their combination with the surface functionalization produced chemical patterns at the micro and nano scale.
The patterned areas were chemically and morphologically characterized and their interaction wit proteins and cells was studied. Finally, their application as biointerfaces in biosensing platforms was proved by surface plasmon resonance imaging.

Resumen

El rendimiento que puede presentar un dispositivo dedicado a la detección molecular o al cultivo celular depende en gran parte de la eficiencia lograda en la interacción entre biomoleculas o células y la superficie. En consecuencia, una parte crucial del dispositivo es la interfaz en la que tienen lugar los procesos de inmovilización. En los procesos de fabricación y optimización de estos dispositivos se abre un campo multidisciplinar de investigación. Los factores que influyen la inmovilización de biomoleculas en las superficies sólidas son, principalmente, la química y la topografía superficial, parámetros con los que se han diseñado diversos dispositivos en el presente trabajo.

En esta tesis se proponen diferentes métodos de fabricación de patrones superficiales que permiten controlar tanto la topografía como la química de la superficie.

En la fabricación de los patrones se han utilizado diferentes materiales bio-funcionales y diferentes técnicas de litografía (litografía por haces de electrones e iones) y el contaste químico de estos patrones fue conseguido combinando. Los materiales utilizados fueron seleccionados atendiendo a sus propiedades bio-adhesivos o anti bio-adhesivos con biomoleculas y células y fueron obtenidos tanto por procesos de plasma como por autoensamblaje. Las superficies creadas con estos materiales mediante técnicas de litografía de electrones o iones muestran contrastes químicos en la micro y nano escala.

Las estructuras fueron caracterizadas química y morfológicamente y su interacción con proteínas y células fue estudiada. Finalmente, su aplicación como intercaras en biosensores fue demostrada con éxito mediante imágenes de resonancia de plasmones superficiales.

Conclusiones generales

Nuevos métodos de fabricación de superficies estructuradas mostrando contrastes químicos han sido explorados en esta tesis. Su aplicación como interfaces en biosensores se ha demostrado mediante imágenes de resonancia de plasmones superficiales.

Las superficies estructuradas han sido fabricadas mediante procesos litográficos basados en haces de electrones o iones. Estos procesos han permitido transferir patrones sin necesidad de emplear mascaras adicionales, lo que ha dado al proceso una gran flexibilidad en la creación de los diseños, y un elevado control en la geometría y la dimensión de las estructuras fabricadas.
Ambas técnicas litográficas, por haces de electrones e iones, han permitido crear estructuras a escala nanométrica con gran repetibilidad. La desventaja que han presentado es la velocidad de fabricación, la cual se ha afrontado disminuyendo el área total estructurada en la superficie.
Las técnicas litográficas han sido combinadas con técnicas de funcionalización de superficies para obtener los contrastes químicos. Para ello materiales mostrando propiedades bio-adhesivos y no bio-adhesivos de interacción con biomoleculas y células han sido utilizados en la funcionalizacion de la superficie. Para ello, se ha recurrido tanto a procesos plasma como de autoensamblaje.

De acuerdo con las diferentes líneas de trabajo seguidas en esta tesis, podemos destacar las siguientes conclusiones específicas:

- Se han depositado películas de ácido acrílico por deposición plasma y los parámetros de deposición han sido optimizados para conseguir una elevada retención de grupos carboxílicos en la película y controlar su solubilidad en agua. Tales condiciones han dado lugar a láminas con propiedades bio-adhesivas.

- La deposición de películas de ácido acrílico con un bajo nivel de reticulación (pdAA) ha permitido la fabricación de patrones en la superficie mediante un aumento selectivo de la reticulación de la película por exposición al haz de electrones. A través de este método se ha evitado la utilización de resinas adicionales, y además, la disolución de la película no expuesta a los electrones en agua ha permitido suprimir los disolventes orgánicos del proceso. De esta forma se han obtenido con éxito estructuras de pdAA en una lámina de PEO depositado por plasma. Su caracterización con proteínas ha mostrado una adherencia preferencial en las partes bio-activas (pdAA). Sin embargo, la presencia de fragmentos bio-adhesivos en la lamina de PEO, detectados mediante XPS y XPEEM, ha dado lugar a una reducción del contraste químico.

- Estructuras de ácido acrílico polimerizado depositadas por plasma (ppAA) fueron fabricadas en un matriz de PEO mediante litografía por haz de electrones. Las características no adhesivas del PEO se conservaron durante el proceso de fabricación al utilizar en el proceso una resina (PMMA) que evito la exposición de la película de PEO al proceso de plasma durante la deposición del ácido acrílico. De esta forma se fabricaron patrones submicrométricos que mostraban un elevado contraste químico. Además, resultados obtenidos mediante SPRi indicaron una mejor detección de proteínas utilizando estructuras a escala manométrica que a escala micrometríca, debido a una reducción de los efectos de difracción en las mismas. Además, la caracterización celular mostró una adhesión selectiva de células en las estructuras bio-adhesivas.

- Las propiedades no bio-adhesivas de las láminas de PEO fueron modificadas con éxito en bio-adherentes, mediante la exposición al haz de electrones. Para incrementar la interacción de las proteínas con la superficie y reducir los tiempos de fabricación, el proceso litográfico fue optimizado reduciendo la energía de los electrones en el proceso litográfico y optimizando la dosis aplicada. Además, reduciendo la energía de los

electrones se obtiene una disminución de electrones retrodispersados en el proceso, por lo que los electrones se confinan dentro de las áreas a exponer, y no modifican las propiedades del la lamina que rodea la estructura.

- Contrastes químicos de oro en una matriz no adherente fueron producidos con litografía por haces de electrones e iones. Las estructuras creadas (compuestas de oro) fueron funcionalizadas mediante adsorción química de un tiol. En concreto, dos métodos de fabricación de estas estructuras (estructuras de oro/PEO-plasma fabricadas con haz de iones y estructuras de oro/PEO-tiol fabricadas con haz de electrones) mostraron mediante SPRi una mayor sensibilidad por área en la adhesión de proteínas que en muestras no estructuradas.

Los diferentes métodos de fabricación expuestos en este trabajo dieron lugar a estructuras bien definidas que presentaron un contraste químico. Una propiedad común a todos los métodos empleados en esta tesis, es la reducción del área activa en la superficie estructurada, lo que permite reducir la cantidad de material biológico en los experimentos y disminuir costes considerablemente.

De los resultados obtenidos en esta tesis, se deriva una gran cantidad de trabajo destinado a explorar la compatibilidad de los procesos litográficos con nuevos materiales y a caracterizar las superficies estructuradas con diferentes biomoléculas y células. Estos estudios podrían abrir una aplicación alternativa de estas superficies en aplicaciones basadas en biosensores.

Acknowledgements

Since I arrived to the JRC I have had the opportunity to work in the field of nanobiosciences. I would like to thank to all those who made it possible, whatever their level of implication.

Firstly, thanks to Dr. François Rossi, Action leader at the Nanobiosciences Unit in JRC and my JRC supervisor, for giving me the opportunity to take part in his research group. To Dr. Pascal Colpo thanks to the support, the advices and the suggestions received. To Dr. Miguel Manso Silván, my supervisor at UAM, thanks for supporting me as PhD student at UAM, and for assisting me especially during the writing period.

In addition, I would like to mention all the researchers that have been involved in this work, Dr. Giacomo Ceccone, for the XPS measurements and for including my patterned surfaces in the experiments carried out with the group of the McMaster University in the ALS. Thanks to Dr. Douglas Gilligand for the ToF-SIMS measurements and especially for his production of nanoparticles. To Dr. Cesar Pascual, Dr. Gerardo Marchesini, Dra. Dora Mehn, Dra. Antonietta Parracino and Dr. Guido Giudetti for the suggestions, for relying and counting on me, and particularly, for the good time spent together in the lab.

My sincere thanks also to Ezio Parnisari for assisting me in PEO deposition.

To the Plasmore group: my good friends Ana and Paola, and to Andrea for helping me every time I needed it, for the advices and the support. THANKS!!

Cesar, que te puedo decir, gracias infinitas, por tu ayuda, tus consejos, tu apoyo, y sobre todo, por las risas, la ironía y el humor mostrados tanto dentro como fuera del trabajo, y…. por esa tortilla de patata que solo tu sabes hacer!!!!

Patricia, I have to give you thanks for so many things…. for welcoming me in the office, for the flat and its marvellous neighbours, the support, …..Uff, I have missed you!!!

To all my friends here, Irene, Lara, Ana, Mari Toñi, Giovanni……. Per tutta l'energia positiva che voi riuscite a darmi!!!!!!

To Rosella e Luca, amici che uno trova per caso una volta e mai più può lasciare de voler benne. Mi avete fatto sentire parte dalla vostra bellissima famiglia.

Y como no, a los míos, a Salome y a Jaime, por estar siempre a mi lado, por vuestros consejos y vuestro apoyo. ¡¡¡Sois lo único que he echado de menos en estos tres años!!!